Dissertation

Cardiac magnetic resonance imaging in the evaluation of left ventricular diastolic function

submitted by

Dr. med. univ. Clemens REITER

for the academic degree of

Doctor of Medical Science
(Dr. scient. med.)

at the

Medical University of Graz
Division of General Radiology, Department of Radiology and
Division of Cardiology, Department of Internal Medicine

under the supervision of

PD Dr. Albrecht SCHMIDT

2025

Statutory Declaration

I hereby declare that this thesis is my own original work and that I have fully acknowledged by name all of those individuals and organizations that have contributed to the research for this thesis. Due acknowledgement has been made in the text to all other material used. Throughout this thesis and in all related publications I followed the “Guidelines of the Medical University of Graz on Good Scientific Practice”.
Furthermore, I hereby declare that if artificial intelligence (AI) tools were used for the generation of certain text passages in the creation of this work, such employment was conducted in compliance with ethical principles, academic integrity, and the regulations of my university. Additionally, it was ensured that this usage was transparently disclosed and appropriately attributed.

Graz, 28.10.2025 Dr. med. univ. Clemens Reiter m.p.

Disclosures

The results of this thesis are published in:

- Reiter C[1,2,3], Reiter U[1], Kräuter C[1,4], Nizhnikava V[1], Greiser A[5], Scherr D[3], Schmidt A[3], Fuchsjäger M[1], Reiter G[1,6]. Differences in left ventricular and left atrial function assessed during breath-holding and breathing. Eur J Radiol. 2021, 141:109756. Doi: 10.1016/j.ejrad.2021.109756 (1).
- Reiter C[1,2,3], Reiter G[1,6], Kräuter C[1,4], Scherr D[3], Schmidt A[3], Fuchsjäger M[1], Reiter U[1]. Evaluation of left ventricular and left atrial volumetric function from native MR multislice 4D flow magnitude data. Eur Radiol. 2024; 34(2):981-993. Doi: 10.1007/s00330-023-10017-3 (2).
- Reiter C[1,2,3], Reiter G[1,6], Kräuter C[1,4], Kolesnik E[3], Greiser A[5], Scherr D[3], Schmidt A[3], Fuchsjäger M[1], Reiter U[1]. Impact of the evaluation method on 4D flow-derived diastolic transmitral and myocardial peak velocities: Comparison with echocardiography. Eur J Radiol. 2024; 170: 111247. Doi: 10.1016/j.ejrad.2023.111247 (3).
- Reiter C[1,2,3], Reiter U[1], Kolesnik E[3], Scherr D[3], Schmidt A[3], Fuchsjäger M[1], Reiter G[1]. MR 4D flow-based diagnosis and grading of left ventricular diastolic dysfunction Eur Radiol. 2025 EPub ahead of print. Doi: 10.1007/s00330-025-11703-0. (4).
- Reiter C[1,2,3], Reiter U[1], Kräuter C[1,4], Kolesnik E[3], Scherr D[3], Schmidt A[3], Fuchsjäger M[1], Reiter G[1]. MR 4D flow-derived left atrial acceleration factor for differentiating advanced left ventricular diastolic dysfunction. Eur Radiol. 2024; 34(6):4065-4076. Doi: 10.1007/s00330-023-10386-9 (5).

Author information:

[1]Department of Radiology, Division of General Radiology, Medical University of Graz, Austria

[2]Department of Radiology, Division of Interventional Radiology, Medical University of Graz, Austria
[3]Department of Internal Medicine, Division of Cardiology, Medical University of Graz, Austria
[4]Department of Biomedical Engineering, Graz University of Technology, Austria
[5]Research & Development, Siemens Healthcare GmbH, Germany
[6]Research & Development, Siemens Healthcare GmbH, Austria

Co-Author contributions:

- **Michel Fuchsjäger**: PI of the funded project of the Anniversary funds of the Austrian National Bank (Grant No. 17934). Supervised project, contributed to study design and manuscript editing.
- **Albrecht Schmidt**: PI of the funded COMET K-project BioPersMed (No. 825329). Supervised project, contributed to study design and manuscript editing.
- **Daniel Scherr**: Supervised project. Contributed to study design and manuscript editing.
- **Ursula Reiter**: PI of the funded project of the Anniversary funds of the Austrian National Bank (Grant No. 15702) and the academic projects (ClinicalTrials.gov, NCT01728597 and NCT03253835). Performed cardiac magnetic resonance imaging, contributed to study design, data analyses and manuscript editing.
- **Gert Reiter**: Performed cardiac magnetic resonance imaging, contributed to study design, data analyses and manuscript editing.
- **Corina Kräuter**: Supported magnetic resonance data analyses and contributed to manuscript editing
- **Ewald Kolesnik**: Supported echocardiographic data analysis and contributed to manuscript editing.
- **Volha Nizhnikava**: Supported magnetic resonance data analysis.
- **Andreas Greiser**: Provided work-in-progress software and contributed to manuscript editing.

During my doctoral studies I contributed to the following publications related to the topic of this doctoral thesis:

- Reiter G, Reiter C, Ovcina I, Fuchsjäger M, Reiter U. 4D flow MRI for a dynamic perspective on the heart and adjacent great vessels. Radiology. 2025; 316(2): e242972 Doi: 10.1148/radiol.242972.
- Kräuter C, Reiter U, Kovacs G, Reiter C, Masana M, Olschewski H, Fuchsjäger M, Stollberger R, Reiter G. Automated vortical blood flow-based estimation of mean pulmonary arterial pressure from 4D flow MRI. Magn Reson Imaging. 2022, 88: 132-141. Doi: 10.1016/j.mri.2022.02.007.
- Reiter G, Kovacs G, Reiter C, Schmidt A, Fuchsjäger M, Olschewski H, Reiter U. Left atrial acceleration factor as a magnetic resonance 4D flow measure of mean pulmonary artery wedge pressure in pulmonary hypertension. Front Cardiovasc Med. 2022, 9:972142. Doi: 10.3389/fcvm.2022.972142.
- Kräuter C, Reiter U, Reiter C, Nizhnikava V, Schmidt A, Stollberger R, Fuchsjäger M, Reiter G. Impact of the Choice of Native T1 in Pixelwise Myocardial Blood Flow Quantification. Magn Reson Imaging. 2021, 53(3):755-765. Doi: 10.1002/mrm.28361.
- Reiter U, Kovacs G, Reiter C, Kräuter C, Nizhnikava V, Fuchsjäger M, Olschewski H, Reiter G. MR 4D flow-based mean pulmonary arterial pressure tracking in pulmonary hypertension. Eur Radiol. 2021, 31(4):1883-1893. Doi: 10.1007/s00330-020-07287-6.

- Reiter U, Reiter C, Kräuter C, Nizhnikava V, Fuchsjäger MH, Reiter G. Quantitative Clinical Cardiac Magnetic Resonance Imaging. Rofo. 2020, 192(3):246-256. Doi: 10.1055/a-0999-5716.
- Reiter G, Reiter C, Kräuter C, Fuchsjäger M, Reiter U. Cardiac magnetic resonance T1 mapping. Part 1: Aspects of acquisition and evaluation. Eur J Radiol. 2018, 109:223-234. Doi: 10.1016/j.ejrad.2018.10.011.
- Reiter U, Reiter C, Kräuter C, Fuchsjäger M, Reiter G. Cardiac magnetic resonance T1 mapping. Part 2: Diagnostic potential and applications. Eur J Radiol. 2018, 109:235-247. Doi: 10.1016/j.ejrad.2018.10.013.

I further contributed to the following publications not directly related to the doctoral thesis:

- Schweiger L, Gütl K, Rief P, Reiter C, Janisch M, Weinberg I, Kolluri R, Miller LE, Brodmann M. Retrievable Scaffold Therapy Combined with Sirolimus-coated Balloon Angioplasty for Infrapopliteal Artery Disease: Final Results from the DEEPER LIMUS Trial. Cardiovasc Intervent Radiol. 2025. Doi: 10.1007/s00270-025-03987-y.
- Gressenberger P, Posch F, Adelsmayr G, Nagy E, Kaufmann-Bühler AK, Steiner J, Janisch M, Reiter C, Eibisberger M, Janek E, Softic N, Fuchsjäger M, Gütl K, Jud P, Silbernagel G, Raggam RB, Brodmann M, Gary T, Schmid J. Lipoprotein (a) is not associated with thrombus burden derived from CT pulmonary angiography in patients with acute pulmonary embolism. Sci Rep. 2024, 14(1): 25962. Doi: 10.1038/s41598-024-77669-z.
- Reiter C, Puseljic M, Fuchsjäger M, Schmid J. Estimating synthetic hematocrit and extracellular volume from native blood pool T1 times at 3 Tesla CMR: Derivation of a conversion equation accuracy and comparison with published formulas. Eur J Radiol. 2024, 178:111659. Doi: 10.1016/j.ejrad.2024.111659.
- Nizhnikava V, Reiter U, Kovacs G, Reiter C, Kräuter C, Olschewski H, Fuchsjäger M, Reiter G. Myocardial strain parameters in pulmonary hypertension are

determined by changes in volumetric function rather than by hemodynamic alterations. Eur J Radiol. 2024, 170:111187. Doi: 10.1016/j.ejrad.2023.111187.

- Haudum CW, Kolesnik E, Colantonio C, Mursic I, Url-Michitsch M, Tomaschitz A, Glantschnig T, Hutz B, Lind A, Schweighofer N, Reiter C, Ablasser K, Wallner M, Tripolt NJ, Pieske-Kraigher E, Madl T, Springer A, Seidel G, Wedrich A, Zirlik A, Krahn T, Stauber R, Pieske B, Pieber TR, Verheyen N, Obermayer-Pietsch B, Schmidt A. Cohort profile: 'Biomarkers of Personalised Medicine' (BioPersMed): a single-centre prospective observational cohort study in Graz/Austria to evaluate novel biomarkers in cardiovascular and metabolic diseases. BMJ Open. 2022, 12(4):e058890. Doi: 10.1136/bmjopen-2021-058890.
- Mischinger J, Schöllnast H, Zurl H, Geyer M, Fischereder K, Adelsmayr G, Igrec J, Fritz G, Merdzo-Hörmann M, Elstner J, Schmid J, Triebl A, Trimmel V, Reiter C, Steiner J, Rosenlechner D, Seles M, Pichler GP, Pichler M, Riedl J, Schöpfer-Schwab S, Strobl J, Hutterer GC, Zigeuner R, Pummer K, Augustin H, Ahyai S, Mannweiler S, Fuchsjäger M, Talakic E. Combining targeted and systematic prostate biopsy improves prostate cancer detection and correlation with the whole mount histopathology in biopsy naïve and previous negative biopsy patients. Front Surg. 2022, 9: 1013389. Doi: 10.3389/fsurg.2022.1013389.
- Schmid J, Nagy E, Kaufmann-Bühler AK, Steiner J, Janisch M, Janek E, Reiter C, Eibisberger M, Softic N, Guss H, Fuchsjäger M, Adelsmayr G. Diagnosing Pulmonary Embolism With Computed Tomography Pulmonary Angiography: Diagnostic Accuracy of a Reduced Scan Range. J Thorac Imaging. 2022, 37(5):323-330. Doi: 10.1097/RTI.0000000000000664.
- Krall M, Gollmer J, Pollheimer MJ, Reiter C, Kolland M, Kirsch AH, Kronbichler A, Eller K, Rosenkranz AR, Odler B. Myocardial infarction with non-obstructive coronary arteries in a patient double-seropositive for anti-glomerular basement membrane and anti-neutrophil cytoplasmic antibodies: A case report. Front Cardiovasc Med. 2022, 9: 893742. Doi: 10.3389/fcvm.2022.893742.
- Zach D, Ablasser K, Kolesnik E, Hoeller V, Fruhwald F, Prüller F, Reiter C, Beham-Schmid C, Lipp R, Rainer PP, Zirlik A, Wölfler A, Verheyen N. Advanced isolated

light chain amyloid cardiomyopathy with negative immunofixation and normal free light chain ratio. ESC Heart Fail. 2021, 8(4):3397-3402. Doi: 10.1002/ehf2.13381.

Acknowledgements

My doctoral studies were funded by the Anniversary fund of the Austrian National Bank (Grant No. 15702 and 17934), COMET K-project BioPersMed (No. 825329), and the European Society of Radiology (EIBIR/ECR Seed grant 2020).

I want to thank my supervisors PD Dr. Albrecht Schmidt, Univ.-Prof. Dr. Daniel Scherr and Univ.-Prof. Dr. Michael Fuchsjäger for agreeing to support me throughout my studies, giving me the opportunity to work in these exciting multi-disciplinary projects. I am very grateful for the inspiring discussions I was able to have with them. The project, taking cardiological, radiological and technical aspects of patient care into account, inspired me and will be the basis of my future carrier.

I thank the whole cardiac magnetic resonance imaging team and my colleagues from the Department of Radiology and Division of Cardiology who supported my clinical research and mentored me with helpful discussions and with their friendship.

I would especially like to thank my parents Ursula and Gert Reiter, who have been mentors throughout my life, and who have always supported me. Furthermore, I would like to thank my parents-in-law Michaela and Manfred Rieger for their help. All above I want to thank my wife Alex and my children Theodor and Konstantin Reiter for their patience, their companionship and their understanding during my academic journey.

Table of Contents

Abbreviations

3D	three-dimensional
2D flow	time-resolved, one-directional phase contrast imaging
4D flow	time-resolved, three-dimensional, three-directional phase contrast imaging
α	left atrial acceleration factor
α_{lower}	left atrial acceleration factor (as originally introduced)
α_{Echo}	left atrial acceleration factor assessed by echocardiography
A	late-diastolic transmitral peak filling velocity
ASE	American Society of Echocardiography
bSSFP	balanced steady-state free-precession
D	early-diastolic pulmonary venous peak velocity
E	early-diastolic transmitral peak filling velocity
e’	early-diastolic myocardial peak velocity
E/A	ratio of early-to-late diastolic transmitral peak velocities
EACVI	European Association of Cardiovascular Imaging
EDV	left ventricular end-diastolic volume
EF	left ventricular ejection fraction
EF_{active}	active left atrial ejection fraction
$EF_{passive}$	passive left atrial ejection fraction
EF_{total}	total left atrial ejection fraction
ESV	left ventricular end-systolic volume
F_A	2D flow-derived late-diastolic transmitral peak flow
F_E	2D flow-derived early-diastolic transmitral peak flow
FLASH	fast low angle shot
ICC	intraclass correlation coefficient
LAVI	left atrial volume index
LAV_{bc}	left atrial volume before atrial contraction
LAV_{max}	maximal left atrial volume

LAV_{min}	minimal left atrial volume
LVM	left ventricular myocardial mass
NFV	phase-contrast derived net flow volume
PAWP	mean pulmonary arterial wedge pressure
PER	left ventricular peak ejection rate
PFR_A	late-diastolic left ventricular peak filling rate
PFR_E	early-diastolic left ventricular peak filling rate
r	Pearson's correlation coefficient
S	systolic pulmonary venous peak velocity
SD	standard deviation
SD_w	within subject standard deviation
sPAP	systolic pulmonary arterial pressure
SV	left ventricular stroke volume
TR	peak tricuspid regurgitation velocity
v_D	left atrial early-diastolic peak inflow velocity
v_E	left ventricular early-diastolic peak outflow velocity
v_S	left atrial systolic peak inflow velocities

List of Figures

List of Tables

Zusammenfassung

Hintergrund: Während die Echokardiographie als etabliertes Standardverfahren zur nicht-invasiven Beurteilung der diastolischen Funktion gilt, gewinnt die kardiale Magnetresonanztomographie für die Diagnose der linksventrikulären diastolischen Funktion zunehmend an Bedeutung. Insbesondere die 4D Flow Bildgebung, welche eine gleichzeitige Ermittlung von Volumen- und Flussparametern aus einer einzigen Messung ermöglicht, eröffnet neue Möglichkeiten für eine standardisierte Beurteilung der linksventrikulären diastolischen Funktion. Ziel dieser Dissertation war es, die Eignung der 4D Flow Bildgebung zur Diagnose und Graduierung der linksventrikulären diastolischen Dysfunktion zu untersuchen, wobei die Echokardiographie als Referenzmethode diente.

Methoden: Zwischen Oktober 2016 und Februar 2022 wurden 94 StudienteilnehmerInnen (mittleres Alter 62 ± 12 Jahre; 50 Frauen; 34 mit struktureller Herzerkrankung) prospektiv in die Studie eingeschlossen und mittels transthorakaler Echokardiographie sowie 4D Flow Bildgebung bei 3-Tesla untersucht. Die echokardiographische Graduierung erfolgte gemäß dem multiparametrischen, schwellenwertbasierten ASE/EACVI 2016 Algorithmus. Aus den 4D Flow Daten wurden sowohl volumetrische Parameter als auch Echokardiographie-äquivalenten diastolischen Geschwindigkeitsgrößen ausgewertet. Zusätzlich wurde die Dauer des vortikalen Blutflusses in der Pulmonalarterie (t_{vortex}) als Surrogatparameter für die echokardiographisch bestimmte maximale Trikuspidalregurgitationsgeschwindigkeit (TR) verwendet. Korrelationen zwischen den Parametern und die Übereinstimmung der linksventrikulären diastolischen Dysfunktions-Graduierung zwischen beiden Methoden wurden statistisch analysiert.

Ergebnisse: Alle untersuchten 4D Flow-basierten Parameter zeigten eine starke bis sehr starke Korrelationen mit den echokardiographischen Parametern (r = 0.75–0.92). Bei volumetrischen Parametern traten signifikante Bias zwischen den Methoden auf,

weswegen für die linksventrikuläre Auswurffraktion und den linksatrialen Volumenindex Bias-korrigierte 4D Flow Schwellenwerte definiert wurden. Bei transmitralen und myokardialen Geschwindigkeitsparameter und Parameter-Verhältnissen wurde bei Verwendung entsprechenden Auswerteworkflows kein Bias zwischen 4D Flow Daten und Echokardiographie festgestellt, weswegen die etablierten echokardiographischen Graduierungs-Schwellwerte bei der 4D Flow-basierten Analyse angewendet werden konnten. Für t_{vortex} wurde ein Schwellenwert von >15 % des Herzzyklus als Surrogatparameter für den echokardiographischen Schwellwert TR > 2.8 m/s definiert. Bei Verwendung eines Echo-äquivalenten, Schwellwert-adaptierten ASE/EACVI 2016 Algorithmus zur Klassifikation der diastolischen Dysfunktion 4D Flow Daten ergab sich bei der Graduierung der linksventrikulären diastolischen Dysfunktion eine nahezu perfekte Übereinstimmung mit der Echokardiographie (gewichtetes Kappa = 0.84). Es gab keinen Hinweis auf systematische Über- oder Unterschätzung des Schweregrads der diastolischen Dysfunktion durch die 4D Flow-basierte Methode (p = 0.53).

Schlussfolgerung: Die Diagnose und Graduierung der linksventrikulären diastolischen Dysfunktion aus einer einzigen 4D Flow Messung zeigte unter Verwendung des im Rahmen dieser Dissertation erarbeiteten Auswertealgorithmus eine nahezu perfekte Übereinstimmung mit der Echokardiographie. Der 4D Flow-basierte links-atriale Beschleunigungsfaktor α stellt einen vielversprechenden Parameter zur Identifikation höhergradiger diastolischer Dysfunktion dar und könnte zur Vereinfachung der 4D Flow-basierten Diagnose der höhergradigen diastolischen Dysfunktion beitragen.

Abstract

Background: While echocardiography is the established standard method for non-invasive assessment of left ventricular (LV) diastolic function, cardiac magnetic resonance imaging is increasingly gaining importance in the evaluation of diastolic dysfunction. 4D flow magnetic resonance imaging in particular, which allows the simultaneous acquisition of volumetric and flow parameters from a single measurement, offers new options for standardized assessment of left ventricular diastolic metrics. The aim of this dissertation was to investigate the feasibility and the accuracy of 4D flow-based diagnosis and grading of left ventricular diastolic dysfunction using echocardiography as the reference method.

Methods: This prospective study included 94 participants between October 2016 and February 2022 (average age: 62 ± 12 years; female participants: 50; individuals with structural cardiac pathology: 34). All participants underwent comprehensive transthoracic echocardiography and 3-Tesla cardiovascular magnetic resonance imaging including 4D flow imaging. Classification of left ventricular diastolic dysfunction followed the established multiparametric ASE/EACVI 2016 algorithm using threshold criteria. The analysis of both volumetric cardiac parameters and velocity measurements equivalent to echocardiography were derived from 4D flow data. Pulmonary arterial vortical flow duration (t_{vortex}) was used as a surrogate marker for echocardiographic tricuspid regurgitant peak velocity (TR) measurements. Parameter correlations and inter-method agreement for diastolic dysfunction grading were analyzed.

Results: All 4D flow-derived measurements showed strong to very strong correlations with echocardiographic parameters ($r = 0.75–0.92$). Volumetric parameters revealed significant biases between methods, requiring the definition of bias-corrected 4D flow thresholds for left ventricular ejection fraction and left atrial volume index calculations. Transmitral and myocardial velocity measurements, along with their ratios, showed no significant biases when employing appropriate data evaluation workflows, allowing the

use of established echocardiographic threshold values for the 4D flow-based grading of left ventricular diastolic dysfunction. A t_{vortex} threshold > 15% was established as equivalent to the echocardiographic tricuspid regurgitation velocity threshold of TR > 2.8 m/s. Employing the threshold-adjusted ASE/EACVI 2016 algorithm for 4D flow-based diastolic dysfunction classification achieved nearly perfect agreement with echocardiographic assessment (weighted kappa coefficient = 0.84). No evidence of systematic over- or under-classification of diastolic dysfunction severity was observed using the 4D flow method ($p = 0.53$).

Conclusion: The diagnostic assessment and severity grading of left ventricular diastolic dysfunction using a single 4D flow acquisition, employing the evaluation algorithm developed in this dissertation, demonstrates nearly perfect agreement with echocardiography. The 4D flow-derived left atrial acceleration factor emerges as a promising single 4D flow parameter for identifying advanced diastolic dysfunction and may facilitate simplified 4D flow-based clinical diagnostics in future applications.

1. Introduction

1.1 Left ventricular diastolic function assessment using cardiac imaging

Heart failure is a clinical syndrome caused by functional impairment of ventricular filling or ejection of blood. Diastolic heart failure, which affects up to 50% of heart failure patients, is both highly prevalent and associated with significant morbidity and mortality. Diagnosing and grading of left ventricular diastolic dysfunction is crucial for managing and treating these patients (6).

While systolic function describes contraction of the ventricles and of blood into the circulation, diastolic function describes the ability of the ventricles to relax and fill with blood after contraction ensuring a satisfying filling for the next ejection. The diastolic phase represents a complex process composed of relaxation, drop of the intraventricular pressure and subsequent flow of blood form the atria into the ventricles (7). The normal filling phase is composed of a rapid early component, a slower following filling and another faster part due to atrial contraction – all of which happen without massive increase of left ventricular pressure in a healthy heart (8). Elevated filling pressures are the hallmark finding of diastolic dysfunction and their non-invasive assessment is complex (9).

The American Society of Echocardiography (ASE) and the European Association of Cardiovascular Imaging (EACVI) endorse echocardiography as the preferred method for noninvasive evaluation of left ventricular diastolic function (10). Current guidelines for this non-invasive assessment of diastolic function with two-dimensional and Doppler echocardiography recommend a validated, multiparametric, threshold-based approach (11). This method involves identifying structural changes in the left atrium and left ventricle associated with diastolic dysfunction, such as atrial enlargement and left ventricular hypertrophy, as well as measurement of velocity parameters that indicate impaired left ventricular relaxation, increased left ventricular stiffness, and elevated left ventricular filling pressures. Key parameters include the early-diastolic transmitral peak velocity (E), the early-diastolic mitral valve tissue peak

velocity (e'), the ratio of early-to-late diastolic transmitral peak velocities (E/A), and the E/e' ratio. Tricuspid regurgitant velocity, an echocardiographic marker of elevated pulmonary arterial pressure, further aids in assessing left ventricular diastolic dysfunction.

1.2 Cardiac magnetic resonance imaging

Cardiac magnetic resonance imaging offers a wide range of different sequences with possibilities to investigate various cardiac parameters (12,13) and cardiac magnetic resonance imaging-based diastolic assessment includes measuring left atrial volumes and ejection fractions (14,15) and analyzing left ventricular filling dynamics through peak filling rates (15–17) from volumetric imaging as well as transmitral blood inflow velocities and early-diastolic myocardial peak velocities using phase contrast imaging (18,19). Furthermore, cardiac magnetic resonance-based analysis of cardiac function is rapidly advancing, especially with the introduction of commercial software that facilitates (semi-)automated cardiac chamber segmentation (20–23).

1.6.1 Volumetric Function

Balanced steady-state free presession (bSSFP) cine imaging is considered the reference standard for assessing left ventricular and left atrial volumetric function due to its high accuracy and consistency (12,24). High-quality cine imaging is essential for precise assessment of cardiac function, and respiratory motion during image acquisition is typically minimized through breath-holding, either during inspiration or expiration. For patients who struggle to hold their breath, cine real-time imaging techniques offer a viable alternative, allowing functional assessment to be performed during breathing (24–31). However, breath-holding has been shown to influence various cardiovascular parameters (32–38), raising the possibility that intrathoracic pressure changes between breath-holding and free breathing may affect measures of cardiac function. Research comparing systolic left ventricular functional parameters

obtained with cine real-time imaging during free breathing and conventional multi-breath-hold segmented cine acquisition has produced mixed results regarding the impact of breath-holding on left ventricular volumes and ejection fraction (25–31,39–42). These conflicting findings suggest that the distinct imaging sequences used might obscure physiological changes associated with breathing (34–36). As differences between breath-hold and free-breathing measurements could affect longitudinal assessments in various respiratory states or comparisons of functional parameters across imaging modalities (e.g., echocardiography, where measurements are typically performed during free breathing (11)), it is relevant to gain a clearer understanding of breathing-induced variations in cardiac function.

1.6.2 Phase contrast imaging

Transmitral diastolic peak velocities obtained from 2D phase contrast imaging (2D flow) in a short-axis orientation tend to be systematically lower than those measured with echocardiography (43–46,18,47–49). Assessing e' with phase contrast magnetic resonance imaging also differs methodologically from echocardiography, as the signal from the mitral valve tissue is limited, although myocardial tissue velocity derived from 2D flow has been shown to correlate with echocardiography, albeit with biases for both e' and E/e' (43,44,47,48). As a result, established echocardiographic thresholds for E, E/A, e’, and E/e’ are not necessarily applicable when assessing diastolic dysfunction using phase contrast magnetic resonance. The lack of standardized acquisition protocols, evaluation methods, and defined grading thresholds, which are often not interchangeable with other techniques (50–52) hinders diagnosis and grading of diastolic dysfunction by cardiac magnetic resonance imaging.

Four-dimensional (4D) flow imaging is increasingly recognized as a valuable tool for noninvasive cardiovascular hemodynamic assessment and is increasingly implemented in routine cardiac magnetic resonance imaging practice (53,54). This technology provides three-dimensional magnitude images along with the comprehensive time-resolved, three-dimensional velocity field of the heart and surrounding vessels and allows positioning of evaluation planes in any region of

interest, such as the transmitral inflow region or the myocardium. The retrospective nature of 4D flow also supports a variety of strategies for assessing velocity parameters, though these different approaches may impact how the parameters relate to those obtained from echocardiography.

Apart from the three-dimensional velocity field, 4D flow measurements also produce three-dimensional anatomical (magnitude) cine images. While many new 4D flow parameters related to cardiac function and velocity have been investigated (55–57), the use of 4D flow magnitude images for assessment of volumetric cardiac function remains underexplored (58–62). Compared to standard cine bSSFP imaging, 4D flow magnitude images use fast low-angle shot (FLASH) readout, which inherently results in lower blood-to-myocardium contrast (63,64). Additionally, 4D flow is typically performed as a 3D sequence, leading to decreased in-flow blood enhancement and thus reduced contrast between blood and myocardium compared to two-dimensional based methods (57,63,65). To mitigate this limitation in 3D acquisitions, volumetric data from 4D flow has been collected using contrast agents like gadobenate dimeglumine, gadopentetate dimeglumine, gadoterate meglumine (60–62), or off-label ferumoxytol (58,59), enabling extraction of ventricular function parameters comparable to those derived from standard cine bSSFP imaging (58–62). However, the use of gadolinium and ferumoxytol as contrast agents is controversial due to safety concerns, making their application difficult to justify when not specifically indicated by the clinical referral (66,67).

A potential alternative is the use of a multislice time-resolved two-dimensional phase contrast sequence with three-directional velocity encoding, known as multislice 4D flow, where volumetric function could be assessed from the native (non-contrast-enhanced) magnitude images. This would be desirable as this could enable to evaluate the parameters of diastolic function from a single measurement, preventing cycle-to-cycle physiological variations, streamlining and shortening magnetic resonance imaging protocols and also enabling investigation of new parameters.

1.3 Aims and scope

The primary objective of this doctoral thesis study was to explore the feasibility of evaluation of left ventricular diastolic function from a single 4D flow measurement. Echocardiographic assessment was used as the reference method for diagnosis and grading of left ventricular diastolic dysfunction following the ASE/EACVI 2016 algorithm. To achieve this, five research milestones (**MS1**-**MS5**) were defined and examined across study cohort subgroups:

MS1: Impact of respiration on functional parameters

This milestone investigated how breath-holding affects ventricular and atrial volumetric and flow parameters compared to free breathing, using cine bSSFP real-time and two-dimensional magnetic resonance flow imaging. This first study specifically examined the impact of inspiratory breath-holding on ventricular and atrial function parameters, applying the same imaging techniques during both, free breathing and breath-holding (1).

MS2: 4D Flow-based evaluation of volumetric function

This milestone assessed whether 4D flow magnitude data allow reliable evaluation of left ventricular and left atrial volumetric function. Free-breathing cine bSSFP realtime imaging was used as reference method. Internal validation was performed by 4D flow-derived pulmonary net flow volumes. The study focused on assessing native multislice 4D flow magnitude images for left ventricular and left atrial volumetric function, and validating these results against bSSFP cine-derived parameters and native multislice 4D flow-derived net forward volumes (2).

MS3: Impact of evaluation strategy on 4D flow-derived diastolic parameters

Different strategies for evaluating 4D flow-derived diastolic function parameters, analogous to those obtained through echocardiography, were compared to echocardiography as the reference (3).

MS4: 4D Flow-based diagnosis and grading of left ventricular diastolic dysfunction

This milestone compared 4D flow magnetic resonance imaging to echocardiography for diagnosing and grading of left ventricular diastolic dysfunction according to the ASE/EACVI 2016 multiparametric threshold approach. Agreement between methods was determined (4).

MS5: Novel 4D Flow metrics characterizing diastolic dysfunction

This milestone explored innovative 4D flow-based metrics for identifying and grading left ventricular diastolic dysfunction. Specifically, the left atrial acceleration factor was evaluated as a potential single-parameter metric to distinguish between normal and more advanced grades of diastolic dysfunction. The proof-of-concept study examined the correlation between α and left ventricular diastolic dysfunction grades as assessed by echocardiograph (5).

2. Material and Methods

The methods of this doctoral thesis have been published in (1–5).

2.1 Study design and participant recruitment

2.1.1 Ethical considerations

The study analyzed data from two prospective, single-center trials designed to evaluate the diagnostic capabilities of 4D flow cardiovascular magnetic resonance in cardiac function assessment. The study protocol received approval from the institutional ethics committee and was conducted in full compliance with the Declaration of Helsinki. All study participants provided written informed consent prior to enrollment.

2.1.2 Inclusion and exclusion criteria

Participants were recruited between October 2016 to February 2022. 61 adults without clinical evidence or symptoms of cardiovascular disease (ClinicalTrials.gov identifier: NCT01728597, for research milestones **MS1**-**MS5**) and 35 adults with documented structural heart disease and confirmed or suspected diastolic dysfunction (ClinicalTrials.gov identifier: NCT03253835, for research milestones **MS4** and **MS5**).

Inclusion criteria were age over 18 years and the capacity to provide written informed consent. Exclusion criteria were contraindications to magnetic resonance imaging (including pregnancy, severe claustrophobia), cardiac rhythm irregularities, significant mitral valve stenosis, and the presence of implanted cardiac devices incompatible with magnetic resonance imaging.

2.1.3 Final study population

All participants underwent echocardiographic assessments for evaluation of left ventricular diastolic function and were examined using native or contrast-enhanced cardiac magnetic resonance imaging (if indicated by clinical referral), including 4D flow imaging.

Two participants were unable to complete magnetic resonance imaging due to severe back pain (n=1) and previously unrecognized claustrophobia (n=1), resulting in a final study cohort of 94 participants. Comprehensive baseline demographic and clinical data included age, gender, medical history, blood pressure measurements, and relevant laboratory results were obtained at enrollment. **Figure 1** provides the study flow chart, illustrating inclusion and exclusion criteria along with the sub-cohorts analyzed for each research milestone **MS1** - **MS5**.

2.2 Echocardiographic protocol

2.2.1 Image acquisition

Echocardiographic evaluations followed the 2016 ASE/EACVI guidelines (10). All participants were investigated with a Vivid E9 system (GE Healthcare, Chicago, Illinois, USA). Image acquisition was performed with concurrent echocardiographic monitoring during shallow respiration, with patients positioned in the left lateral decubitus position. Each measured parameter was acquired across three to five consecutive cardiac cycles, with all images stored for subsequent analysis using the Vivid E9 software (GE Healthcare, Chicago, Illinois, USA).

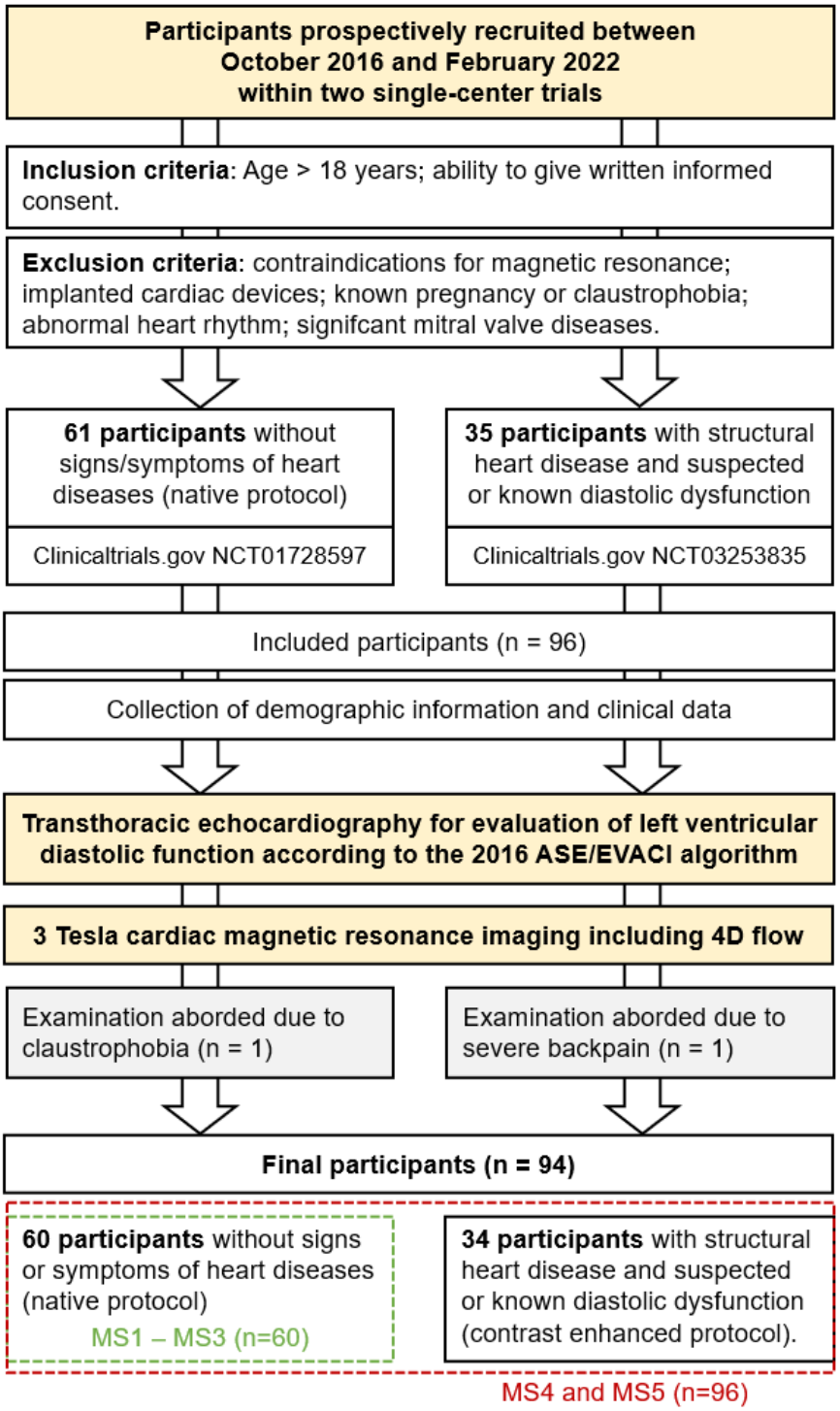

Figure 1: Study flow chart. Reproduced with modifications from Reiter C et al. Eur Radiol 2025 (4).

MS = research milestones

2.2.2 Volumetric and functional parameters

The left ventricular ejection fraction (EF) and the maximum left atrial volume indexed to the body surface area (LAVI) were determined from apical four-chamber and two-chamber view images using the biplane Simpson method and the biplanar area-length method, respectively (**Figure 2**).

Early- and late-diastolic transmitral peak velocities (E and A, respectively) as well as the early diastolic tissue Doppler mitral annular peak velocities (e') were acquired in the apical four-chamber view. Average e' was assessed as the average of septal and lateral velocities. Continuous-wave Doppler was used to measure peak tricuspid regurgitation velocity (TR) in the apical four-chamber view, and systolic pulmonary arterial pressure (sPAP/pTR) was estimated from TR (in m/s) using the formula sPAP (in mmHg) = $4 \cdot TR^2 + 5$ mmHg (68).

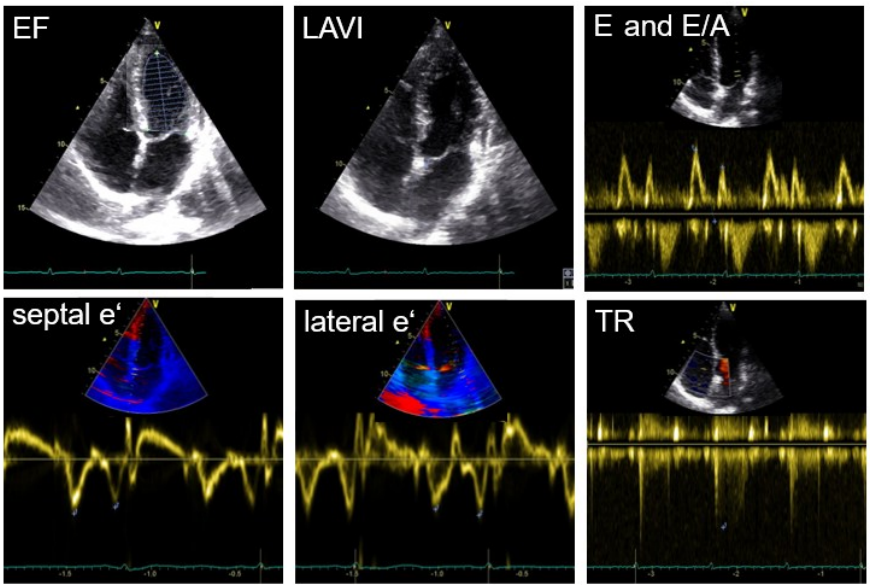

Figure 2: Echocardiographic left ventricular diastolic dysfunction parameters.
EF = left ventricular ejection fraction, LAVI = left atrial maximal volume index, E = early-diastolic transmitral peak velocity, E/A = early-to-late diastolic transmitral peak velocity ratio, e' = early diastolic tissue Doppler mitral annular peak velocity, TR = peak tricuspid regurgitation velocity.

Systolic and early-diastolic pulmonary venous peak velocities (S and D, respectively) were assessed in the right upper or lower pulmonary vein visualized in the apical four-chamber view, positioning the Doppler sample volume approximately 0.5 cm within the pulmonary vein.

2.2.3 Echocardiographic characterization of diastolic function

Diastolic function characterization and grading followed the ASE/EACVI algorithm (10), where participants with normal left ventricular ejection fraction (≥ 50%) were graded based on cut-off values for e', E/e', TR, and LAVI. Diastolic function was classified from parameter cut-off values as normal (grade 0, fewer than half of cut-offs met), indeterminate (50% of cut-offs met), or diastolic dysfunction (over 50% of cut-offs met). For participants with diastolic dysfunction, reduced left ventricular ejection fraction, or participants with structural heart disease, left ventricular diastolic dysfunction severity (grades I-III) was assessed using these parameters together with E and E/A.

2.3 Cardiac magnetic resonance imaging protocol

2.3.1 Image acquisition

Cardiac magnetic resonance imaging was performed on a 3-Tesla scanner (Magnetom Skyra, Siemens Healthcare, Erlangen, Germany) equipped with an 18-channel body array matrix and spine matrix coil. Electrocardiographic gating was employed for all sequences.

2.3.2 Cine function imaging

Left ventricular and left atrial volumetric function was assessed from cine bSSFP real-time series acquired in left ventricular two- and four-chamber orientations, contiguous slice stacks covering the left ventricle in short-axis orientation, and contiguous slice

stacks covering the entire left heart in four-chamber orientation. Typical imaging parameters were: Spatial resolution = 2.5 × 4.2 × 8.0 mm^3 for short-axis images and 2.3 × 3.9 × 7.0 mm^3 for long-axis images, temporal resolution = 35 - 38 ms (using echo sharing), data acquisition time per cardiac phase = 55 - 61 ms, echo time = 1.1 ms, flip angle = 40°, parallel acquisition factor = 3. The data acquisition window was set to exceed one heartbeat to ensure coverage of the entire cardiac cycle. For inspiratory breath-hold acquisitions (**MS1**), series were acquired in multiple stacks, ensuring breath-holding not exceeding 15 heartbeats.

To evaluate reproducibility of volumetric function assessment, five participants underwent both, short- and long-axis stacks measurements twice - once during breath-holding and once during free breathing - with the initial measurements used for comparison.

2.3.3 2D flow imaging

A prototype sequence using a retrospectively electrographically gated 2D flow technique with respiratory gating was employed to evaluate transmitral inflow during inspiratory breath-holding and free-breathing (**MS1** and **MS3**). Images were acquired parallel to the mitral valve annulus at the level of the valve tips. Typical imaging parameters were: Voxel size = 1.8 × 2.5 × 5.0 mm^3, echo time = 2.5 ms, temporal resolution = 45 ms (interpolated to yield 30 cardiac phases per cycle), flip angle = 15°, velocity encoding = 100 - 120 cm/s (preventing aliasing), breath-hold period = 12 heartbeats. Respiratory gating was used for free-breathing measurements, with respiratory gating positioning a navigator on the right diaphragm dome (gating window = ±3 mm).

2.3.4 4D flow imaging

4D flow imaging was preformed using a two-dimensional phase contrast sequence with three-directorial velocity encoding (69) which was either electrocardiographically or

pulse gated. The image stack was orientated in the three-chamber view and covered at least the left ventricle, left atrium, and the main pulmonary artery.

Protocol parameters were: voxel size = 1.8 × 2.5 × 4 mm^3, echo time = 3.1 ms, temporal resolution = 41.8 ms (interpolated to 30 cardiac phases per cycle), flip angle = 12°, velocity encoding = 100 - 190 cm/s in all directions (preventing aliasing), parallel acquisition factor = 2, averaging factor = 2 (to compensate breathing motion). The acquisition time per slice was typically 45 seconds (52 heartbeats), resulting in a 4D flow measurement time of about 22 minutes for 20 - 40 contiguous.

2.4 Cardiac magnetic resonance image analysis

Left ventricular and left atrial volumetric function, as well as 2D flow series were analyzed using dedicated software (syngo.via and Argus Flow, Siemens Healthineers, Erlangen, Germany; cvi42, Circle Cardiovascular Imaging Inc., Calgery, Canada). 4D flow data were evaluated by a prototype software (4Dflow, Siemens Healthineers, Erlangen, Germany). Repeatability (**MS1**) and intra- and inter-observer variability of parameters were assessed in 20 participants which were evaluated twice by one observer and once by a second observer (**MS1 - MS3, MS5**). All evaluations were performed blinded to prior results.

2.4.1 Volumetric function

Left ventricular volumes in end-diastole (EDV), end-systole (ESV), the stroke volume (SV), and the EF were evaluated from short-axis image stacks (and additionally from four-chamber image stacks in **MS1**) following guideline recommendations (70), including trabeculae, papillary muscles, and the left ventricular outflow tract to the left ventricular cavity.

For the volumetric evaluation of cine bSSFP short-axis series the mitral valve insertion points in left ventricular two-chamber and four-chamber series were identified to define the left ventricular base, carefully excluding left atrial segments from the left ventricular cavity (**Figure 3A**). Contours and mitral valve points were automatically

propagated across all cardiac phases and manually adjusted as needed. Left ventricular peak ejection rate (PER), and early-diastolic (PFR_E) as well as late-diastolic (PFR_A) left ventricular peak filling rates, were calculated from the left ventricular volume time-curve derivative.

Left atrial maximum (LAV_{max}), pre-contraction (LAV_{bc}), and minimum (LAV_{min}) volumes, along with the body surface area-normalized maximum left atrial volume index, were measured either from segmented four-chamber stacks using the Simpson's method (syngo.via software, **MS1**) or from manual segmentation of left ventricular two- and four-chamber series using the bi-planar area-length method (cvi42, Circle Cardiovascular Imaging Inc., Calgery, Canada, **MS2** and **MS5**). The left atrial appendage was included, and pulmonary vein insertion regions were excluded from the left atrial volumes using straight-line contours (71). Calculated left atrial ejection fractions included the total ($EF_{total} = 100 \times (LAV_{max} - LAV_{min}) / LAV_{max}$), the passive ($EF_{passive} = 100 \times (LAV_{max} - LAV_{bc}) / LAV_{max}$), and the active ($EF_{active} = 100 \times (LAV_{bc} - LAV_{min}) / LAV_{bc}$) ejection fractions.

The cine bSSFP volumetric evaluation was used as reference method (**MS2**) for the evaluation of left ventricular volumetric function from 4D flow magnitude data. To employ the same evaluation strategy, left ventricular function parameters and myocardial mass (LVM) were calculated from manual segmentation of end-diastolic and end-systolic endo- and epicardial contours in short axis series (**Figure 3B**). A discrepancy over 5% between end-diastolic and end-systolic LVM was defined as segmentation error and corrected as needed, with the final LVM reported as the average of both measurements.

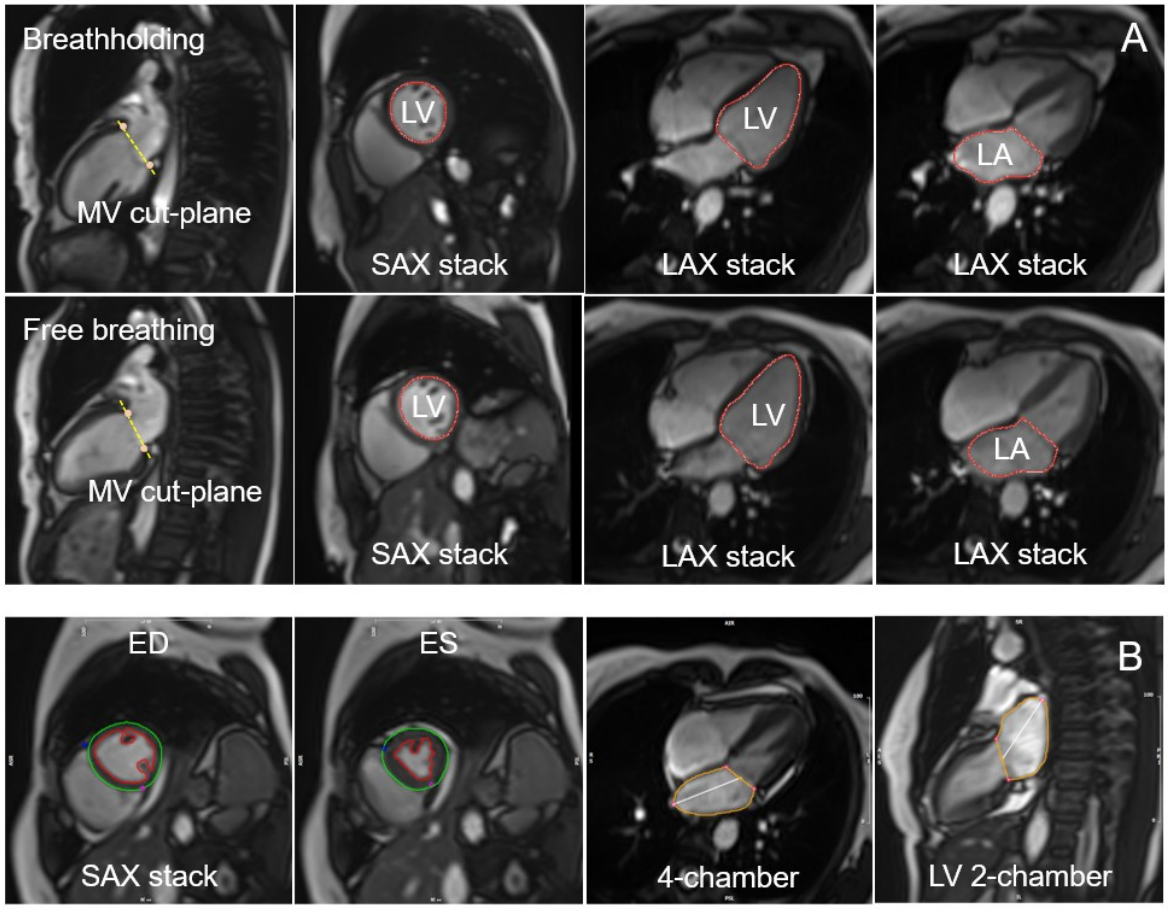

Figure 3: Evaluation of left ventricular and left atrial volumetric function. Reproduced with modifications from Reiter C et al. Eur J Radiol 2021 (1)

For comparison of breath-hold versus free-breathing and short-axis versus long-axis orientation acquisition (**MS1**) the Simpson method was employed for the left ventricle and left atrium using the mitral valve plane as baseplane (A). For comparison of acquisition sequence (**MS2**) left ventricular volumes were acquired from short-axis series and left atrial function was evaluated using the bi-planar area-length method (B). MV = mitral valve, SAX = short-axis, LAX = 4-chamber orientation.

2.4.2 2D flow magnetic resonance imaging

To assess left ventricular filling velocities and flow from transmitral 2D flow (**MS1** and **MS3**), manual segmentation of the mitral valve opening area was performed on transmitral phase contrast images across all diastolic cardiac phases using dedicated software (Argus software, Siemens Healthineers, Erlangen, Germany). Transmitral peak velocities and peak flows in the early-diastole (E and F_E, respectively) and late-

diastole (A and F_A, respectively) were derived from velocity-time curves and flow-time curves.

The early-diastolic myocardial peak velocity was calculated as the peak average velocity in early diastole within a myocardial region in the lateral myocardial wall, measured from the same phase contrast series (**Figure 4**). Due to the proximity of the imaging plane to the left ventricular outflow tract, septal myocardial velocity could not be derived reliably.

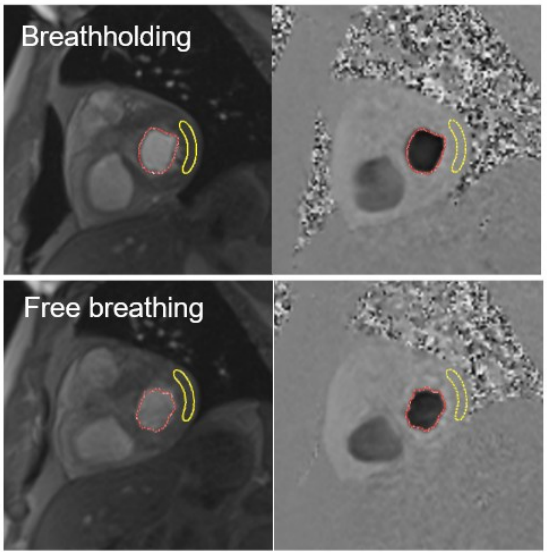

Figure 4: Evaluation of transmitral and myocardial tissue velocities from 2D flow magnetic resonance imaging. Reproduced with modifications from Reiter C et al. Eur J Radiol 2021 (1).
Red contour = segmentation of the mitral valve opening area; yellow contour = segmentation of the lateral myocardial tissue.

During both breath-hold (**MS1**) and free-breathing (**MS1** and **MS3**) conditions, cardiac intervals (RR-intervals) were defined as the average intervals during 2D flow assessment.

Breathing depth and rate were assessed by the diaphragmatic motion, quantified as the displacement between inspiratory and expiratory positions, and as respiratory frequency calculated from the time interval between two successive inspiratory peaks (**MS1**).

2.4.3 4D flow magnitude data

4D flow magnitude data were multiplanar reconstructed in long-axis views (left ventricular two-chamber and four-chamber views), and a set of consecutive short-axis slices (8 mm thickness) to cover the left ventricular cavity. Cine 4D flow series were created for further analysis (**Figure 5A**) of left ventricular and left atrial volumetric function parameters using standard software (cvi42, Circle Cardiovascular Imaging Inc., Calgery, Canada). All contours were manually traced (**Figure 5B**). Left ventricular end-diastole and end-systole were defined visually in a mid-ventricular short-axis slice as the phases with the largest and smallest left ventricular cross-sectional areas, respectively (72,73). Left ventricular end-diastolic, end-systolic, and stroke volume, left ventricular EF, and left ventricular myocardial mass were assessed similar to the evaluation described for cine bSSFP series.

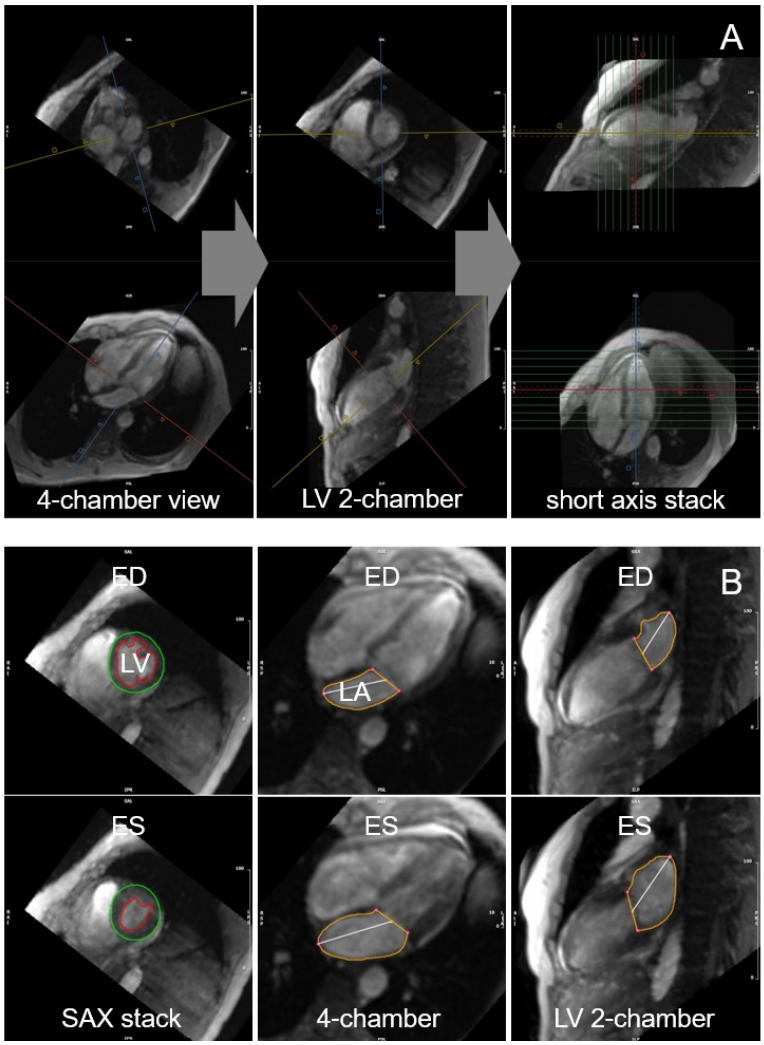

Figure 5: Processing of 4D flow magnitude data. Reproduced with modifications from Reiter C et al. Eur Radiol 2023 (2).

Left ventricular long- and short-axis reconstruction (A). Chamber segmentation for left ventricular and left atrial volumetric function evaluation (B). ED = end-diastole, ES = end-systole, green line = epicardial segmentation, red line = endocardial segmentation, orange line = segmentation of the left atrium.

2.4.4 4D flow velocity data

Prior to analysis, corrections for background phases were performed, along with aliasing correction if required. Automatic segmentation of the left ventricle, left atrium, and surrounding large vessels was performed by using a segmentation threshold (**Figure 6**). Additionally, the velocity vector fields for the left ventricle and left atrium

were visually examined to identify any unknown cardiac shunts or notable valve regurgitations.

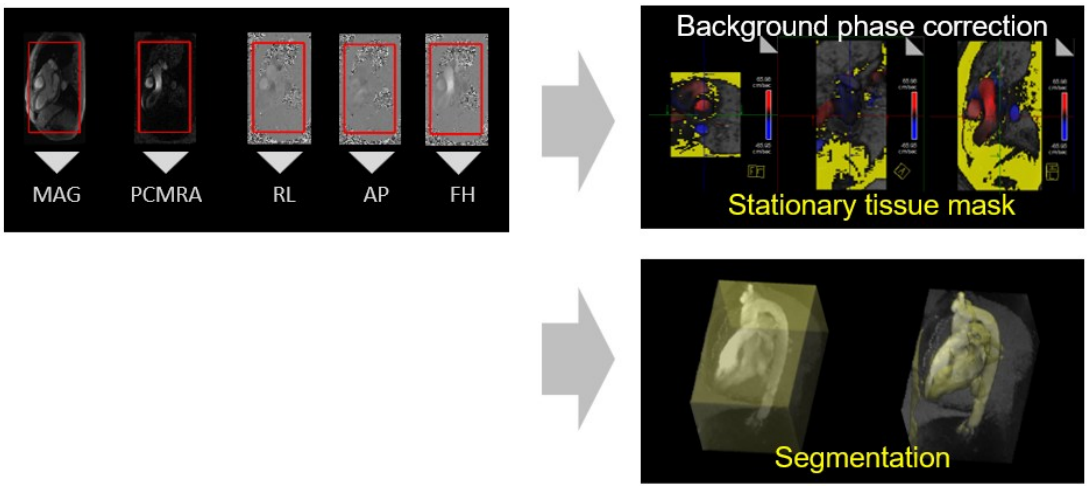

Figure 6: 4D flow pre-processing workflow.
MAG = magnitude image series, PCMRA = phase contrast magnetic resonance angiographic image series, RL = right-left velocity encoded image series, AP = anterior-posterior velocity encoded image series, FH = feet-head velocity encoded image series.

Transmitral peak velocities

To establish a workflow for evaluating transmitral diastolic peak velocities, three different evaluation pathways were examined using multiplanar reconstructed images in left ventricular two-chamber, four-chamber, and short-axis orientations (**Figure 7**).

- *4D flow SA method*: An evaluation plane was reconstructed parallel to the mitral valve at the level of the valve tips during early diastole, similar to conventional 2D flow assessment. Early- and late-diastolic peak velocities were determined by manually segmenting the mitral valve opening across all diastolic phases to obtain 3D peak velocities.
- *4D flow 4-chamber method*: Early- and late-diastolic peak velocities were assessed as 3D peak velocities from a region of interest between the mitral leaflet tips in a

multiplanar reconstructed 4-chamber view similar to echocardiographic assessment.

- *4D flow max-velocity method*: Voxels with the highest early- and late-diastolic velocities within the 3D velocity field of the transmitral inflow region were identified between the mitral valve ring and tips from a velocity magnitude overlay reconstruction.

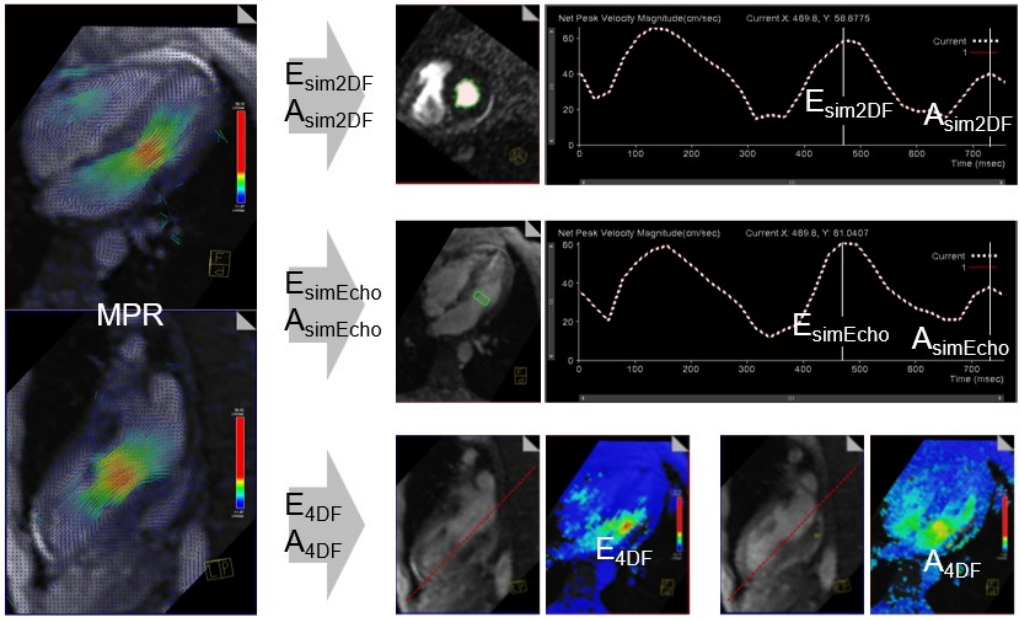

Figure 7: Approaches for assessing diastolic transmitral peak velocities from 4D flow velocity data. Reproduced with modifications from Reiter C et al. Eur J Radiology 2023 (3).
E_{sim2DF} and A_{sim2DF} refer to early- and late-diastolic peak velocities from a static short-axis image at the mitral valve tips; $E_{simEcho}$ and $A_{simEcho}$ are early- and late-diastolic peak velocities from a static 4-chamber view; E_{4DF} and A_{4DF} indicate maximal early- and late-diastolic velocities in the transmitral inflow volume.

Myocardial peak velocity

Peak early-diastolic myocardial velocities in the septal and lateral myocardial regions were assessed from evaluation planes which were aligned perpendicular to posterior septal and anterior lateral myocardium (**Figure 8**).

Average e' was calculated as the average of septal and lateral e', respectively. These velocities were derived from the average through-plane velocity-time curves.

Voxels representing blood or pericardial tissue were carefully excluded to ensure accuracy in the myocardial measurements.

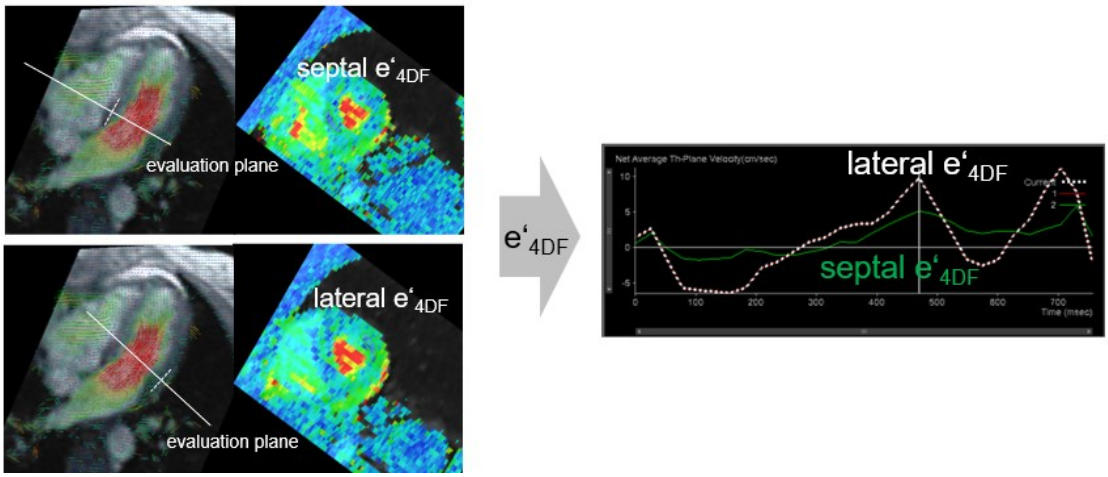

Figure 8: Assessment of early-diastolic myocardial tissue velocities from 4D flow data. Reproduced with modifications from Reiter C et al. Eur J Radiology 2023 (3).
e'$_{4DF}$ = early-diastolic myocardial tissue velocity.

Pulmonary artery net flow volume

To assess the net flow volume of the pulmonary artery, an evaluation plane was multiplanar reconstructed above the pulmonary valve aligned perpendicular to the course of the vessel (**Figure 9**). The cross-sectional area of the pulmonary artery was automatically segmented and manually adjusted as needed.

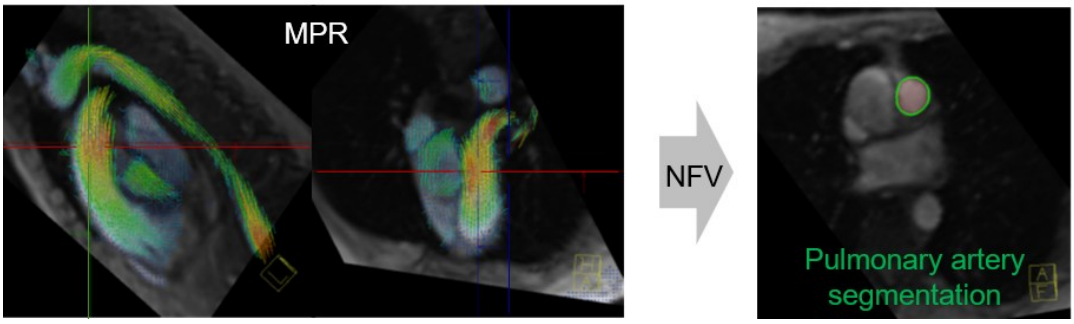

Figure 9: Assessment of pulmonary artery net flow volume from 4D flow velocity data. Reproduced with modifications from Reiter C et al. Eur Radiology 2023 (3).
MPR = multiplanar reconstruction, NFV = net flow volume.

Elevated mean pulmonary arterial pressure

Vortical blood flow along the main pulmonary artery, was assessed visually from multiplanar reconstructed 3D velocity vector fields in right ventricular outflow tract orientation (**Figure 10**). the duration of vortical flow (t_{vortex}) was quantified as previously described (74).

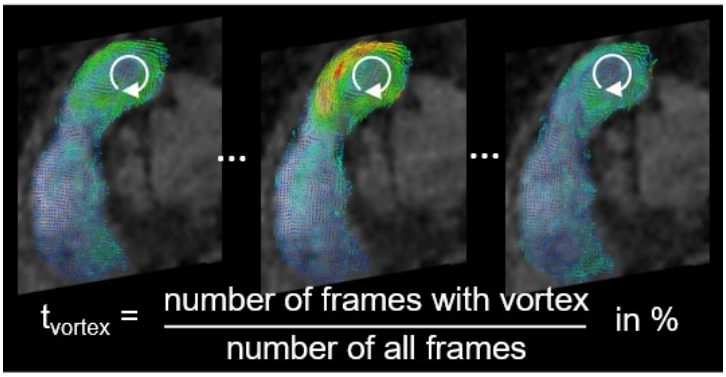

Figure 10: Evaluation of vortical blood flow along the main pulmonary artery from observed vortical flow patterns. Reproduced with modifications from Reiter C et al. Eur Radiol 2025 (4).
t_{vortex} = relative duration of vortical flow in the pulmonary artery during the cardiac interval.

Left atrial peak inflow and outflow velocities

The left atrial peak early-diastolic (v_E) outflow velocity was measured from the voxel with the highest mitral valve velocity at the level of the annulus during early diastole. Left atrial peak systolic (v_S) and early-diastolic (v_D) inflow velocities were measured in cross-sections of the left and right lower and upper pulmonary veins at the level of the junctions with the atrium (**Figure 11**).

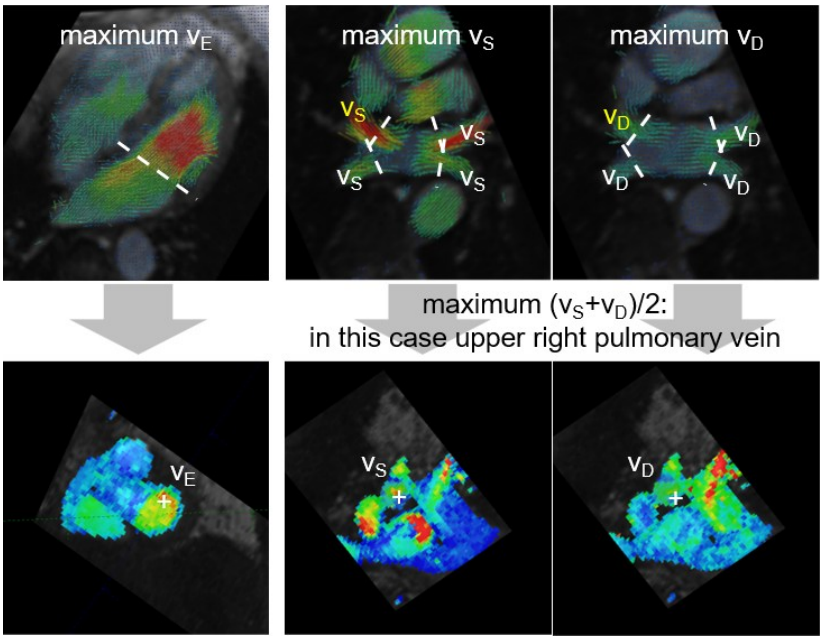

Figure 11: Assessment of early-diastolic peak outflow and peak inflow velocities of the left atrium from 4D flow data during systole and early diastole. Reproduced with modifications from Reiter C et al. Eur Radiol 2023 (5).
v_E = early-diastolic peak left atrial outflow velocity; v_S = systolic peak left atrial inflow velocity; v_D = early-diastolic peak left atrial inflow velocity.

Left atrial acceleration factor

In the present study the left atrial acceleration factor α was calculated from the formula $\alpha = v_E/[(v_S + v_D)/2]$ using the maximum value of $v_S + v_D$ across all pulmonary veins. Moreover, the left atrial acceleration factor α_{lower} was determined the maximum $v_S + v_D$ values among the lower pulmonary veins, as per the original definition of this metrics in Reiter et al. (75).

2.5 Statistical analysis

Statistical analysis was performed using SPSS® (SPSS Software v25-v28, Chicago, IL, USA) and NCSS (NCSS 11 Statistical Software, Kaysville, Utah, USA). Statistical significance was defined as $p < 0.05$ for all analyses. Non-overlapping 95% confidence intervals were interpreted as differing.

2.5.1 Descriptive statistics and normality assessment

Continuous variables are presented as mean ± standard deviation for normally distributed data and as median with interquartile range for non-normally distributed data. Normality of distributions was assessed using the Shapiro-Wilk test and visual inspection of QQ-plots.

2.5.2 Agreement Analysis and correlation

Differences of non-paired samples were compared by t-test or Mann-Whitney U test, differences of paired samples by paired t-Test or Wilcoxon signed-rank test, as appropriate. Significance of biases was investigated by one sample t-test, percentages were compared with Pearson's Chi-Square test. Means of different groups of diastolic (dys)function were compared by analysis of variance with Dunett-T3 as post hoc test or Kruskal-Wallis test. Relationships of continuous parameters were investigated by Pearson correlation (r), linear regression, and Bland-Altman analysis. Inter- and intra-observer variability and repeatability was studied by two-way mixed effect model, single measure, absolute agreement intra-class correlation coefficients (ICC) and within-subject standard deviation in a variance component analysis (synonymously standard error of measurements).

A segmented linear model was fitted to the relationship between pTR and t_{vortex}, with t_{vortex} = 0% up to a treshhold of pTR and increasing linearly afterwards. Diagnostic agreement and grading of left ventricular diastolic dysfunction between 4D flow and echocardiography were studied by contingency table analysis; agreement was assessed by Cohen's weighted kappa and over- or underestimated was tested by McNemar's test.

Correlations were classified as very high for r = 0.9–1.0, high for r = 0.7–0.9, moderate for r = 0.5–0.7, low for r = 0.3–0.5, and negligible for r = 0.0-0.3 (76). Interobserver reliability were classified as excellent for ICC = 0.9–1.0, good for ICC = 0.75–0.9, moderate for ICC = 0.5–0.75, and poor for ICC =0.0–0.5 (77).

2.5.3 Threshold Determination and Validation

Receiver operating characteristic curve analysis was employed to determine optimal threshold values for four-dimensional flow-derived parameters in detecting diastolic dysfunction grades. 95% confidence intervals were derived for area under the receiver operating characteristics curve. Youden's index was used to suggest cut-off values. Sensitivity, specificity, positive predictive value, and negative predictive value were calculated for thresholds.

3. Results

The results of this doctoral thesis have been published in (1–5).

3.1 Cohort demography and clinical characterization

3.1.1 Study population overview

Data from 94 participants were analyzed. The average age of the cohort was 62 ± 12 years, of whom 53% (n=50) were females. The baseline demographic profile, echocardiographic findings, and laboratory parameters are summarized in **Table 1**.

3.1.2 Diastolic function distribution

Echocardiographic evaluation revealed normal diastolic function in 54% (n=51) of participants. Diastolic dysfunction was distributed as follows: Grade I diastolic dysfunction in 14% (n=13), grade II diastolic dysfunction in 14% (n=13), and grade III diastolic dysfunction in 9% (n=8). Indeterminate diastolic function classification was observed in 10% (n=9) of the cohort. None of the participants showed significant mitral regurgitation, aortic regurgitation or shunts. Ten participants exhibited reduced left ventricular ejection fraction (<50%). The temporal interval between echocardiographic and 4D flow cardiovascular magnetic resonance assessments was 3 ± 7 days.

3.1.3 Baseline clinical parameter

Participants with advanced diastolic dysfunction (Grades II-III) demonstrated elevated N-terminal pro-brain natriuretic peptide levels compared to those with normal function or mild dysfunction ($p < 0.001$).

Table 1: Study population characterization. Reproduced with modifications from *Reiter C* et al. (4,5).

Characteristics	Total (n=94)	Grade0 (n=51)	Ind (n=9)	Grade I (n=13)	Grade II (n=13)	Grade III (n=8)	P value
Demography							
Age (years)	62±12	61±9	59±8	58±17	68±15	65±14	0.212
Sex female n (%)	50 (52)	29 (57)	7 (78)	5 (39)	6 (46)	3 (38)	0.326
Height (cm)	170±10	171±9	166±8	172±11	167±10	171±10	0.249
Weight (kg)	77±15	75±13	76±21	80±19	77±13	86±10	0.106
BMI (kg/m^2)	26±4	25±3	28±6	27±4	28±5	30±4	0.082
BSA (m^2)	1.90±0.21	1.88±0.20	1.86±0.27	1.95±0.28	1.88±0.18	2.01±0.15	0.237
sBP (mmHg)	136±19	134±17	144±15	138±20	140±26	136±20	0.578
dBP (mmHg)	76±11	75±10	77±7	73±9	77±15	86±12	0.790
HR (min^{-1})	67±11	67±10	66±9	69±10	61±11	75±17	0.079
Laboratory parameters							
Hb (g/L)	14±2	14±1	14±1	15±2	14±1	13±3	0.065
eGFR (ml/min)	76±18	80±10^{3}	82±13^{3}	78±25^{3}	74±22	48±16^{i,1,2}	<0.001
NTproBNP (pg/ml)*	1298± 5986	76±124^{2,3}	84±53^{2,3}	561±647^{3}	689± 770^{0,i,3}	15233± 18651^{0,i,1,2}	<0.001
Triglycerides (mg/dL)	113±60	105±49	97±63	141±49	132±96	114±76	0.075
HDL (mg/dL)	62±20	65±21	72±23	50±16	57±12	48±13	0.029
LDL (mg/dL)	135±43	154±31^{1,2}	136±45	99±34^{0}	92±40^{0}	121±44	<0.001
Echocardiographic parameters							
EF_{Echo} (%)	59±10	61±6	61±5	60±11	55±14	52±19	.068
E_{Echo} (cm/s)	82±21	78±16^{3}	79±15^{3}	74±13^{3}	92±32	109±18^{0,i,1}	<0.001
E/A_{Echo}	1.23±0.54	1.10±0.29^{3}	1.14±0.27^{3}	1.03±0.32^{3}	1.16±0.35^{3}	2.66± 0.53^{0,i,1,2}	<0.001
e'_{Echo} (cm/s)	8.5±7.1	10.6±9.0^{2,3}	7.9±1.4^{2,3}	6.6±2.6	5.4±1.3^{0,i}	4.1±1.8^{0,i}	0.023
E/e'_{Echo}	12.7±8.8	8.3±2.2^{i,2,3}	10.0±1.1^{0,2,3}	13.2±6.2	19.6±5.7^{0,i}	31.8±14.3^{0,1}	<0.001
$LAVI_{Echo}$ (ml/m^2)	34±13	28±6^{i,2}	36±4^{0}	32±11^{2}	51±18^{0,1}	46±17	<0.001
TR (cm/s)	2.3±0.5	2.2±0.4^{2}	2.3±0.3	2.1±0.4	2.7±0.4^{0}	2.9±0.6	<0.001
sPAP (mmHg)	27.3±8.1	24.2±4.2^{2}	25.6±5.2	24.0±7.3^{2}	35.3±8.4^{0,1}	39.4±11.8	<0.001

Categorical data presented as frequencies with percentages in parentheses; continuous data presented as means with standard deviations in parentheses. P value refers to analysis of variance. Superscripts 0, i, 1, 2, 3 indicate significant differences from grade 0, indeterminate, I, II, III, respectively. Ind = indeterminate, BMI = body mass index (calculated as BMI = weight/height^2, weight measured in kilograms, height measured in meters), BSA = body surface area (calculated as BSA = weight$^{0.425}$ × height$^{0.725}$ × 0.007184; weight measured in kilograms, height measured in meters), sBP = systolic blood pressure, dBP = diastolic blood pressure, HR = heart rate, eGFR = estimated glomerular filtration rate, NTproBNP = N-terminal prohormone of brain natriuretic peptide, HDL = high-density lipoprotein, LDL = low-density lipoprotein, EF_{Echo} = ejection fraction, E_{Echo} = early-diastolic transmitral peak velocity, E/A_{Echo} = early-to-late-diastolic transmitral peak velocity ratio, e_{Echo}' = early-diastolic mitral valve tissue peak velocity, $LAVI_{Echo}$ = left atrial volume index, TR = peak tricuspid regurgitation velocity, sPAP = systolic pulmonary arterial pressure. *Values of NTproBNP were log-transformed for comparison.

Estimated glomerular filtration rate showed progressive decline with increasing diastolic dysfunction severity, reaching statistical significance in Grade III dysfunction ($p < 0.001$). Systolic pulmonary arterial pressure measurements increased progressively across diastolic dysfunction grades, with the highest values observed in Grade III dysfunction (39.4 ± 11.8 mmHg, $p < 0.001$).

3.2 Cardiac magnetic resonance volumetric function measurements

3.2.1 Effect of respiration on cardiac function parameters

Analysis of respiratory effects on cardiac function was performed in 56 participants without cardiovascular disease symptoms (mean age 58 ± 14 years), following the exclusion of four participants due to inadequate image quality (**MS1**). The cohort included 33 women (mean age 56 ± 16 years) and 23 men (mean age 62 ± 10 years). The average cardiac interval remained stable between respiratory conditions with 922 ± 126 ms during breath-holding versus 937 ± 120 ms during breathing ($p = 0.064$). Respiratory parameters during free breathing included mean respiratory depth of 13 ± 4 millimeters and respiratory rate of 11 ± 2 breaths per minute, with no significant differences observed between genders.

The left ventricular volumetric function parameters showed strong correlations between inspiratory breath-holding and free breathing conditions. During free breathing, both end-systolic and end-diastolic volumes were higher, while ejection fraction and peak ejection rate decreased. Among the diastolic parameters, peak filling rate during early diastole showed only moderate correlation between the respiratory conditions and was the sole parameter exhibiting higher values during free breathing compared to breath-holding. Comparisons of left ventricular volumetric function parameters are presented in **Table 2** and **Figure 12**.

Table 2: Effect of respiration on left ventricular and left atrial volumetric function. Reproduced with modifications from Reiter C et al. Eur J Radiol 2021 (1).

Parameter	Breath-hold	Breathing	Bias	SD	P value	r
Left ventricle						
EDV (ml)	132±29	139±30	-7	15	0.002	0.87
ESV (ml)	48±15	56±18	-7	8	<0.001	0.91
SV (ml)	84±16	83±15	1	11	0.631	0.77
EF (%)	64±6	61±6	3	4	<0.001	0.79
PER (ml/s)	-437±90	-416±85	22	51	0.002	0.83
PFR_E (ml/s)	395±127	429±127	-34	110	0.025	0.63
PFR_A (ml/s)	279±83	287±96	-8	61	0.313	0.78
PFR_E/PFR_A	1.57±0.68	1.69±0.72	-0.11	0.49	0.095	0.76
Left atrium						
LA_{max} (ml)	89±21	95±20	-6	13	0.001	0.79
LA_{bc} (ml)	67±17	68±17	-1	10	0.422	0.81
LA_{min} (ml)	49±13	48±13	0	8	0.841	0.82
EF_{total} (%)	46±6	50±6	-4	4	<0.001	0.72
EF_{active} (%)	27±6	29±6	-2	5	0.013	0.67
$EF_{passive}$ (%)	25±6	29±5	-4	4	<0.001	0.73

EDV = end-diastolic volume, ESV = end-systolic volume, SV = stroke volume, EF = ejection fraction, PER = systolic peak emptying rate, PFRE = early-diastolic peak filling rate, PFRA = late-diastolic peak filling rate, LA_{max} = maximal left atrial volume, LA_{bc} = left atrial volume before contraction, LA_{min} = minimal left atrial volume, EF_{total} = total left atrial ejection fraction, EF_{active} = active left atrial ejection fraction, $EF_{passive}$ = passive left atrial ejection fraction

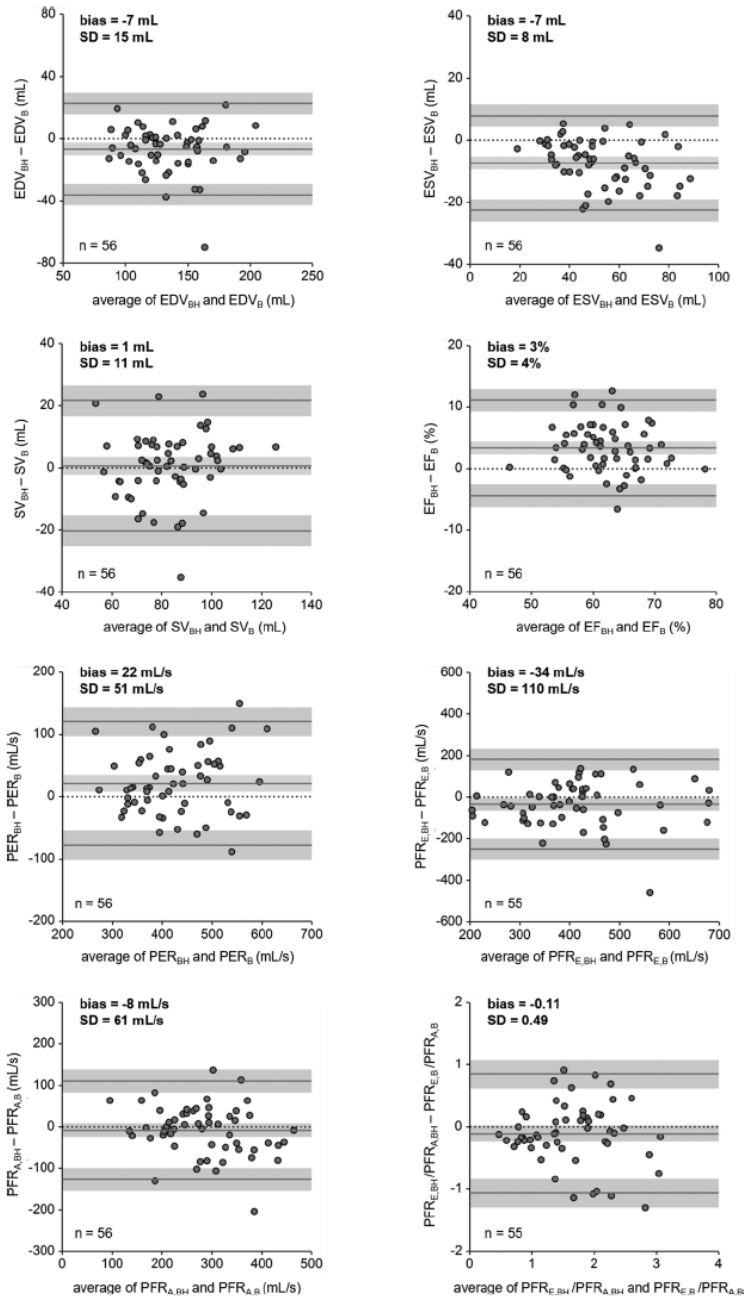

Figure 12: Bland-Altman plots comparing left ventricular function during breath-holding and breathing. Reproduced with modifications from Reiter C et al. Eur J Radiol 2021 (1).

Parameter are evaluated from stacks of short-axis images. BH = breath-holding, B = breathing, n = number of participants, SD = standard deviation of differences, EDV = end-diastolic volume, ESV = end-systolic volume, SV = stroke volume, EF = ejection fraction, PER = systolic peak emptying rate, PFR_E = early-diastolic peak filling rate, PFR_A = late-diastolic peak filling rate. Grey bars = 95% confidence intervals of bias and 95% limits of agreement,

Breath-hold-to-breathing differences in left ventricular volumetric function parameters did not correlate significantly with their average values. Gender related differences were observed in breath-hold-to-breathing biases: 14 ml in males vs. 1 ml in females for EDV ($p = 0.004$), 11 ml in males vs. 5 ml in females for ESV ($p = 0.005$), 3 ml in males vs. -3 ml in females for SV ($p = 0.027$), and -86 ml/s in males vs. 3 ml/s in females for PFR_E ($p = 0.002$).

Both LAV_{max} and all left atrial ejection fractions were lower during breath-holding. Strong correlations were observed between left atrial volumes acquired during free breathing and breath-holding. A detailed comparison of volumetric function parameters of the left atrium during free breathing and breath-holding is provided in **Table 2**, with corresponding Bland-Altman plots displayed in **Figure 13**.

Breath-hold-to-breathing biases for LAV_{max} (11 ml in men vs. 2 ml in women, $p = 0.033$), LAV_{bc} (5 ml in men vs. -1 ml in women, $p = 0.038$), and LAV_{min} (2 ml in men vs. -2 ml in women, $p = 0.042$) were greater in men than in women. However, same as with left ventricular parameters the breath-hold-to-breathing differences did not correlate significantly with the average values of the respective left atrial parameters.

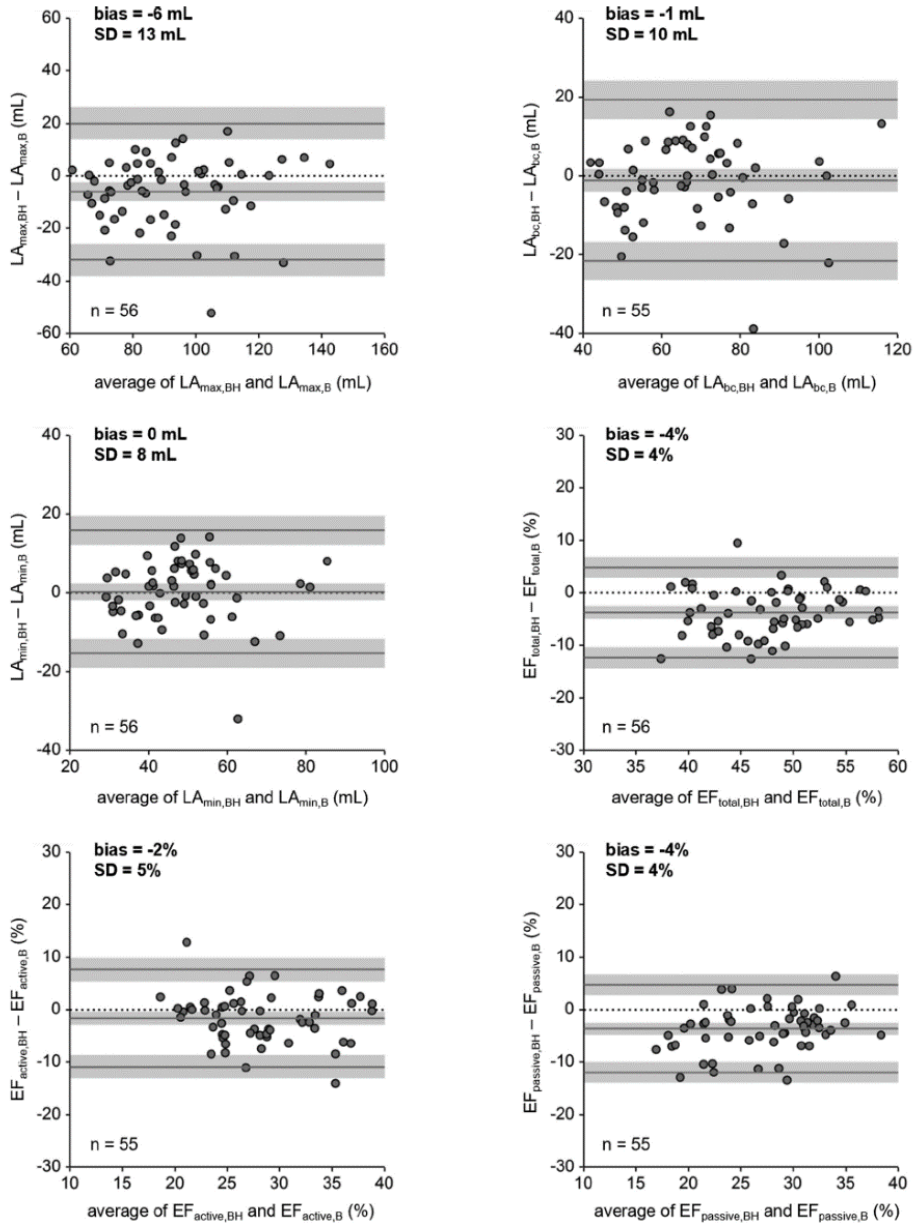

Figure 13: Bland-Altman plots comparing left atrial (LA) volumetric function parameters acquired during breathholding and free breathing. Reproduced with modifications from Reiter C et al. Eur J Radiol 2021 (1).

BH = breath-holding. B = breathing. n = number of participants, SD = standard deviation of differences. LA_{max} = Maximal left atrial volume. LA_{bc} = pre-contraction left atrial volume. LA_{min} = minimal left atrial volume, EF = ejection fraction. Grey bars = 95% confidence intervals of bias and 95% limits of agreement.

3.2.2 Impact of image orientation

Left ventricular volumetric function parameters derived from stacks of four-chamber cine series correlated strongly and demonstrated similar changes during breath-holding and breathing with the ones derived from stacks of short-axis cine series. The comparison of left ventricular volumetric function parameters derived from four-chamber cine stack images during breath-holding and breathing is provided in **Table 3**, together with the correlations between parameters derived from short-axis and four-chamber stacks during breath-holding and breathing, respectively.

Table 3: Impact of breath-holding on volumetric function evaluated from 4-chamber cine series. Reproduced with modifications from Reiter C et al. Eur J Radiol 2021 (1).

Parameter	Breath-hold	Breathing	Bias	SD	P value	r	$r_{SA,BH}$	$r_{SA,B}$
EDV (ml)	145 ± 32	150 ± 31	-5	18	0.044	0.83	0.93	0.94
ESV (ml)	62 ± 17	66 ± 19	-4	10	0.003	0.85	0.91	0.90
SV (ml)	83 ± 18	84 ± 15	-1	11	0.532	0.78	0.87	0.82
EF (%)	58 ± 5	56 ± 5	1	3	0.012	0.78	0.78	0.62
PER (ml/s)	426 ± 96	419 ± 80	7	46	0.234	0.88	0.84	0.88
PFR_E (ml/s)	320 ± 98	359 ± 86	-39	63	<0.001	0.78	0.86	0.82
PFR_A (ml/s)	287 ± 81	311 ± 85	-24	61	0.004	0.73	0.64	0.80
PFR_E/PFR_A	1.21 ± 0.52	1.25 ± 0.49	-0.04	0.43	0.455	0.64	0.73	0.81

Breath-hold and breathing values are given as means ± standard deviations. p refers to comparison between breath-hold and breathing mean values. SD = standard deviation of differences, $r_{SA,BH}$ = Pearson's correlation coefficient between parameters derived from short-axis and 4-chamber stacks during breath-holding, $r_{SA,B}$ = Pearson's correlation coefficient between parameters derived from short-axis and 4-chamber stacks during breathing, r = Pearson's correlation coefficient between parameters derived from 4-chamber stacks during breath-holding and breathing. EDV = end diastolic volume. ESV = end systolic volume. SV = stroke volume. EF = ejection fraction. PER = peak ejection rate. PFR_E = early-diastolic peak filling rate. PFR_A = late-diastolic peak filling rate.

Of note, absolute differences to left ventricular volumetric parameters obtained from stacks of short-axis series are comparable with previously published values (78).

3.2.3 Repeatability volumetric function measurements

The results of repeatability measurements for left ventricular and left atrial volumetric function parameters assessed during both breath-holding and breathing are summarized in **Table 4**. While short-axis-derived parameters showed better repeatability during breath-hold measurements, the repeatability of parameters from four-chamber series was comparable between breath-holding and breathing. Notably, within-subject standard deviations for repeatability measurements in both conditions were smaller than the standard deviations of differences observed between breath-hold and breathing measurements.

Table 4: Repeatability of left ventricular and left atrial volumetric function for different respiratory conditions. Reproduced with modifications from Reiter C et al. Eur J Radiol 2021 (1)

Parameter	Breath-hold		Breathing		SD
	ICC	SD_w	ICC	SD_w	
Short-axis orientation					
EDV (ml)	1.00	1	1.00	1	15
ESV (ml)	1.00	1	1.00	2	8
SV (ml)	1.00	2	0.99	4	11
EF (%)	0.99	1	0.99	2	4
PER (ml/s)	0.94	39	0.99	24	51
PFR_E (ml/s)	0.99	17	0.99	20	110
PFR_A (ml/s)	0.95	19	0.97	26	61
PFR_E/PFR_A	0.81	0.23	0.90	0.36	0.49
LA_{max} (ml)	0.99	5	0.98	6	13
LA_{bc} (ml)	0.98	5	0.98	5	11
LA_{min} (ml)	0.98	4	0.98	4	8
EF_{total} (%)	0.87	2	0.90	2	6
EF_{active} (%)	0.68	3	0.95	2	5
$EF_{passive}$ (%)	0.81	3	0.81	3	7
4-chamber orientation					
EDV (ml)	1.00	3	1.00	4	18
ESV (ml)	1.00	2	0.99	4	10
SV (ml)	0.98	4	0.99	3	11
EF (%)	0.97	2	0.93	3	3
PER (ml/s)	0.98	20	0.91	42	46
PFR_E (ml/s)	0.77	56	0.94	29	63
PFR_A (ml/s)	0.91	36	0.68	67	61
PFR_E/PFR_A	0.85	0.17	0.85	0.38	0.43

Left ventricular (LV) volumetric function data derived from stacks of short-axis cine series and left atrial (LA) volumetric function data derived from stacks of 4-chamber cine series for measurements taken under breath-hold and breathing. SD_w = within subject standard deviation, ICC = intra-class correlation, SD = breath-hold-to-breathing standard deviation of differences (for comparative reasons). EDV = end-diastolic volume, ESV = end-systolic volume, SV = stroke volume, EF = ejection fraction, PER = peak ejection rate, PFR_E = early-diastolic peak filling rate, PFR_A = late-diastolic peak filling rate, LA_{max} = maximal left atrial volume, LA_{bc} = left atrial before contraction volume, LA_{min} = minimal LA volume, EF_{total} = total left atrial ejection fraction, EF_{acive} = active left atrial ejection fraction, $EF_{passive}$ = passive left atrial ejection fraction.

3.2.4 Volumetric function evaluation from 4D flow magnitude data

This analysis included the 60 participants (35 females) without signs or symptoms of heart failure or cardiac diseases **(MS2**). Left ventricular and left atrial volumetric parameters measured from 4D flow and cine bSSFP series exhibited high to very high correlations. Detailed results for parameters are provided in **Table 5**, scatter plots (**Figure 14**) and Bland-Altman plots (**Figure 15**).

Table 5: Left ventricular and atrial volumetric parameters derived from cine 4D flow and cine bSSFP images. Reproduced with modifications from Reiter C et al. Eur Radiol 2023 (2).

Parameter	4D flow-cine	bSSFP-cine	r	Bias	P value
EDV (ml)	137.9±28.6	140.8±28.8	0.98	-2.9±5.8	<0.001
ESV (ml)	46.2±12.7	48.6±13.2	0.96	-2.3±3.8	<0.001
sSV (ml)	91.7±18.4	92.3±18.1	0.95	-0.6±5.8	0.433
LVM (g)	157.8±37.6	118.8±30.6	0.96	39.0±11.4	<0.001
EF (%)	66.7±4.6	65.8±4.4	0.84	0.9±2.6	0.005
LAV_{max} (ml)	78.6±17.5	77.8±17.9	0.96	0.8±4.4	0.152
LAV_{min} (ml)	36.3±11.1	35.6±12.0	0.97	0.7±3.4	0.143
LATEF (%)	54.2±7.1	54.7±8.1	0.83	-0.5±4.6	0.380

r is the Pearson-correlation coefficient between 4D flow-cine and bSSFP-cine parameters. EDV = end-diastolic volume, ESV = end-systolic volume, SV = stroke volume, LVM = left ventricular mass, EF = ejection fraction, LAV_{max} = maximal left atrial volume, LAV_{min} = minimal left atrial volume, LATEF = total left atrial ejection fraction

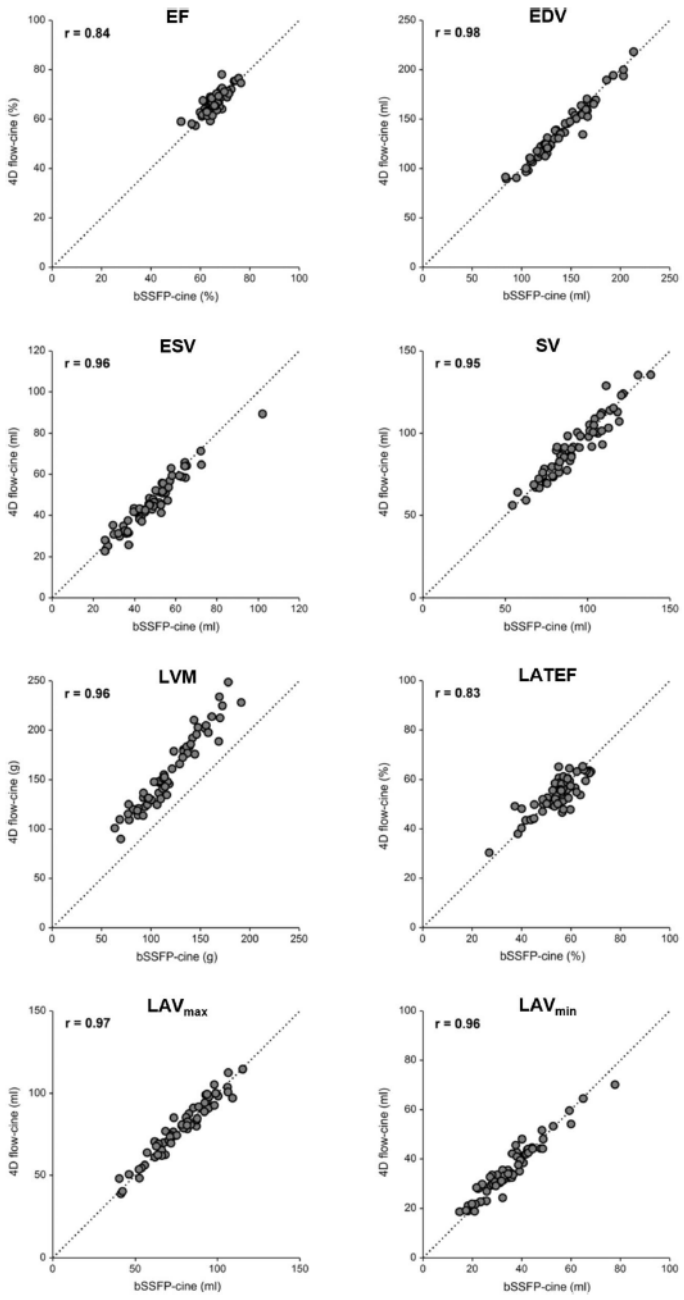

Figure 14: Scatter-plots of left ventricular and left atrial volumetric function parameters from cine 4D flow and cine bSSFP images. Reproduced with modifications from Reiter C et al. Eur Radiol 2023 (2).
The dotted lines refer to the line of identity. r = correlation coefficients. EDV = end-diastolic volume, ESV = end-systolic volume, SV = stroke volume, LVM = left ventricular mass, EF, ejection fraction, LAV_{max} = maximal left atrial volume, LAV_{min} = minimal left atrial volume, LATEF = total left atrial ejection fraction.

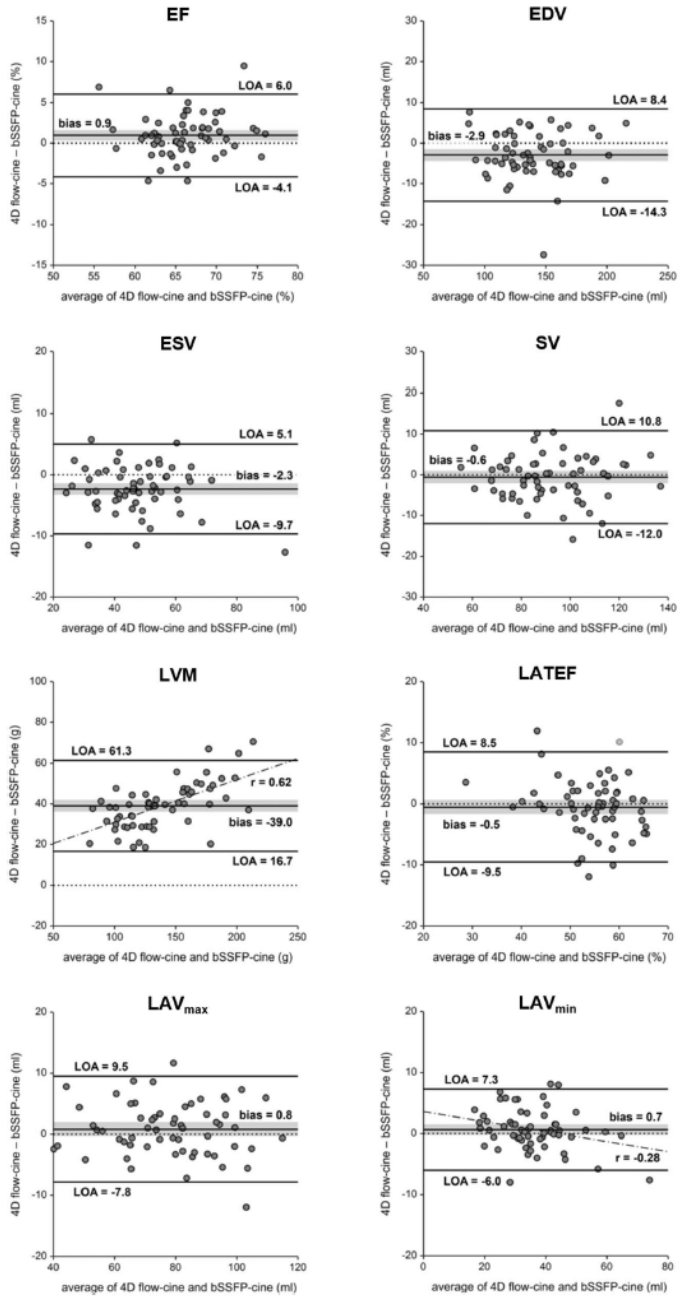

Figure 15: Bland-Altman plots comparing left ventricular and left atrial volumetric function parameters from cine 4D flow and cine bSSFP images. Reproduced with modifications from Reiter C et al. Eur Radiol 2023 (2).

LOA, limits of agreement, EDV = end-diastolic volume, ESV = end-systolic volume, SV = stroke volume, LVM = left ventricular mass, EF, ejection fraction, LAV_{max} = maximal left atrial volume, LAV_{min} = minimal left atrial volume, LATEF = total left atrial ejection fraction. Grey bar = 95% confidence intervals of bias, dotted line = regression line for significant correlations between differences and averages of a parameter, r = correlation coefficient.

Significant biases were observed across all left ventricular volumetric function parameters except for stroke volume; biases were generally small (less than 5% of each parameter's mean value) with the exception of LVM. Differences in LVM between 4D flow and cine bSSFP measurements showed a moderate correlation (r = 0.61) with LVM average values. Additionally, LVM was the only parameter with a significant gender-related bias difference (46.2 ± 11.5 g for males vs. 33.9 ± 8.3 g for females, p < 0.001).

Observer variability

Inter- and intraobserver agreement of left ventricular and left atrial volumetric function parameters were excellent (**Table 6**).

Table 6: Inter- and intraobserver agreement of left ventricular and left atrial volumetric function evaluated from cine 4D flow and cine bSSFP series. Reproduced with modifications from Reiter C et al. Eur Radiol 2023 (2)

Parameter	Inter-observer variability (n = 20)		Intra-observer variability (n = 20)	
	4D flow-cine	bSSFP-cine	4D flow-cine	bSSFP-cine
EDV (ml)	0.986 [0.966–0.994]	0.995 [0.988–0.998]	0.971 [0.930–0.988]	0.994 [0.978–0.998]
ESV (ml)	0.980 [0.950–0.992]	0.983 [0.957–0.993]	0.973 [0.926–0.990]	0.994 [0.985–0.998]
SV (ml)	0.964 [0.913–0.986]	0.987 [0.969–0.995]	0.959 [0.900–0.984]	0.983 [0.946–0.994]
LVM (g)	0.994 [0.984–0.997]	0.995 [0.989–0.998]	0.996 [0.989–0.998]	0.991 [0.977–0.996]
EF (%)	0.873 [0.708–0.948]	0.869 [0.704–0.946]	0.911 [0.792–0.963]	0.889 [0.738–0.955]
LAV_{max} (ml)	0.995 [0.985–0.998]	0.983 [0.959–0.993]	0.997 [0.990–0.999]	0.995 [0.989–0.998]
LAV_{min} (ml)	0.995 [0.988–0.998]	0.992 [0.980–0.997]	0.997 [0.992–0.999]	0.996 [0.988–0.999]
LATEF (%)	0.974 [0.936–0.989]	0.900 [0.763–0.959]	0.974 [0.936–0.989]	0.953 [0.882–0.981]

Intraclass correlation coefficients (ICCs) and their 95% confidence intervals in brackets. EDV = end-diastolic volume, ESV = end-systolic volume, SV = stroke volume, LVM = left ventricular mass, EF = ejection fraction, LAV_{max} = maximal left atrial volume, LAV_{min} = minimal left atrial volume, LATEF = total left atrial ejection fraction

No difference for cine 4D flow and cine bSSFP derived parameters was observed.

Validation of stroke volumes

Net forward volumes measured using 4D flow imaging demonstrated a very strong correlation with volumetric stroke volumes obtained from both cine 4D flow and cine bSSFP imaging (r = 0.91 for both comparisons). There was no significant bias between net forward volumes and volumetric stroke volumes (p = 0.218 for cine 4D flow imaging and p = 0.058 for cine bSSFP imaging-derived stroke volumes). Scatter as well as Bland-Altman plots illustrating these comparisons are provided in **Figure 16**.

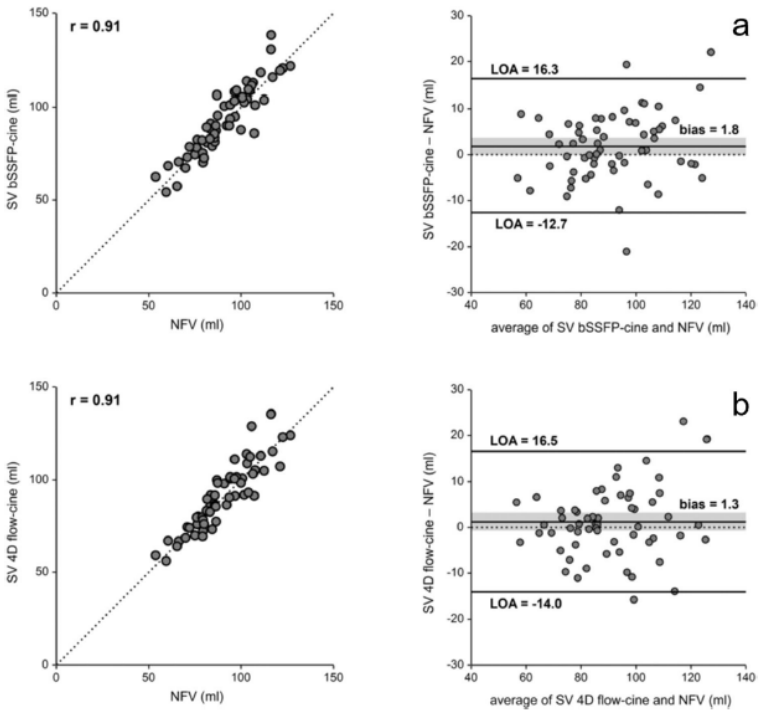

Figure 16: Scatter plots and Bland-Altman plots comparing left ventricular stroke volume evaluated from cine bSSFP series and cine 4D flow series with the pulmonary artery net flow volume. Reproduced with modifications from Reiter C et al. Eur Radiol 2024 (2).
SV = left ventricular stroke volume, NFV = pulmonary artery net flow volume, r = correlation coefficient, LOA = limits of agreement. Dotted line in scatter plots = line of identity, grey bar = 95% confidence intervals of bias.

3.3 2D flow measurements

3.3.1 Impact of breath-holding on 2D flow measurements

E and A wave were fused in two participants during breath-holding and breathing such that late-diastolic transmitral velocities could not be evaluated. In another two participants the lateral myocardium was corrupted by partial volume of the left atrium therefore evaluation of e' was not possible.

During breathing, all early-diastolic velocities and flows (E, F_E, e') were significantly higher, while only the late-diastolic peak velocity A showed a marked increase. As a result, there were no significant changes in the velocity ratios E/A and E/e' between breath-holding and breathing. Diastolic function parameters derived from 2D flow imaging under different respiratory conditions are presented in **Table 7**, Bland-Altman plots shown in **Figure 17**.

Table 7: Diastolic 2D flow-derived transmitral and myocardial tissue metrics during breath-holding and free breathing. Reproduced with modifications from Reiter C et al. Eur J Radiol 2021 (1).

Parameter	Breath-hold	Breathing	Bias	SD	P value	r
E_{2DF} (cm/s)	60±14	66±12	-6	13	<0.001	0.53
A_{2DF} (cm/s)	51±11	54±13	-3	9	0.021	0.72
F_E (ml/s)	313±110	340±81	-27	86	0.024	0.63
F_A (ml/s)	259±75	268±87	-8	64	0.335	0.70
E/A_{2DF}	1.23±0.41	1.31±0.43	-0.07	0.32	0.101	0.71
F_E/F_A	1.31±0.61	1.43±0.62	-0.12	0.34	0.011	0.84
e'_{2DF} (cm/s)	9.2±3.1	11.0±4.0	-1.8	2.9	<0.001	0.68
E/e'_{2DF}	7.1±2.0	6.7±2.1	-0.4	2.0	0.115	0.53

Breath-hold and breathing values are given as mean ± standard deviation. p refers to comparison between breath-holding and breathing mean values. SD = standard deviation of differences, r = Pearson's correlation coefficient between breath-hold and breathing parameters, E_{2DF} = early-diastolic transmitral peak velocity, A_{2DF} = late-diastolic transmitral peak velocity, F_E = early-diastolic transmitral peak flow, F_A = late-diastolic transmitral peak flow, e'_{2DF} = early-diastolic myocardial peak velocity.

The differences in E/e' between breath-holding and breathing were different for women and men (0.96 vs. -0.37, p = 0.010). Notably, cine bSSFP imaging-derived early- and late-diastolic peak filling rates, along with their ratio, showed moderate to strong correlations with the corresponding flows from 2D flow imaging during breathing (r = 0.70, 0.69, and 0.70 for E, A, and E/A, respectively) and breath-holding (r = 0.85, 0.53, and 0.78 for E, A, and E/A, respectively).

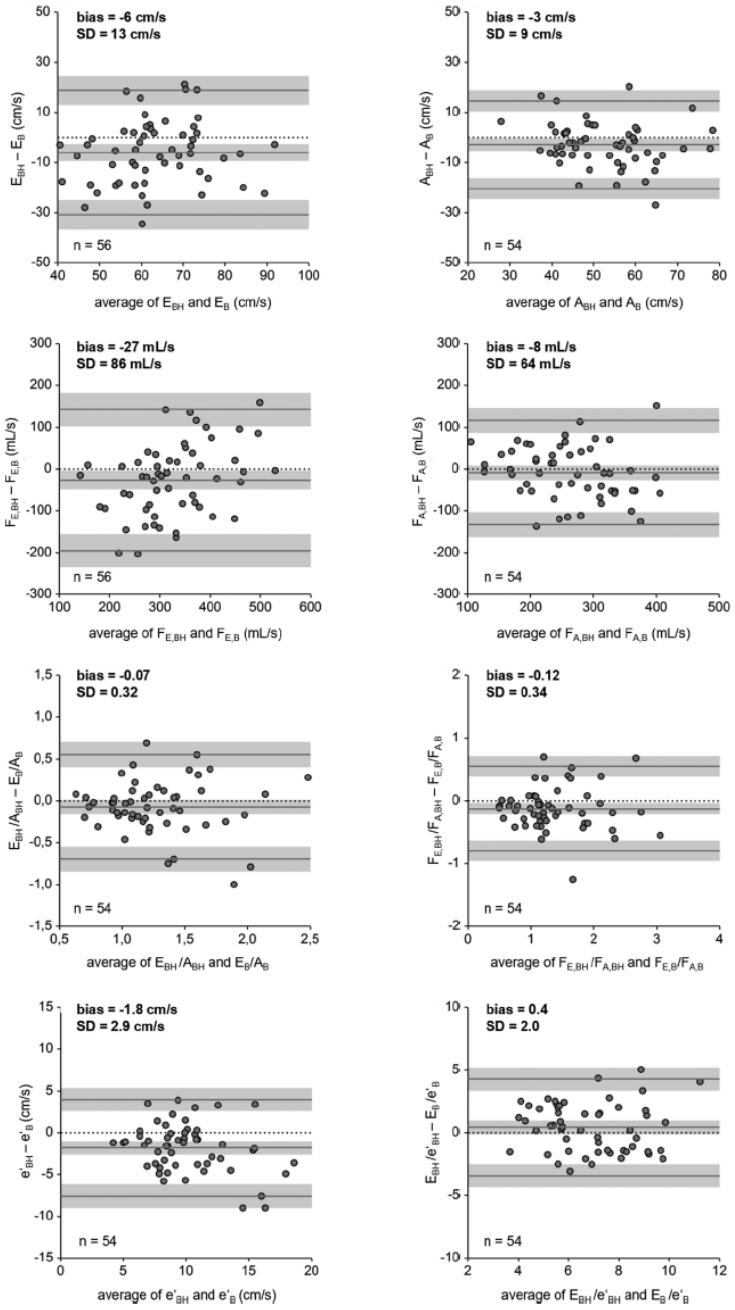

Figure 17: Bland-Altman plots comparing transmitral and myocardial tissue 2D flow measurements under breath-holding and breathing. Reproduced with modifications from Reiter C et al. Eur J Radiol 2021 (1).

BH = breath-hold, B = breathing, E = early-diastolic transmitral peak velocity, A = late-diastolic transmitral peak velocity, F_E = early-diastolic transmitral peak flow, F_A = late-diastolic transmitral peak flow, e' = early-diastolic myocardial peak velocity. n = number of participants, SD = standard deviation of differences. Grey bars = 95% confidence intervals of bias and 95% limits of agreement.

3.3.2 Comparison with echocardiography

Moderate correlations have been observed between echocardiographic and 2D flow transmitral diastolic peak velocities (**Table 8**). 2D flow, however, significantly underestimated both, echocardiographic E and A.

Table 8: Comparison of diastolic transmitral peak velocities evaluated from 2D flow and Doppler echocardiography. Reproduced with modifications from Reiter C et al. Eur J Radiol 2024 (3).

Parameter	Echo	2D-flow	Bias	r	P value
E (cm/s)	78 ± 16	66 ± 12	12 ± 12	0.70	<0.001
A (cm/s)	73 ± 15	53 ± 12	19 ± 10	0.74	<0.001
E/A	1.11 ± 0.29	1.31 ± 0.43	-0.20 ± 0.33	0.65	<0.001

Bias is the mean difference between echocardiographic and 2D-flow measurments. E = early-diastolic peak velocity, A = late-diastolic peak velocity, r = correlation with Echo; p = significance of the bias.

3.3.3 Impact of myocardial motion on diastolic peak filling rates

In 23 participants without symptoms of cardiopulmonary diseases, left ventricular PFR_E and PFR_A were obtained from left ventricular volume-time curves. These measurements were corrected with the myocardial wall velocity e'_{2D} as background phase to obtain corrected F_E and corrected F_A to compare corrected and uncorrected transmitral 2D flow metrics with volumetrically obtained peak filling rates.

The peak filling rates PFR_E = 396 ± 128 ml/s and PFR_A = 294 ± 90 ml/s demonstrated a significant bias when compared to the uncorrected 2D flow-derived peak flow measurements F_E = 316 ± 114 ml/s ($p<0.001$) and F_A = 249 ± 72 ml/s ($p=0.005$). However, no significant bias was found for the myocardial velocity-corrected values F_E = 383 ± 90 ml/s ($p = 0.196$) and F_A = 306 ± 94 ml/s ($p = 0.438$).

Correlations between volumetric peak filling rates and 2D flow-derived peak flows were similar, with correlation coefficients of r = 0.93 and 0.94 for PFR_E with uncorrected and corrected F_E, respectively, and r = 0.67 and 0.69 for PFR_A with uncorrected and corrected F_A, respectively. The ratio of filling rates PFR_E/PFR_A = 1.48 ± 0.63 showed a

strong correlation of r = 0.85 and no significant bias compared to the uncorrected F_E/F_A ratio of 1.36 ± 0.63 (p = 0.150), as well as a strong correlation r = 0.82 and no significant bias compared to the myocardial velocity-corrected F_E/F_A ratio of 1.38 ± 0.69 (p = 0.260).

3.4 4D flow measurements

The comparison between 4D flow-derived E, A and e' with echocardiographic measurements was performed in the 60 participants of whom 35 were female (**MS3**). Cardiac magnetic resonance imaging followed on average 4 ± 3 days after echocardiography. The cardiac intervals during cardiac magnetic resonance imaging (68 ± 11 bpm) and echocardiography (69 ± 11 bpm) did not differ (p = 0.367).

3.4.1 Transmitral diastolic velocities

In two participants, E and A velocities were fused wherefore the late-diastolic peak velocities could not be assessed. **Table 9** and **Figure 18** present the comparisons of different 4D flow evaluation strategies for transmitral peak velocities and echocardiography.

Table 9: Comparison of 4D flow and Doppler echocardiography derived diastolic transmitral and myocardial peak velocities and velocity ratios. Reproduced with modifications from Reiter C et al. Eur J Radiol 2024 (3).

Method	mean ± SD	bias ± SD	r	p
E (cm/s)				
Echo	78 ± 16			
$4DF_{SA}$	69 ± 13	9 ± 9	0.65	<0.001
$4DF_{4CH}$	68 ± 13	10 ± 10	0.72	<0.001
$4DF_{max}$	76 ± 15	2 ± 11	0.73	0.128
A (cm/s)				
Echo	73 ± 15			
$4DF_{SA}$	56 ± 15	18 ± 11	0.75	<0.001
$4DF_{4CH}$	61 ± 12	12 ± 9	0.80	<0.001
$4DF_{max}$	69 ± 13	5 ± 8	0.83	<0.001
septal e' (cm/s)				
Echo	8.2 ± 2.1			
4DF	8.0 ± 2.1	0.2 ± 1.7	0.64	0.350
lateral e' (cm/s)				
Echo	10.1 ± 2.2			
4DF	10.0 ± 2.0	0.1 ± 1.5	0.77	0.536
average e' (cm/s)				
Echo	9.1 ± 1.8			
4DF	9.0 ± 1.8	0.2 ± 1.1	0.81	0.262
E/A ratio				
Echo	1.11 ± 0.29			
$4DF_{SA}$	1.32 ± 0.42	-0.22 ± 0.29	0.74	<0.001
$4DF_{4CH}$	1.14 ± 0.30	-0.04 ± 0.19	0.79	0.139
$4DF_{max}$	1.14 ± 0.29	-0.04 ± 0.15	0.86	0.067
E/e' ratio				
Echo	8.7 ± 1.9			
$4DF_{SA}$	7.8 ± 1.5	0.9 ± 1.6	0.54	<0.001
$4DF_{4CH}$	7.7 ± 1.4	1.1 ± 1.5	0.61	<0.001
$4DF_{max}$	8.6 ± 1.5	0.1 ± 1.5	0.64	0.462

Data given as mean ± standard deviation. Bias is the mean difference of echocardiographic and 4D flow MRI measurements. Subscripts specify the 4D flow evaluation method at the mitral valve tips (SA), between the mitral valve leaflets (4CH) and in the transmitral inflow volume (max). E = early-diastolic transmitral peak velocity, A = late-diastolic transmitral peak velocity, SD = standard deviation=, r = correlation with Echo, p = significance of the bias.

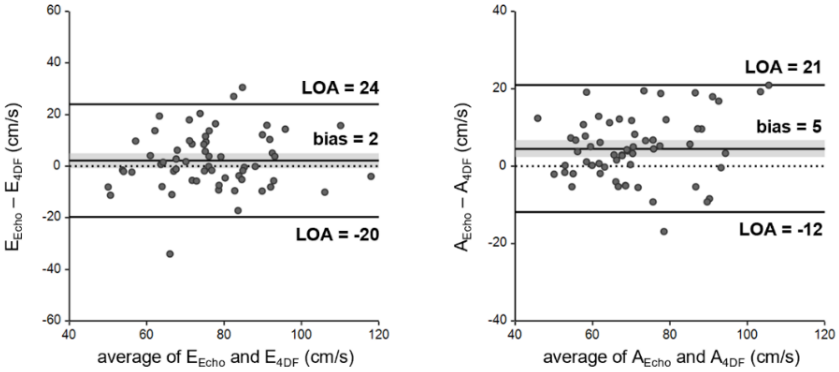

Figure 18: Bland-Altman plots comparing transmitral peak velocities from 4D flow and echocardiography. Reproduced with modifications from Reiter C et al. Eur J Radiol 2024 (3).
LOA = limits of agreement, E_{Echo} = echocardiographic early-diastolic transmitral peak velocity, A_{Echo} = echocardiographic late-diastolic transmitral peak velocity, E_{4DF} = 4D flow-derived early-diastolic transmitral peak velocity, A_{4DF}.= 4D flow-derived late-diastolic transmitral peak velocity. Gray bars = 95% confidence interval of bias.

Moderate to high correlations were observed between echocardiographic and 4D flow-derived diastolic transmitral peak velocities. The *4D flow SA method*, and *4D flow 4-chamber method* significantly underestimated transmitral peak velocities; however, the *4D flow max-velocity method* displayed a much smaller bias, which remained significant for late-diastolic transmitral velocity. Importantly, neither the differences nor the absolute values of these differences between methods correlated significantly with time or heart rate discrepancies between magnetic resonance imaging and echocardiography. Notably, velocities obtained from 2D flow and the *4D flow SA method* showed high correlations (r = 0.87 for E and 0.89 for A) and displayed only a slight but statistically significant bias for early-diastolic transmitral velocity (p = 0.004).

3.4.2 Myocardial velocities

Myocardial tissue peak velocities assessed from 4D flow data and their comparison with echocardiography are demonstrated in **Table 9** and **Figure 19**.

Strong correlations between echocardiographic and 4D flow-derived early-diastolic septal and lateral myocardial tissue peak velocities were observed, without significant bias. The highest correlation was found between the averaged early-diastolic myocardial tissue peak velocities from the lateral and septal regions, comparing 4D flow to echocardiography. Similar to the transmitral peak velocities, no significant correlations were found between differences or absolute values of differences and time or heart rate differences between echocardiographic and 4D flow-derived tissue velocities.

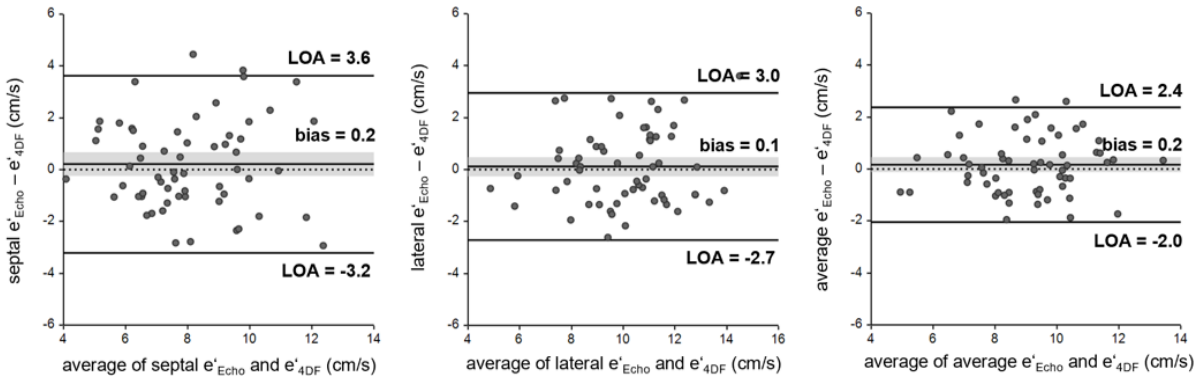

Figure 19: Bland-Altman plots comparing 4D flow with echocardiographic transmitral peak velocities. Reproduced with modifications from Reiter C et al. Eur J Radiol 2024 (3).

Gray bars = 95% confidence interval of bias, LOA = limits of agreement, e'$_{Echo}$ = echocardiography-derived early-diastolic mitral valve tissue peak velocity, e'$_{4DF}$ = 4D flow-derived early-diastolic myocardial tissue peak velocities.

3.4.3 Velocity ratios

Comparison of E/A and E/e' ratios evaluated from 4D flow and echocardiography are summarized in **Table 9**; Bland-Altman plots shown in **Figure 20**. Moderate to high correlations between echocardiographic and 4D flow E/A and E/e' ratios were observed, with the highest correlations for parameters obtained by the *4D flow max-velocity method*. While no bias was observed only for E/A assessed from the *4D flow 4-chamber method*, no significant bias for E/A and E/e' was observed using the *4D flow max-velocity method*.

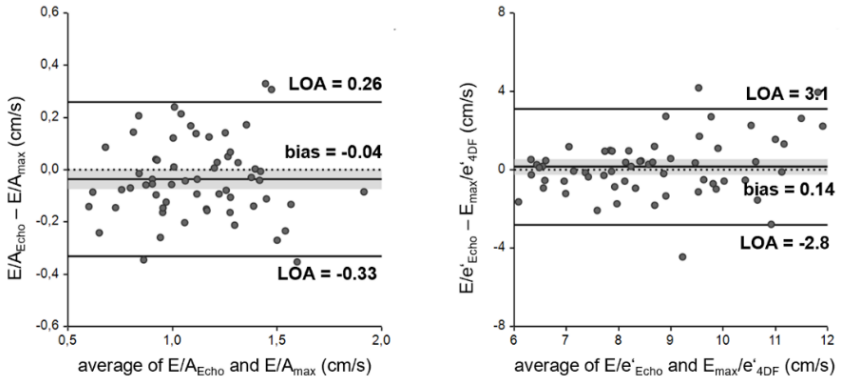

Figure 20: Bland-Altman plots comparing echocardiographic with 4D flow E/A and E/e' ratios using the *4D flow max-velocity-method*. Reproduced with modifications from Reiter C et al. Eur J Radiol 2024 (3). Gray bar = 95% confidence interval of bias, LOA = limits of agreement, E/A_{Echo} = echocardiography-derived ratio of early- and late-diastolic transmitral peak velocities, E/A_{4DF} = 4D flow-derived ratio of early- and late-diastolic transmitral peak velocities.

3.4.4 Interobserver variability

Interobserver agreement was excellent across all 4D flow-derived measurements, except for the early-diastolic transmitral peak velocity evaluated from the *4D flow SA-method* and the *4D flow 4-chamber method*. The least observer variability was observed for the *4D Flow max-velocity method*, making it the most consistent approach for measuring transmitral peak velocities and ratios (**Table 10**).

Table 10: Interobserver variability for 4D flow-derived diastolic velocity parameter. Reproduced with modifications from Reiter C et al. Eur J Radiol 2024 (3).

Method	ICC	SEM
E (cm/s)		
$4DF_{SA}$	0.895 [0.758 - 0.957]	5.1 [3.9 - 7.4]
$4DF_{4CH}$	0.872 [0.695 - 0.948]	4.6 [3.5 - 6.8]
$4DF_{max}$	0.988 [0.970 - 0.995]	1.6 [1.3 - 2.4]
A (cm/s)		
$4DF_{SA}$	0.945 [0.866 - 0.978]	5.4 [4.1 - 7.8]
$4DF_{4CH}$	0.940 [0.792 - 0.979]	3.4 [2.6 - 5.0]
$4DF_{max}$	0.988 [0.967 - 0.995]	1.6 [1.2 - 2.3]
e' (cm/s)		
septal	0.971 [0.927 - 0.989]	0.4 [0.3 - 0.6]
lateral	0.963 [0.911 - 0.985]	0.4 [0.3 - 0.6]
average	0.983 [0.952 - 0.994]	0.2 [0.2 - 0.3]
E/A' ratio		
$4DF_{SA}$	0.961 [0.905 - 0.984]	0.12 [0.09 - 0.17]
$4DF_{4CH}$	0.907 [0.781 - 0.962]	0.11 [0.08 - 0.15]
$4DF_{max}$	0.987 [0.967 - 0.995]	0.04 [0.03 - 0.05]
E/e' ratio		
$4DF_{SA}$	0.915 [0.798 - 0.965]	0.60 [0.46 - 0.88]
$4DF_{4CH}$	0.917 [0.801 - 0.967]	0.52 [0.44 - 0.84]
$4DF_{max}$	0.975 [0.939 - 0.990]	0.31 [0.23 - 0.45]

Intraclass correlation coefficients (ICCs) and standard error of measurement (SEM) are given with corresponding 95%-confidence intervals in brackets. Subscripts specify the 4D flow evaluation method at the mitral valve tips (SA), between the mitral valve leaflets (4CH) and in the transmitral inflow volume (max). E = early-diastolic transmitral peak velocity, A = late-diastolic transmitral peak velocity, e' = early-diastolic myocardial peak velocity.

3.5 4D flow grading parameters

The feasibility and accuracy of left ventricular diastolic dysfunction grading by 4D flow magnetic resonance imaging using the ASE/EACVI 2016 echocardiographic grading as reference method (**MS4**) was investigated in 94 participants within 3 ± 7 days. Mean participants' heart rates at echocardiography and 4D flow imaging did not differ (p = 0.33).

3.5.1 Volumetric grading parameter

High correlations were observed between volumetric parameters measured by 4D flow and echocardiography, the values derived from 4D flow, however, were significantly higher than those from echocardiography (**Table 11** and **Figure 21**).

The echocardiographic grading cutoff values for EF < 50% and LAVI > 34 ml/m² (10) were therefore bias-corrected to EF < 55% and LAVI > 47 ml/m² for 4D flow grading, respectively. The accuracy of 4D flow parameters, using above bias-adjusted cutoff values, for identifying echocardiographic EF < 50% and LAVI > 34 ml/m² was 91% (CI: 83%, 96%) for EF and 77% (CI: 67%, 85%) for LAVI.

Table 11: Comparison of ASE/EACVI 2016 grading parameters from echocardiography and 4D flow. Reproduced with modifications from Reiter C et al. 2024 (4).

Parameter	Echo	4D flow	Bias	r	P value
Volumetric grading parameter					
EF (%)	59 ± 10	64 ± 9	-5	<0.001	.75
LAVI (mL/m²)	35 ± 14	48 ± 15	-13	<0.001	.80
Velocity grading parameter					
E (cm/s)	82 ± 21	80 ± 21	2.00	0.065	0.87
E/A	1.23 ± 0.54	1.23 ± 0.48	0.01	0.820	0.84
septal e‘ (cm/s)	7.0 ± 2.5	6.8 ± 2.4	0.20	0.201	0.80
lateral e‘ (cm/s)	8.8 ± 3.0	8.8 ± 2.7	0.00	0.884	0.86
E/e‘	12.3 ± 7.7	11.7 ± 6.4	0.60	0.069	0.92

Parameters are presented as means ± standard deviations. The P value refers to the significance of the bias, r to the correlation between echocardiographic and 4D flow measurements. EF = ejection fraction, LAVI = left atrial volume index, Echo = echocardiography, E = early-diastolic transmitral peak velocity, A = late-diastolic transmitral peak velocity, e’ = early-diastolic myocardial peak velocity, r = correlation with Echo, p = significance of the bias.

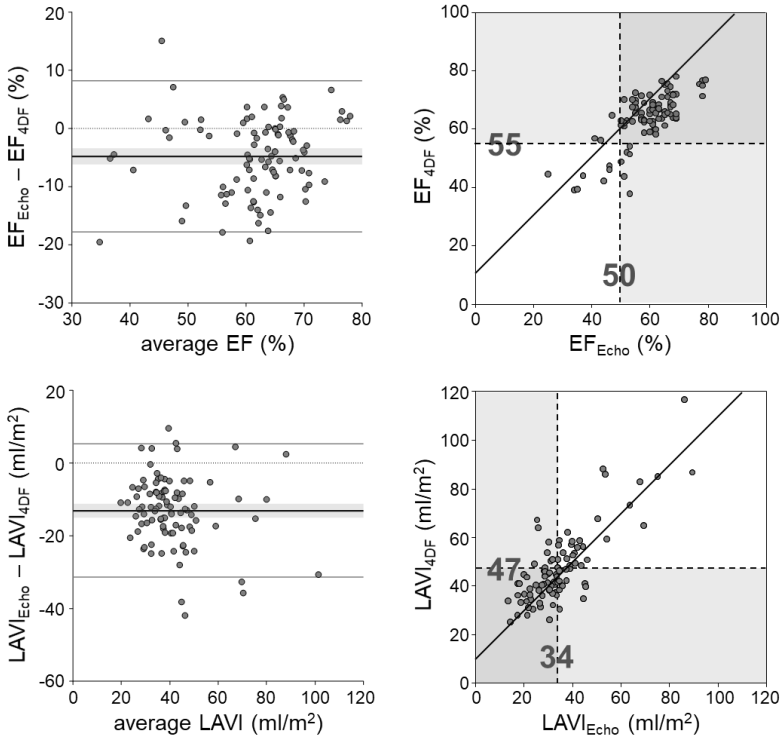

Figure 21: Bland-Altman and scatter plots comparing 4D flow with echocardiographic left ventricular EF and LAVI. Reproduced with modifications from Reiter C et al. 2024 (4).
Bland-Altman plots: dotted line = line of identity, bold solid line with grey bars = bias with 95% confidence interval, upper and lower solid lines = 95% limits of agreement. Scatter plot: bold line = bias-adjusted line of identity, dashed lines = echocardiographic and bias-adjusted 4D flow grading cutoffs. Echo = echocardiography, 4DF = 4D flow, EF = ejection fraction, LAVI = left atrial volume index.

3.5.2 Velocity grading parameters

High to very high correlations were observed between echocardiographic and 4D flow-derived E and E/A (**Figure 22**), septal e', lateral e', and E/e' values (**Figure 23**), with no significant bias between methods (**Table 11**). Consequently, the bias-adjusted 4D flow grading cutoffs were set to match the established echocardiographic thresholds (10). The predictive accuracies of 4D flow for identifying echocardiographic thresholds were as follows: E > 50 cm/s at 97% (CI: 91%, 99%), E/A > 0.8 at 91% (CI: 83%, 96%), E/A < 2.0 at 97% (CI: 91%, 99%), septal e' < 7 cm/s at 78% (CI: 68%, 86%), lateral e' < 10 cm/s at 88% (CI: 80%, 94%), and E/e' > 14 at 93% (CI: 85%, 97%).

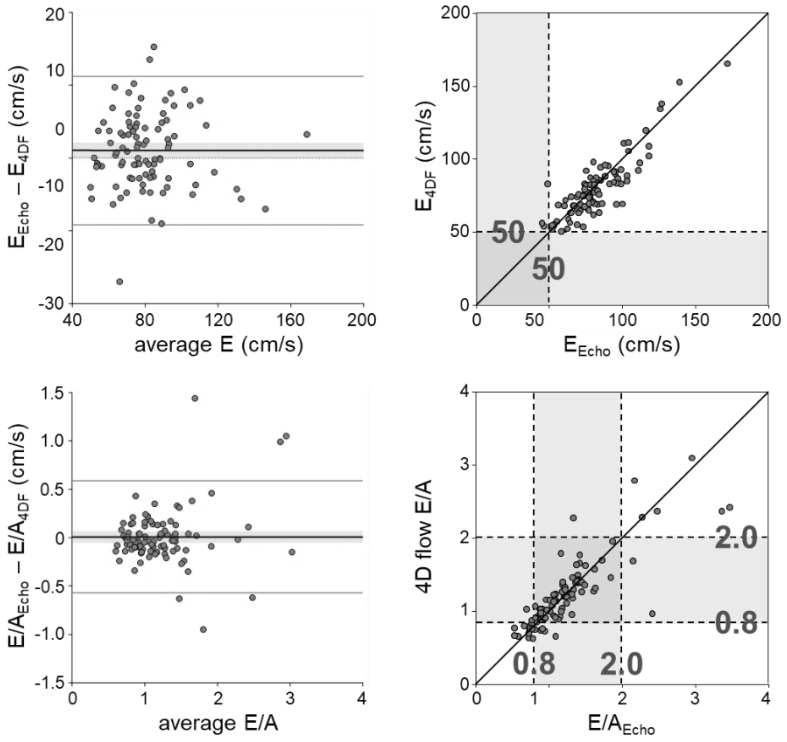

Figure 22: Bland-Altman and scatter plots comparing 4D flow with echocardiographic E and E/A. Reproduced with modifications from Reiter C et al. 2024 (4).

Bland-Altman plots: dashed lines = line of identity, bold solid lines with the grey bars = bias with 95% confidence interval, upper and lower solid lines = 95% limits of agreement. Scatter plot: bold lines = bias-adjusted line of identity, dotted lines = echocardiographic and 4D flow grading cutoffs. Echo = echocardiography, 4DF = 4D flow, E = early-diastolic transmitral peak velocity, E/A = ratio of early-to-late diastolic transmitral peak velocities.

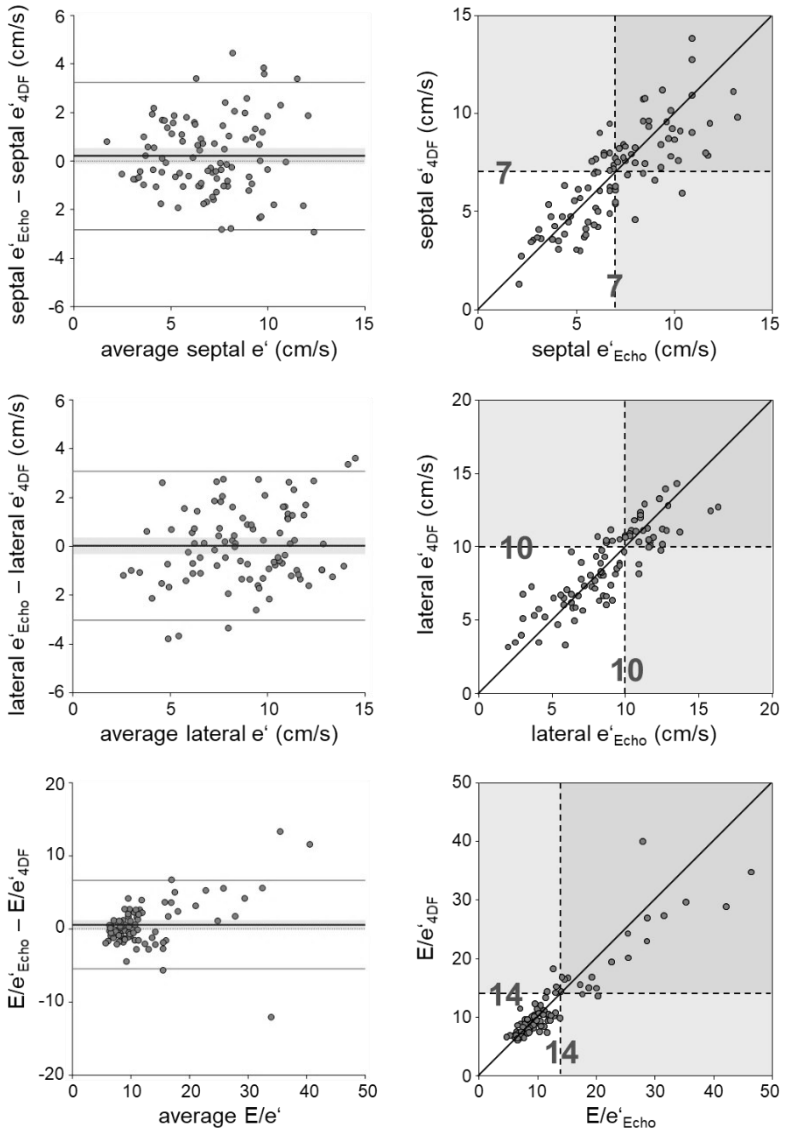

Figure 23: Bland-Altman and scatter plots comparing 4D flow with echocardiographic septal and lateral e' and E/e'. Reproduced with modifications from Reiter C et al. 2024 (4).

Bland-Altman plots: dashed lines = line of identity, bold solid lines with the grey bars = bias with 95% confidence interval, upper and lower solid lines = 95% limits of agreement. Scatter plot: bold lines = bias-adjusted line of identity, dotted lines = echocardiographic and 4D flow grading cutoffs. Echo = echocardiography, 4DF = 4D flow, e' = early-diastolic mitral annular/myocardial peak velocity, E/e' = ratio of early-diastolic transmitral peak velocity to average early-diastolic mitral annular/myocardial peak velocity.

3.5.3 Elevated pulmonary arterial pressure

In 69 out of 94 participants (73%) a tricuspid regurgitation was identified via echocardiography. In these 69 individuals, the relationship between echocardiographic peak tricuspid regurgitation pressure pTR and 4D flow-derived t_{vortex} was well characterized (square root of the coefficient of determination = 0.88) by a segmented linear model with a threshold pTR_0 = 18.4 mmHg and a slope = 1.19 %/mmHg (**Figure 24**). This model estimates t_{vortex} = 15% (CI: 13%, 17%) as 4D flow-based grading cutoff for the TR = 2.8 m/s (or equivalently pTR = 31.4 mmHg) echocardiographic grading cutoff.

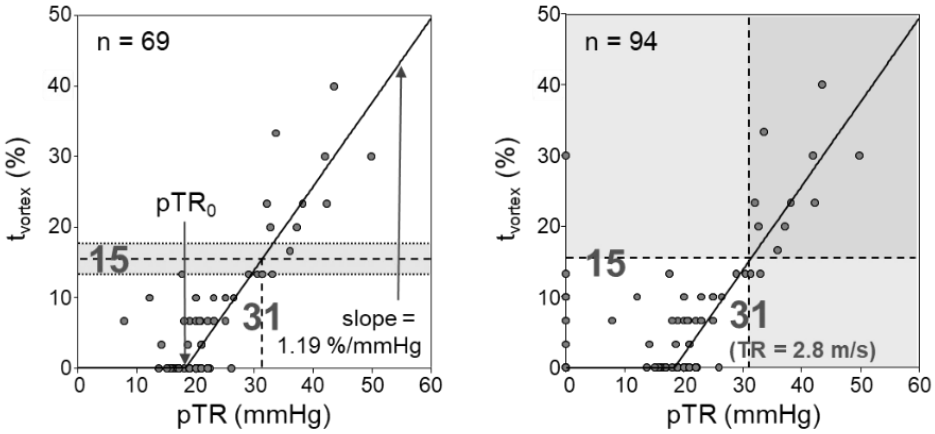

Figure 24: Scatter plot of duration of vortical blood flow along the main pulmonary artery derived from 4D flow versus echocardiographic peak tricuspid pressure gradient. Reproduced with modifications from Reiter C et al. 2024 (4).

Left: Scatter plot of 69 participants with tricuspid regurgitation, right: scatter plot of all participants. Solid line = fitted segmented linear model for t_{vortex} on pTR, vertical dashed lines = echocardiographic grading cutoff for TR, horizontal dashed lines = 4D flow grading cutoff for t_{vortex}. pTR = peak tricuspid pressure gradient, t_{vortex} = vortex duration along the main pulmonary artery, TR = tricuspid regurgitant peak velocity, pTR_0 = threshold value of the segmented linear model.

For all participants with echocardiographic detectable tricuspid regurgitation, the accuracy of 4D flow-derived t_{vortex} > 15% in predicting TR > 2.8 m/s was 99% (CI: 92%,

100%). However, one individual with t_{vortex} > 15% but no visible tricuspid regurgitation on echocardiography reduced this accuracy to 98% (CI: 93%, 100%) for all participants.

3.6 Diagnosis and grading of diastolic dysfunction

The modified ASE/EACVI 2016 algorithm for assessing diastolic dysfunction, using 4D flow with bias-adjusted grading parameters and their respective thresholds are summarized in **Figure 25**. The comparison between echocardiography and 4D flow-based grading of diastolic dysfunction showed nearly perfect agreement (**Table 12**), with a weighted kappa coefficient = 0.84 (95%-CI: 0.78-0.91). No significant overestimation or underestimation of diastolic dysfunction grades was observed when employing the suggested 4D flow method (p = 0.53).

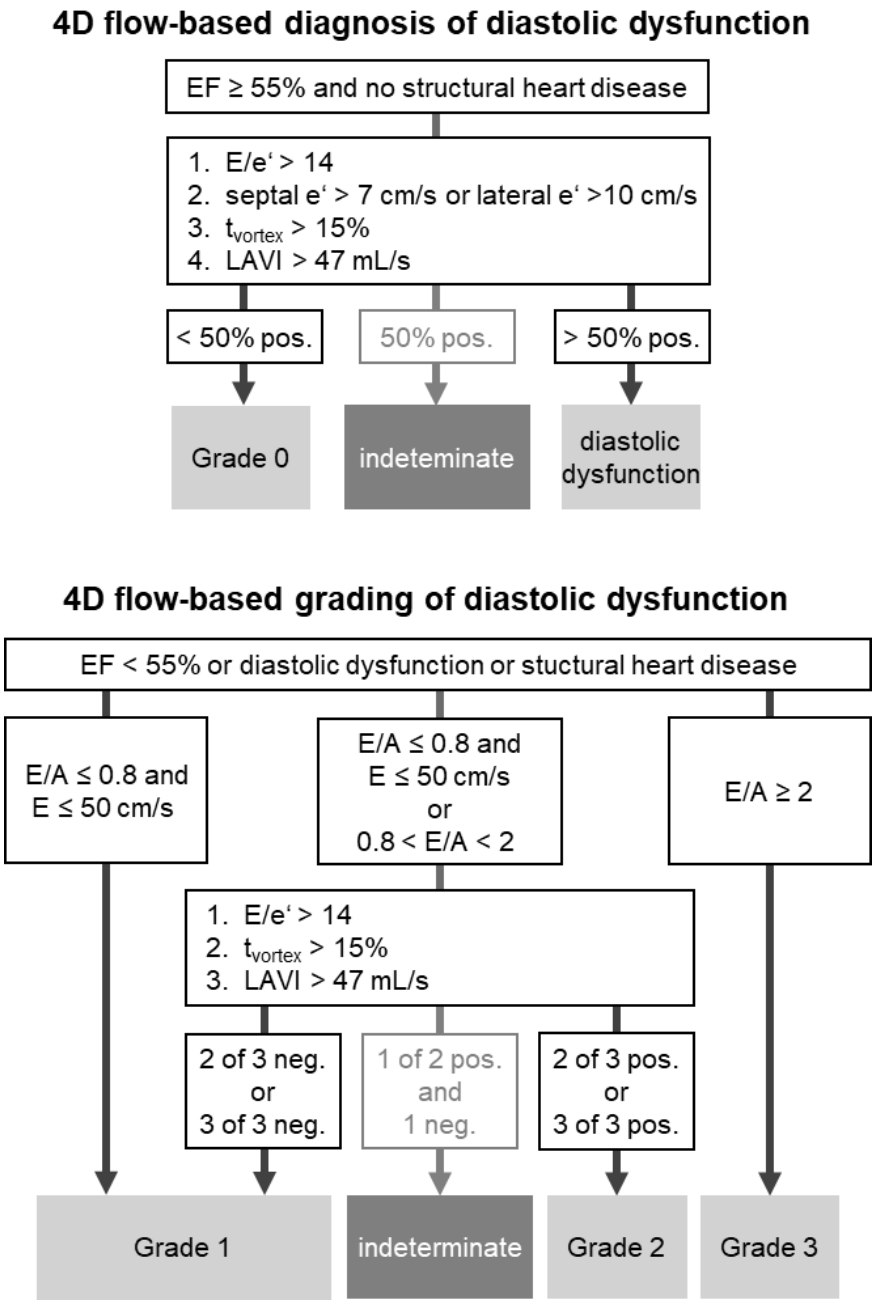

Figure 25: 4D flow-based diagnosis and grading of left ventricular diastolic dysfunction along with the 4D flow parameter thresholds following ASE/EACVI 2016 algorithm. Reproduced with modifications from Reiter C et al. 2024 (4).

EF = left ventricular ejection fraction, LAVI = maximal left atrial volume index, E = transmitral early-diastolic peak velocity, E/A = transmitral early-to-late diastolic peak velocities, e' = average of septal and lateral early-diastolic myocardial peak velocities, E/e' = transmitral early-diastolic peak velocity to average of septal and lateral early-diastolic myocardial peak velocities ratio, t_{vortex} = duration of vortical blood flow along the main pulmonary artery.

Table 12: Comparison of echocardiographic and 4D flow-based grading of left ventricular diastolic dysfunction. Reproduced with modifications from Reiter C et al. 2024 (4).

		Echocardiography					
	Grade	0	ind.	I	II	III	total
4D flow	0	**44**	6	0	0	0	50
	ind	7	**3**	0	0	0	10
	I	0	0	**12**	4	0	16
	II	0	0	1	**8**	2	11
	III	0	0	0	1	**6**	7
	total	51	9	13	13	8	94

Grade 0 = normal left ventricular diastolic function, ind. = indeterminate left ventricular diastolic function, I/II/III = grade I/II/III left ventricular diastolic dysfunction

3.7 The left atrial acceleration factor

The association of the severity of left ventricular diastolic dysfunction with the left atrial acceleration factor (79) was investigated in 94 participants (**MS5**).

Peak left atrial inflow and outflow velocities, along with corresponding α for the entire study population and for subgroups of patients with diastolic dysfunction are summarized in **Table 13**. The highest average left atrial inflow velocities were detected in either the upper left (56%) or upper right (32%) pulmonary vein in 83 cases (88%), while the left lower pulmonary vein showed the highest inflow velocities in 8 (9%) and the right lower vein in 3 participants (3%).

Significant correlations were observed between α and echocardiographic EF ($r = -0.27$, $p = 0.01$), E ($r = 0.40$, $p < 0.001$), E/A ($r = 0.60$, $p < 0.001$), e' ($r = -0.37$, $p = 0.009$), E/e' ($r = 0.66$, $p < 0.001$), LAVI ($r = 0.43$, $p < 0.001$), TR ($r = 0.42$, $p < 0.001$), and sPAP ($r = -0.49$, $p < 0.001$). Additionally, the left atrial acceleration factor demonstrated significant differences between participants with normal ($\alpha = 1.35 \pm 0.46$) and reduced ($\alpha = 1.99 \pm 0.70$) left ventricular ejection fraction ($p < 0.001$).

Table 13: 4D flow-derived left atrial velocities and left atrial acceleration factor. Reproduced with modifications from Reiter C et al. Eur Radiol 2023 (5).

Parameter	Total (n=94)	grade 0 (n=51)	ind. (n=9)	Grade I (n=13)	Grade II (n=13)	Grade III (n=8)	P value
All pulmonary veins							
v_E (cm/s)	57.0 ± 13.2	52.8 ± 8.3^{2,3}	51.5 ± 6.7^{3}	57.0 ± 10.8	61.1 ± 7.8^{0}	83.7 ± 21.7^{0,i}	<0.001
maximum v_S (cm/s)	50.1 ± 11.7	54.4 ± 9.0^{2,3}	52.1 ± 8.7^{3}	50.5 ± 10.1^{3}	43.0 ± 10.9^{0}	30.9 ± 11.2^{0,i,1}	<0.001
maximum v_D (cm/s)	36.2 ± 9.4	38.1 ± 8.5	35.8 ± 4.4	37.1 ± 11.4	29.8 ± 8.4	34.0 ± 13.7	0.072
maximum $(v_S+v_D)/2$ (cm/s)	43.1 ± 9.1	46.2 ± 7.6^{2}	43.9 ± 6.1	43.8 ± 8.8	36.4 ± 7.2^{0}	32.5 ± 11.5	<0.001
α	1.41 ± 0.50	1.17 ± 0.14^{1,2,3}	1.20 ± 0.07^{2,3}	1.33 ± 0.15^{0,2,3}	1.77 ± 0.18^{0,i,1,3}	2.79 ± 0.69^{0,i,1,2}	<0.001
Lower pulmonary veins							
maximum $(v_S+v_D)/2$ cm/s	35.6 ± 8.4	37.0 ± 7.4	38.8 ± 5.4	36.9 ± 11.0	31.1 ± 6.3	28.6 ± 10.6	0.012
α_{lower}	1.68 ± 0.59	1.46 ± 0.23^{2,3}	1.33 ± 0.12^{1,2,3}	1.60 ± 0.24^{i,2,3}	2.00 ± 0.30^{0,i,1}	3.14 ± 0.87^{0,i,1}	<0.001

Superscripts 0, i, 1, 2 and 3 indicate significant differences from grade 0, indeterminate, grade I, grade II and grade III diastolic dysfunction, respectively. v_E = early-diastolic left atrial peak outflow velocity, v_S = systolic left atrial peak inflow velocity, v_D = early-diastolic left atrial peak inflow velocity, α = left atrial acceleration factor from all pulmonary veins, α_{lower} = left atrial acceleration factor derived from only the lower pulmonary veins.

Correlations between α and laboratory markers were observed for haemoglobin (r = -0.25, p = 0.02), estimated glomerular filtration rate (r = -0.49, p < 0.001), N-terminal prohormone of brain natriuretic peptide (r = 0.53, p < 0.001), and low-density lipoprotein (r = -0.34, p < 0.001). Maximum values of v_E, v_S, $(v_S + v_D)/2$ and α differed among groups with varying grades of diastolic function, showing a decrease in v_S and $(v_S + v_D)/2$ and an increase in α with higher diastolic dysfunction grades. Specifically, mean α values for diastolic dysfunction grades II and III differed from mean α in all other groups (**Figure 26**).

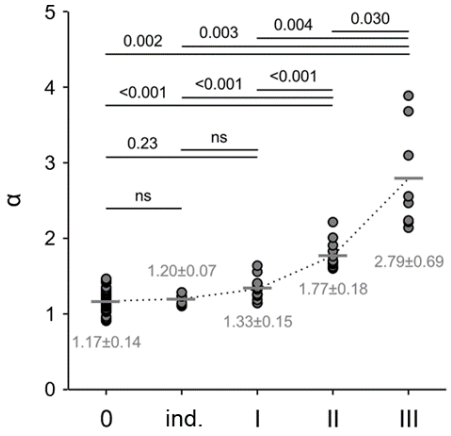

Figure 26: Left atrial acceleration factor alterations in left ventricular diastolic dysfunction. Reproduced with modifications from Reiter C et al. Eur Radiol 2023 (5).
Comparisons of group means by Dunett-T3 post hoc test are indicated by lines together with p-values. ns = non-significant; ind. = indeterminate.

3.7.1 Advanced left ventricular diastolic dysfunction

In cases of advanced diastolic dysfunction (grade ≥ II), α was significantly higher compared to normal, indeterminate, and grade I diastolic dysfunction, with values of 2.16 ± 0.66 versus 1.20 ± 0.15 ($p < 0.001$). The area-under-curve for detecting advanced diastolic dysfunction based on α was 0.998 (95% CI: 0.958–1.000) (**Figure 27**). With a cut-off value of α ≥ 1.58, the sensitivity and specificity for identifying advanced diastolic dysfunction were 100% (95% CI: 84–100%) and 99% (95% CI: 93–100%), respectively. For distinguishing grade III diastolic dysfunction, the area-under-curve was also 0.998 (95% CI: 0.976–1.000). Using a threshold of α ≥ 2.14, sensitivity and specificity for detecting grade III diastolic dysfunction were 100% (95% CI: 63–100%) and 99% (95% CI: 94–100%).

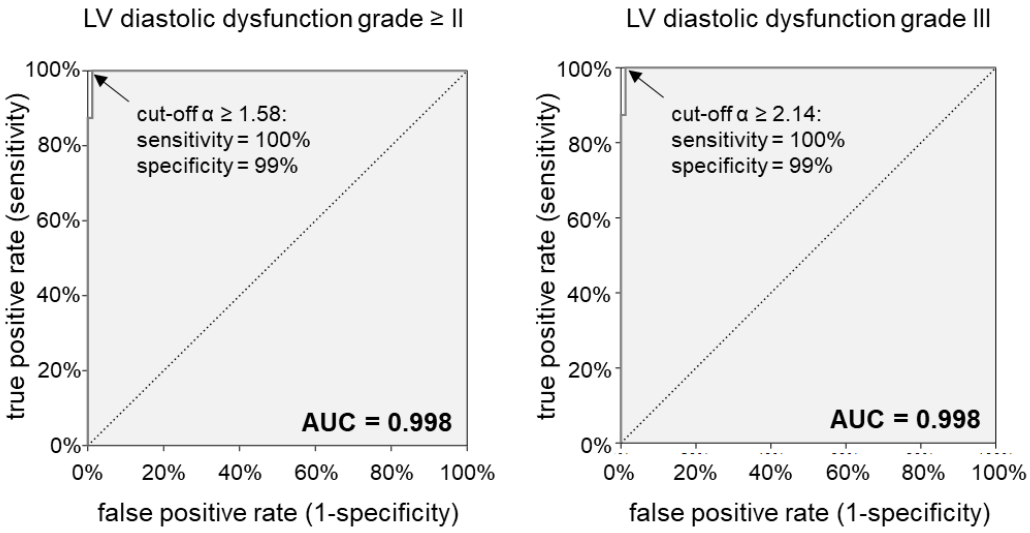

Figure 27: Left atrial acceleration factor-based discrimination of advanced diastolic dysfunction and grade III diastolic dysfunction. Reproduced with modifications from Reiter C et al. Eur Radiol 2023 (5). Cutoff values at maximum of Youden's index are given together with their sensitivity and specificity. AUC, area under the curve.

Among participants with non-advanced diastolic dysfunction, the area-under-curve for differentiating normal diastolic function using α was 0.711 (95% CI: 0.569–0.812), with a sensitivity of 71% (95% CI: 56–83%) and specificity of 68% (95% CI: 45–86%) at a cutoff value of α ≤ 1.22. For detecting grade I diastolic dysfunction, the area-under-curve was 0.797 (95% CI: 0.646–0.888), with a sensitivity of 77% (95% CI: 46–95%) and specificity of 72% (95% CI: 59–83%) at a cutoff value of α ≥ 1.24.

3.7.2 Left atrial acceleration factor from lower pulmonary veins α_{lower}

As summarized in **Table 13**, assessment of α_{lower} from the lower pulmonary veins similar to the original study (79) resulted in smaller α values in both, the entire study population and within groups categorized by their diastolic function status (p = <0.001 to 0.045). A very high correlation (r = 0.90, p < 0.001) but also a significant bias of -0.27 (p < 0.001) was observed between α and α_{lower}.

The area-under-curve for detecting advanced diastolic dysfunction using α_{lower} was 0.961 (95% CI: 0.899–0.990). At a threshold of α_{lower} ≥ 1.77, the sensitivity and

specificity for predicting advanced diastolic dysfunction were 90% (95% CI: 70–99%) and 89% (95% CI: 80–95%), respectively.

3.7.3 Echocardiographic left atrial acceleration factor

As the pulmonary veins could only be inadequately visualization in the apical 4-chamber view, S and D measurements were not feasible in 5 participants; among the remaining 89, the right lower pulmonary vein was assessed in 81 participants (91%) and the right upper pulmonary vein in 8 participants (9%). **Table 14** summarizes the mean values of E, S, D, and (S + D)/2, along with the corresponding echocardiographic left atrial acceleration factor α_{Echo} for the overall study population and subgroups of patients with diastolic dysfunction.

Table 14: Echocardiography-derived left atrial velocities and left atrial acceleration factor. Reproduced with modifications from Reiter C et al. Eur Radiol 2023 (5).

Parameter	Total (n=94)	grade 0 (n=51)	ind. (n=9)	Grade I (n=13)	Grade II (n=13)	Grade III (n=8)	P value
E_{Echo} (cm/s)	82.0 ± 20.7	77.6 ± 15.8[3]	79.0 ± 15.0[3]	74.4 ± 13.0[3]	103.8 ± 31.5[3]	110.9 ± 18.8[0,i,1]	<0.001
S_{Echo} (cm/s)	55.8 ± 14.8	57.5 ± 11.9	55.3 ± 5.0	56.0 ± 17.5	61.4 ± 21.8	36.3 ± 15.7	0.005
D_{Echo} (cm/s)	48.7 ± 13.1	43.7 ± 8.0	46.1 ± 8.7	53.3 ± 11.2	61.0 ± 16.0	63.6 ± 23.0	<0.001
$(S_{Echo}+D_{Echo})/2$ (cm/s)	51.2 ± 12.3	50.6 ± 8.4	50.7 ± 6.4	54.7 ± 12.5	61.2 ± 15.2	49.9 ± 19.0	0.719
α_{Echo}	1.64 ± 0.51	1.58 ± 0.42	1.56 ± 0.28	1.44 ± 0.49	1.74 ± 0.54	2.44 ± 0.75	<0.001

Superscripts 0, i, 1, 2 and 3 indicate significant differences from grade 0, indeterminate, grade I, grade II and grade III diastolic dysfunction, respectively. E_{Echo} = early diastolic transmitral peak velocity, S_{Echo} = systolic pulmonary venous peak velocity, D_{Echo} = early diastolic pulmonary venous peak velocity, α_{Echo} = LA acceleration factor derived from echocardiographic measurements.

There was a significant bias between α and α_{Echo} (-0.25, $p < 0.001$), with a large standard deviation of differences (SD = 0.53) and a low correlation ($r = 0.48$, $p < 0.001$). The area-under-curve for detecting advanced diastolic dysfunction based on α_{Echo} was 0.692 (95% CI: 0.535–0.848).

3.7.4 Interobserver reliability

Interobserver reliability for determining peak velocities used to calculate α ranged from good to excellent, while the reliability for both α and α_{lower} was consistently excellent (**Table 15**).

Table 15: Interobserver reliability for 4D flow-derived left atrial peak inflow and outflow velocities and left atrial acceleration factor determined from all or just the lower pulmonary veins. Reproduced with modifications from Reiter C et al. Eur Radiol 2023 (5).

Parameter	SD_w	ICC
All pulmonary veins		
v_E (cm/s)	3.4	0.97 [0.92 - 0.99]
maximum v_S (cm/s)	3.1	0.95 [0.88 - 0.98]
maximum v_D (cm/s)	3.5	0.86 [0.68 - 0.94]
maximum (v_S+v_D)/2 cm/s	3.1	0.90 [0.77 - 0.96]
α	0.14	0.96 [0.91 - 0.99]
Lower pulmonary veins		
maximum (v_S+v_D)/2 cm/s	3.4	0.83 [0.61 - 0.93]
α_{lower}	0.20	0.93 [0.84 - 0.97]

Intraclass correlation coefficients (ICC) are given together with their 95%-confidence intervals. SD_w = within subject standard deviation, v_E = early-diastolic left atrial peak outflow velocity, v_S = systolic left atrial peak inflow velocity, v_D = early-diastolic left atrial peak inflow velocity, α = left atrial acceleration factor from all pulmonary veins, α_{lower} = left atrial acceleration factor derived from only the lower pulmonary veins.

4. Discussion

4.1 Principal findings and clinical implications

The results of this doctoral thesis demonstrate that 4D flow-based diagnosis and grading of left ventricular diastolic dysfunction, adapted from the 2016 ASE/EACVI echocardiographic guidelines, is feasible and closely aligns with echocardiographic results (4). The 4D flow approach included the setting of bias-adjusted thresholds for volumetric parameters, definition of equivalent cutoffs for diastolic transmitral and myocardial peak velocities and ratios, and using the duration of vortical blood flow in the main pulmonary artery (t_{vortex} > 15%) as alternative grading parameter for the echocardiographic TR > 2.8 m/s criterion (**MS4**).

The first key consideration of the study included the different conditions under which echocardiography (free breathing) and standard magnetic resonance imaging (inspiratory breath-holding) are performed (**MS1**). Breath-holding was found to impact left ventricular and left atrial volumes, EF, and transmitral flow rates (1): left ventricular volumes were higher and EF lower, LAV_{max} was higher, and early-diastolic velocities where higher during breathing, with notable variability in parameters between breath-hold and breathing. Given the impact of breath-holding, it was investigated if free-breathing 4D flow magnitude data could be used for left ventricular and left atrial volumetric function assessment, potentially reducing inconsistencies by evaluating all parameters from the same heartbeats (**MS2**). Study results showed that left ventricular and left atrial volumetric function can be accurately assessed from 4D flow magnitude images, with all parameters highly correlated with cine bSSFP data, and no significant differences in SV, left atrial volumes, or left atrial total ejection fraction (2). To provide a standardized evaluation workflow for 4D flow assessment of E, E/A, e', and E/e' for diagnosis and grading of left ventricular diastolic dysfunction analogously to the ASE/EACVI 2016 echocardiographic algorithm, different evaluation strategies were investigated, achieving high concordance with echocardiography and low intraobserver variability for the evaluation of grading parameters from the transmitral inflow volume

(**MS3**). This approach especially enables to use the established echocardiographic E, E/A, e', and E/e' cutoff values for 4D flow-based grading of left ventricular diastolic dysfunction (3).

Finally, the left atrial acceleration index α, a novel 4D flow metric associated with PAWP was introduced as 4D flow-based method diagnosing left ventricular diastolic dysfunction (**MS5**). α successfully differentiated normal left ventricular diastolic function and lower-grade diastolic dysfunction from higher-grade diastolic dysfunction, potentially simplifying the cardiac magnetic resonance multiparametric cutoff-value based diagnosis of left ventricular diastolic dysfunction to a single-parameter approach (5).

4.2 Methodological advances in diastolic function assessment

Cardiac magnetic resonance imaging is recognized as the gold standard for assessing ventricular and atrial volumetric function through cine imaging (13). Left ventricular ejection fraction and left atrial volume index calculated from multiplanar-reconstructed 4D flow magnitude data have shown high correlation with volumetric function parameters obtained from standard cine balanced steady-state free precession imaging, as well as comparable inter- and intraobserver variability (2). Consistent with previous studies that compare echocardiographic ejection fraction with that derived from cardiac magnetic resonance imaging (80–82), there is a strong correlation between ejection fraction values obtained via 4D flow and echocardiography. In this analysis, 4D flow-derived ejection fraction was measured by manually segmenting the left ventricular endocardial borders, with exclusion of papillary muscles and trabeculae from the left ventricular cavity (13), which may account for the minor but significant bias factored into the bias-adjusted ejection fraction cutoff. Additionally, studies comparing left atrial volume index values from echocardiography with those from cardiac magnetic resonance imaging show high correlation between the two methods, though echocardiography tends to underestimate left atrial volume index (83,84). This discrepancy has been attributed to limitations in echocardiographic imaging, such as reduced clarity of the left atrial endocardial wall and potential foreshortening (83).

Therefore, biases had to be accounted for cutoffs of volumetric grading parameters. Meanwhile 4D flow provided a means to assess diastolic transmitral flow and myocardial velocity grading parameters without significant bias relative to echocardiography. Studies have reported strong correlations between echocardiographic values and those derived from both 2D flow and 4D flow for E, E/A, e', and E/e' parameters (3,85–90), with 2D flow measurements generally showing a tendency to underestimate echocardiographic E, A, and e' values (3,87–90). Unlike 2D flow, 4D flow can capture the highest transmitral velocities across the entire inflow volume and offers a posteriori optimization of myocardial cut planes, effectively overcoming the issue of underestimation seen in 2D E, A, and e' measurements (3,86). This likely accounts for the minor differences between echocardiographic and 4D flow-derived values for E, E/A, e', and E/e' observed in the current study.

In contrast to the 2016 ASE/EACVI echocardiographic algorithm, the proposed echo-equivalent 4D flow algorithm eliminates the need for a separate distinction in cases where not all grading parameters are available (10). By deriving all grading parameters from a single measurement and enabling a posteriori evaluation, this method ensures that all parameters are available, a common limitation in echocardiographic or comprehensive cardiac magnetic resonance imaging protocols that rely on cine function, 2D, and 4D phase contrast imaging (90,91). The observed level of agreement for grading between echocardiography and 4D flow is similar to previously reported repeated echocardiographic evaluations (92), representing the upper limit of achievable agreement across methods.

4.2.1 Respiratory considerations in assessment of cardiac function

The cardio-respiratory interaction, frequently overlooked in the interpretation of cardiac magnetic resonance imaging-derived functional parameters, represents a complex physiological process marked by changes in intrathoracic pressure and associated variations in ventricular volumes (93,94). During the first 30 seconds of breath-holding, swift alterations in cardiovascular parameters have been noted, with a reduce in venous return due to increased intrathoracic pressure as the likely main contributor (33,37).

Moreover, additional cardiovascular and autonomic regulatory mechanisms have also been recognized as influencing these observed changes (37,38).

With both EDV and ESV shown to be greater during breathing than during breath-holding, only EF and PER—but not SV—were higher in the free breathing state. The consistency of these findings in systolic left ventricular volumetric function parameters, regardless of variations in breathing depth or frequency and across both short-axis and 4-chamber views, implies that these changes stem from physiological responses rather than systematic measurement errors, such as slice position shifts during breathing. Similar breathing-induced left ventricular volume alterations have been documented previously (93,94); however, prior studies' typically focus on the end-inspiratory state during breathing does not directly compare to inspiratory breath-holding with a closed glottis. Research examining the feasibility of left ventricular volumetric function assessment during breathing, using cine real-time or cine real-time compressed sensing imaging, against standard segmented cine multi-breath-hold imaging as a reference, has reported varied outcomes on systolic left ventricular function differences between breath-holding and breathing (25,29–31,39–42). These inconsistent results likely arise from differences in protocols, including imaging sequence techniques, spatial and temporal resolution, post-processing approaches, and breath-hold maneuvers, in addition to the small sample sizes involved in these studies.

The effect of breathing on left atrial volumetric function has not been previously explored using cardiac magnetic resonance imaging. However, given that left atrial volumetric function is a key echocardiographic marker of diastolic function (11), understanding the influence of breath-holding on cardiac magnetic resonance imaging-derived left atrial parameters gains significant clinical relevance (15,19,95). In this study, similar to left ventricular volumes, LA_{max} was found to be higher during breathing. However, unlike left ventricular EF, left atrial ejection fractions were also elevated during breathing. The observation that the differences between breath-holding and breathing for $EF_{passive}$ and EF_{total} are double those for EF_{active} suggests that active left atrial contraction may help offset the pressure variations that occur between breath-holding and breathing.

All early-diastolic metrics investigated in this study (PFR_E, E, F_E, e') were elevated during breathing, consistent with the fact that early-diastolic parameters are more influenced by pressure changes than late-diastolic parameters (96). Importantly, ratios such as E/A, PFR_E/PFR_A, and E/e' remained stable regardless of the breathing state. Transmitral F_E and F_A, which represent phase contrast analogs of PFR_E and PFR_A, exhibited similar breathing-induced variations as observed with PFR_E and PFR_A. The discrepancy between peak filling rates and peak flows can be attributed to the motion of the mitral valve plane during transmitral peak flow. For instance, assuming an average mitral valve opening area of 8 cm^2 and a mean e' of 10 cm/s yields a flow of roughly 80 ml, which would need to be added to F_E and F_A to obtain peak flow values that match peak filling rates. Additionally, considering the variability in e' and the mitral valve opening area, this helps explaining the moderate to strong correlations observed between peak filling rates and peak flows.

The comparison of repeatability during breath-holding and breathing reveals that the standard deviations of breath-hold-to-breathing differences are larger, indicating significant inter-individual variability in these differences. This variation is likely due to individual physiological responses to breath-holding, potentially influenced by variations in sympatho-vagal balance (38). Such findings suggest that the respiratory state can substantially impact cardiac magnetic resonance imaging-based functional parameters for left ventricular systolic and diastolic as well as left atrial measurements. This has important clinical implications, in particular when comparing results across imaging modalities or tracking changes in individual patients over time.

4.2.2 Volumetric function evaluation from 4D flow data

The observed biases for volumetric parameters obtained from standard bSSFP cines and 4D flow in this study are likely attributable to the use of FLASH for 4D flow magnitude data. Previous studies have reported up to a 19% overestimation of LVM when using native 2D cine FLASH, compared to cine bSSFP imaging, attributing this discrepancy to lower contrast in FLASH images, which impairs accurate differentiation between endocardial voxels containing blood or epicardial voxels with fat and the

myocardium (58–62). Similar to these studies, left ventricular stroke volumes were consistent across techniques in our study; however, unlike findings from contrast-enhanced 4D flow studies, this study revealed that native multislice 4D flow imaging slightly underestimated left ventricular volumes and overestimated left ventricular ejection fraction, with a more pronounced overestimation of left ventricular mass.

The larger bias observed here could be due to the lower in-plane resolution of reformatted magnitude cine images compared to the 2D cine FLASH images in prior studies, a limitation that may be less pronounced in contrast-enhanced data. left atrial volumes and ejection fraction (LATEF) showed high correlation between the two techniques, with no significant differences. Unlike the left ventricular myocardial wall, the left atrial wall is smooth, enabling accurate delineation of the left atrial cavity on reformatted 4D flow series comparable with cine bSSFP series. Employing the biplanar area-length method for volumetric evaluation of left atrium particularly benefits from retrospective reconstruction of evaluation planes, facilitating to assess optimally orientated left ventricular long axis cut planes (97).

In the present study the orientation and angulation of cine bSSFP long-axis images was carefully inspected and readjusted if necessary, resulting in a level of precision that may sometimes be overlooked in routine clinical cardiac magnetic resonance imaging assessments.

In our study cohort, which was free of cardiac shunts and significant valve regurgitations, mass conservation was applied to validate stroke volumes (57,98). Both volumetric stroke volumes exhibited a very high correlation with 4D flow-derived NFV without significant bias, which serves as mutual validation for both free-breathing cine bSSFP volumetry and 4D flow velocity data, as well as an added validation for 4D flow volumetry. Interestingly, the correlation between cine bSSFP and 4D flow SV with 4D flow-derived NFV did not differ, despite the fact that the 4D flow results were obtained from the same measurement. This is noteworthy, as a lower correlation might typically be anticipated between cine bSSFP SV and 4D flow NFV due to their sequential acquisition. The consistency in heart rate across measurements and the unchanged respiratory state indicate a stable physiological condition, which is often not given

between different sequences due to patient adjustments to the scanner, discomfort, anxiety, or contrast agent administration (99).

4.2.3 Diastolic velocity parameter evaluation from 4D flow data

Current guidelines for the non-invasive assessment of left ventricular diastolic function emphasize the need for precise measurement of parameters such as E, E/A, e', and E/e' (11). Consistent with previous studies that evaluated diastolic transmitral peak velocities using through-plane-encoded 2D flow measurements (18,43–48,100,101), this study found underestimation of E and A compared to echocardiography. A similar underestimation was observed for transmitral peak velocities derived from 4D flow when measured from a static short-axis plane at the mitral valve tips, a limitation noted previously for this approach (100,102). This underestimation of peak velocities derived from 2D flow, compared to those from 4D flow, can be attributed to the three-dimensional complexity of the transmitral velocity field, which is not fully captured by through-plane 2D flow; this discrepancy may be even greater in cases of valve pathology or abnormal flow patterns. Although 4D flow-derived E/A, evaluated from the region between the mitral valve leaflets in a 4-chamber view, showed no significant bias relative to echocardiography, transmitral peak velocities were still underestimated. Possible reasons for this include the thinner slice thickness in the multiplanar reconstructed planes and potential movement of the Doppler sample volume during measurement. Peak maximal velocities within the transmitral inflow volume provided the highest correlation with echocardiography across all 4D flow methods, allowing a bias free assessment of E and E/A relative to echocardiography. The underestimation of A might result from the high temporal resolution of the 4D flow protocol, set at the upper recommended limit (57), and the relatively short duration of the A-wave compared to the E-wave in healthy individuals (103). These findings align with recent research using a streamline-based approach for diastolic peak velocity assessment (104), underlining the need for a volume-based rather than slice-based evaluation strategy for accurate 4D flow-derived diastolic velocity assessment. While the *4D flow max-velocity method* demonstrated low intraobserver variability, indicating high

reproducibility for identifying the voxel with the highest velocity, variability was higher for other methods due to differences in slice selection among observers.

4D flow-derived septal, lateral, and average e' values, as well as E/e' from the *4D flow max-velocity method*, showed no significant differences compared to echocardiographic measurements. In contrast, 2D flow studies have reported a significant bias in e' measurements relative to echocardiography (43,47,48,18,101,105,106), potentially due to suboptimal slice positioning or orientation. A key advantage of 4D flow over 2D flow imaging is its capacity for a posteriori definition of evaluation planes, allowing for individualized optimization in terms of location and angulation to be perpendicular to the septal and lateral myocardium. Importantly, the high velocity encoding used in the 4D flow protocol did not impede the assessment of the low myocardial velocities in this study. Although a lower velocity encoding could have improved the velocity-to-noise ratio (63), it would require a separate measurement. As myocardial velocity assessment in this context is region of interest-based, averaging over numerous voxels produced a precise estimate of e'. Consistent with these findings, high correlations between 2D flow-derived and echocardiographic e' have been reported using velocity encoding values of 100 cm/s (44), low velocity encoding (43,47,48,101,105), or dual velocity encoding (106) protocols. Additionally, an alternative approach for deriving e' by cardiac magnetic resonance imaging is mitral valve insertion point tracking from cine bSSFP imaging (107). A study comparing e' from cine bSSFP with echocardiographic measurements in healthy subjects (108) found a minimal bias; however, the limits of agreement were nearly twice as wide as those observed in the present study.

The study population consisted of individuals without cardiovascular disease symptoms. The observation that differences between parameters derived from 4D flow and echocardiography did not vary with the magnitude of the parameters suggests that similar outcomes may be achievable in subjects with diastolic dysfunction, even with broader velocity ranges. A retrospective analysis of patients with diastolic dysfunction supported this generalization for both the 4-chamber and *4D flow max-velocity method* (3). Additionally, the more pronounced discrepancy in transmitral peak velocity E between echocardiography and the 4D flow SA-method in patients, compared to the

asymptomatic study population, highlights the advantage of using a volume-based approach to assess peak velocities.

4.3 Novel diagnostic parameter and clinical implications

4.3.1 Pulmonary arterial vortical flow as surrogate parameter for tricuspid regurgitation velocity

Phase contrast imaging could theoretically directly assess tricuspid regurgitant peak velocity, comparable to echocardiography (109,110); however, this approach would require an additional high velocity encoding flow measurement. Therefore, this study adopted a surrogate grading parameter for tricuspid regurgitation, as previously recommended (91). As described by the simplified Bernouilli equation, the peak tricuspid pressure gradient is directly related to systolic pulmonary arterial pressure, aside from right atrial pressure (111). A cutoff of TR > 2.8 m/s is commonly used to indicate possible pulmonary hypertension (112). The 4D flow-derived duration of vortical blood flow along the main pulmonary artery has demonstrated a segmented linear relationship to mean pulmonary arterial pressure, allowing elevated mean pressure (in mmHg) to be estimated from t_{vortex} via the formula: t_{vortex} via $16 + 0.63 \cdot t_{vortex}$ (113). Given the approximate proportionality between systolic and mean pulmonary arterial pressures (114), the close segmented linear relationship observed between pTR and t_{vortex} in this study is consistent with these findings. The model-derived 4D flow grading cutoff of t_{vortex} > 15%, employed as a surrogate for the echocardiographic TR > 2.8 m/s threshold, aligns with a mean pulmonary arterial pressure of approximately 25 mmHg—the former benchmark for pulmonary hypertension (112). Using these grading cutoffs, there was strong agreement between 4D flow and echocardiography in predicting elevated pulmonary arterial pressures, both in participants with detectable TR and across the entire cohort (with non-detectable TR interpreted as TR ≤ 2.8 m/s). It is noteworthy, however, that the current cutoff of t_{vortex} > 15% (corresponding to a mean pressure >25 mmHg) may not be the optimal threshold for 4D flow-based

detection of pulmonary hypertension. Lowering the threshold to t_{vortex} > 13% (reflecting a mean pressure >24 mmHg) would remain within the confidence interval for a TR of 2.8 m/s and more closely match the pulmonary hypertension definition. Nevertheless, this lower cutoff could reduce agreement between 4D flow and echocardiography, which aligns with the observation that t_{vortex} more accurately reflects elevated mean pulmonary arterial pressures than echocardiography when compared to measurements from a right heart catheter (115).

4.3.2 The left atrial acceleration factor as discriminator for advanced diastolic dysfunction

The left atrial acceleration factor derived from 4D flow, was initially proposed as a non-invasive approach to estimate PAWP in individuals at risk of or suffering from pulmonary hypertension (75). Results of the present study support the link between α and PAWP across a non-pulmonary hypertension cohort, showing that α can effectively differentiate between normal, indeterminate, or grade I diastolic dysfunction and more advanced diastolic dysfunction, where increased left ventricular filling pressures are present. Although α exhibited significant, yet only low to moderate correlations with echocardiographic parameters such as E, E/A, E/e', and LAVI, these levels of correlation are comparable to those found between echocardiographic metrics and invasive PAWP measurements (116,117). This result supports α's relevance as a PAWP indicator within a study group including individuals with normal left ventricular ejection fraction and patients with conditions like hypertrophic cardiomyopathy, restrictive cardiomyopathy, or aortic stenosis. Identifying advanced diastolic dysfunction—or elevated left ventricular filling pressures—is crucial not only for diagnosing heart failure, especially when left ventricular ejection fraction is preserved, but also for highlighting patients at greater risk for cardiovascular events and mortality across various conditions These conditions include patients undergoing hemodialysis (118,119), those with chronic kidney disease (120), individuals with either reduced or normal left ventricular ejection fraction (121,122), ischemic heart failure (123), post-

cardiac surgery (124), and patients who have undergone transcatheter aortic valve replacement (125,126).

The current standard for non-invasive detection of elevated left ventricular filling pressures involves comprehensive grading of left ventricular diastolic dysfunction using a detailed multiparametric echocardiographic algorithm, with specific thresholds set for parameters like E, E/A, E/e', e', TR, and LAVI (11). Although cardiac magnetic resonance imaging-based assessment could replicate the echocardiographic diagnostic flowchart (43,48,68) it is not yet widely adopted. In contrast, the 4D flow-derived parameter α offers a straightforward and reliable single-parameter alternative, achieving a level of diagnostic accuracy that other parameters—whether from echocardiography or cardiac magnetic resonance imaging—cannot match. The commonly used diastolic parameter E/e' has limited accuracy in cases with normal left ventricular ejection fraction (127,128) as well as in patients with pulmonary hypertension (129,130), hypertrophic cardiomyopathy (131), and in those with acutely decompensated reduced EF (132). Similarly, the relationship between enlarged LAVI and elevated left ventricular filling pressures is weakened in groups such as athletes, individuals with mitral valve disease, patients with atrial fibrillation (11,133), and those with persistent left atrial dilation following heart failure treatment (134). Although reduced left atrial strain has shown superior predictive power for elevated left ventricular filling pressures over other single diastolic markers (133,135–137), its diagnostic performance is lower compared to α.

In the model introduced in (75) for estimating PAWP non-invasively, α_{lower} was calculated using the maximum pulmonary venous inflow velocities from either the lower left or right pulmonary veins. In contrast, this study derived α from the highest inflow velocities observed across all pulmonary veins. Interestingly, the highest $(v_S+v_D)/2$ values were most commonly found in the upper left or right pulmonary vein for most subjects. Due to the strong correlation between α and α_{lower}, there was no notable difference in their effectiveness for identifying advanced diastolic dysfunction, suggesting that this condition could potentially be diagnosed with a shorter scan focusing on a 4D flow stack that excludes the full left atrium volume. However, it should be noted that because of a bias between α and α_{lower}, using the formula PAWP = -6.2

+ 10.1·α_{lower} from (75) would result in an approximate underestimation of PAWP by 3 mmHg when applied to α. For example, an α threshold of 1.58 for diagnosing advanced diastolic dysfunction would correspond to a PAWP of 13 mmHg rather than 10 mmHg, closely matching the pressures reported by Andersen et al. (117) across different levels of diastolic dysfunction.

The slightly higher α observed in the group with grade I diastolic dysfunction compared to the group with normal diastolic function, along with significant area-under-curves for differentiating normal from grade I diastolic function within non-advanced cases, suggests a marginally elevated PAWP in grade I diastolic dysfunction, though still within the normal range. The α difference of 0.14 between normal and grade I diastolic function would correspond to an estimated PAWP difference of about 1.5 mmHg, a finding consistent with invasive measurements reported in (138).

The echocardiographic analogue α_{Echo} derived through recommended methods for measuring peak pulmonary venous velocities (S and D) and early-diastolic transmitral E, showed poor correlation with α and lacked accuracy for identifying advanced diastolic dysfunction. Contributing to this result are factors such as the derivation of left atrial inflow velocities from only one pulmonary vein and suboptimal quality in pulmonary venous flow assessment by transthoracic echocardiography (9,139). Additionally, these findings may largely reflect the anatomical differences in the locations of left atrial inflow and outflow velocity measurements in echocardiography versus cardiac magnetic resonance tomography. As demonstrated in 4D flow datasets, the correlation between PAWP and the left atrial acceleration factor significantly diminishes when velocity measurements are taken at the mitral valve tips and 1 cm into the pulmonary vein rather than at the atrioventricular junction and pulmonary vein orifice (75).

4.4 Limitations of the study

This doctoral thesis study has several limitations. Although the present study was a prospective, medium-sized, single-center study, echocardiography and cardiac magnetic resonance imaging were performed at different times, which may have introduced variability in parameters. This timing difference was considered acceptable for assessing clinically relevant left ventricular diastolic dysfunction, as no changes in medication, particularly with vasodilators or diuretics, occurred between assessments that could influence loading conditions and therefore measurements (92). Subjects with irregular heart rhythms were excluded to avoid potential biases to echocardiography. As previous studies demonstrated high inter-rater reliability for all parameters used in the multiparametric algorithm (3,142), intra-observer reliability of grading was not assessed. Manual evaluation of 4D flow data as well as scan times limit the broader clinical applicability of the method; however, recent advances in magnetic resonance image acquisition and evaluation using artificial intelligence-supported accelerated protocols and automated segmentation algorithms could enhance its utility in the future.

Additional limitations of the study include the non-standard spatial and temporal resolution of cine real-time protocols for assessing the impact of respiration on cardiac function parameters. Since similar protocols were employed for breath-holding and free breathing image acquisitions, any acquisition protocol-dependent impact is expected to be minimal. Breath-holding was performed during inspiration, and parameter differences under expiratory breath-holding are assumed to be less pronounced (19,20). Patients with heart failure, valvular diseases, atrial fibrillation, arrhythmias, or pulmonary conditions were excluded to avoid potential variability in results due to altered intrathoracic pressures (145–147).

Moreover, the feasibility of assessment of volumetric function from 4D flow magnitude data was studied in individuals without cardiovascular symptoms, which offered the possibility to apply the principle of mass conservation for validation of the volumetric ventricular stroke volume with the pulmonary arterial net flow volume. Observed results could differ in patient populations with cardiovascular disease. Velocity encoding for 4D flow was optimized for intracardiac blood flow. The value of

velocity encoding does not impact the quality of 4D flow magnitude images (148), indicating that observed results would remain consistent for higher velocity encoding.

The fact that echocardiography and cardiac magnetic resonance tomography were not performed immediately after each other, might have impacted parameter correlation in the study. Physiological variations between echocardiography and cardiac magnetic resonance imaging measurements are likely mitigated by the large cohort size and stable heart rate between modalities.

Whole-heart 4D flow imaging required an average acquisition time of 22 minutes. Limiting the volumetric coverage to the main pulmonary artery, the left ventricle and the left atrium could reduce this time.

The postprocessing method of 4D flow mitral valve tracking (149) was not available for the present study. Adapting the evaluation plane in late diastole could alter results for diastolic peak velocities, and correction by myocardial tissue velocities would increase all transmitral velocities, consistent with echocardiographic determinations that do not incorporate this factor.

The introduction of the 4D flow-derived left atrial acceleration factor as novel 4D flow metrics for predicting advanced left ventricular diastolic dysfunction finally was a single-center proof-of-concept study. Invasive hemodynamic measurements were not available, and while the interval between cardiac magnetic resonance imaging and echocardiography was minimized, potential changes in filling pressures may have occurred. Additionally, the left atrial acceleration factor was derived from both, native and post-contrast 4D flow datasets. The use of contrast agent, however, is not expected to have a direct impact on velocities measured by 4D flow imaging (150).

5. Conclusion

In conclusion the results of this thesis project show that left ventricular diastolic dysfunction can be diagnosed and graded in nearly perfect agreement with echocardiography from a single 4D flow measurement (**MS4**). The suggested 4D flow-based algorithm could serve as a valuable noninvasive alternative approach to echocardiography, particularly for patients undergoing cardiac magnetic resonance imaging as part of a diagnostic evaluation or patients with poor echocardiographic image quality. Furthermore, this method may support future studies in validating new 4D flow parameters for assessing left ventricular diastolic dysfunction, especially through the use of concurrently acquired data.

Using cardiac magnetic resonance imaging for diagnosing left ventricular diastolic dysfunction comparable to echocardiographic results, respiratory state should be considered, particularly for follow-up results (**MS1**). 4D flow imaging enables accurate assessment of left ventricular and left atrial volumetric parameters during free breathing; however, aside from stroke volume, left ventricular volumetric measurements exhibit biases when compared to cine bSSFP imaging that have to be considered when comparing volumetric function parameter against their respective normal values (**MS2**). 4D flow provides accurate and reproducible measurement of transmitral and myocardial peak velocities for assessing left ventricular diastolic function, particularly when employing the *4D flow max-velocity method* (**MS3**). This approach supports the use of established echocardiographic thresholds for transmitral and myocardial tissue velocities and velocity ratios for echo-equivalent 4D flow-based evaluation of left ventricular diastolic dysfunction. Finally, the 4D flow-derived left atrial acceleration factor α effectively distinguishes advanced diastolic dysfunction (grade II and higher) from less advanced grades (**MS5**). The left atrial acceleration factor calculated from standard echocardiographic measurements, in contrast, cannot effectively differentiate advanced diastolic dysfunction.

6. Bibliography

1. Reiter C, Reiter U, Kräuter C, Nizhnikava V, Greiser A, Scherr D, et al. Differences in left ventricular and left atrial function assessed during breath-holding and breathing. European Journal of Radiology. 2021 Aug;141:109756.

2. Reiter C, Reiter G, Kräuter C, Scherr D, Schmidt A, Fuchsjäger M, et al. Evaluation of left ventricular and left atrial volumetric function from native MR multislice 4D flow magnitude data. Eur Radiol. 2024 Feb;34(2):981–93.

3. Reiter C, Reiter G, Kräuter C, Kolesnik E, Greiser A, Scherr D, et al. Impact of the evaluation method on 4D flow-derived diastolic transmitral and myocardial peak velocities: Comparison with echocardiography. European Journal of Radiology. 2024 Jan;170:111247.

4. Reiter C, Reiter G, Kräuter C, Kolesnik E, Scherr D, Schmidt A, et al. Magnetic resonance 4D flow-based diagnosis and grading of left ventricular diastolic dysfunction. (under review). 2024;

5. Reiter C, Reiter U, Kräuter C, Kolesnik E, Scherr D, Schmidt A, et al. MR 4D flow–derived left atrial acceleration factor for differentiating advanced left ventricular diastolic dysfunction. Eur Radiol. 2023 Nov 13;34(6):4065–76.

6. Heidenreich PA, Bozkurt B, Aguilar D, Allen LA, Byun JJ, Colvin MM, et al. 2022 AHA/ACC/HFSA Guideline for the Management of Heart Failure: A Report of the American College of Cardiology/American Heart Association Joint Committee on Clinical Practice Guidelines. Circulation [Internet]. 2022 May 3 [cited 2024 Jun 29];145(18). Available from: https://www.ahajournals.org/doi/10.1161/CIR.0000000000001063

7. Oh JK, Park SJ, Nagueh SF. Established and Novel Clinical Applications of Diastolic Function Assessment by Echocardiography. Circ: Cardiovascular Imaging. 2011 Jul;4(4):444–55.

8. Klein AL, Garcia MJ, ScienceDirect (Online service), editors. Diastology: clinical approach to diastolic heart failure. 1st ed. Philadelphia: Saunders/Elsevier; 2008. 451 p. (ClinicalKey).

9. Nagueh SF, Appleton CP, Gillebert TC, Marino PN, Oh JK, Smiseth OA, et al. Recommendations for the evaluation of left ventricular diastolic function by echocardiography. Eur J Echocardiogr. 2009 Mar;10(2):165–93.

10. Nagueh SF, Smiseth OA, Appleton CP, Byrd BF, Dokainish H, Edvardsen T, et al. Recommendations for the Evaluation of Left Ventricular Diastolic Function by Echocardiography: An Update from the American Society of Echocardiography

and the European Association of Cardiovascular Imaging. Journal of the American Society of Echocardiography. 2016 Apr;29(4):277–314.

11. Nagueh SF, Smiseth OA, Appleton CP, Byrd BF, Dokainish H, Edvardsen T, et al. Recommendations for the Evaluation of Left Ventricular Diastolic Function by Echocardiography: An Update from the American Society of Echocardiography and the European Association of Cardiovascular Imaging. Journal of the American Society of Echocardiography. 2016 Apr;29(4):277–314.

12. Schulz-Menger J, Bluemke DA, Bremerich J, Flamm SD, Fogel MA, Friedrich MG, et al. Standardized image interpretation and post-processing in cardiovascular magnetic resonance - 2020 update: Society for Cardiovascular Magnetic Resonance (SCMR): Board of Trustees Task Force on Standardized Post-Processing. J Cardiovasc Magn Reson. 2020 Dec;22(1):19.

13. Kawel-Boehm N, Hetzel SJ, Ambale-Venkatesh B, Captur G, Francois CJ, Jerosch-Herold M, et al. Reference ranges (“normal values”) for cardiovascular magnetic resonance (CMR) in adults and children: 2020 update. Journal of Cardiovascular Magnetic Resonance. 2020 Jan;22(1):87.

14. Maceira AM, Cosín-Sales J, Roughton M, Prasad SK, Pennell DJ. Reference left atrial dimensions and volumes by steady state free precession cardiovascular magnetic resonance. J Cardiovasc Magn Reson. 2010;12(1):65.

15. Aquaro GD, Pizzino F, Terrizzi A, Carerj S, Khandheria BK, Di Bella G. Diastolic dysfunction evaluated by cardiac magnetic resonance: the value of the combined assessment of atrial and ventricular function. Eur Radiol. 2019 Mar;29(3):1555–64.

16. Mendoza DD, Codella NC, Wang Y, Prince MR, Sethi S, Manoushagian SJ, et al. Impact of diastolic dysfunction severity on global left ventricular volumetric filling - assessment by automated segmentation of routine cine cardiovascular magnetic resonance. J Cardiovasc Magn Reson. 2010;12(1):46.

17. Kawaji K, Codella NCF, Prince MR, Chu CW, Shakoor A, LaBounty TM, et al. Automated Segmentation of Routine Clinical Cardiac Magnetic Resonance Imaging for Assessment of Left Ventricular Diastolic Dysfunction. Circ Cardiovasc Imaging. 2009 Nov;2(6):476–84.

18. Bollache E, Redheuil A, Clément-Guinaudeau S, Defrance C, Perdrix L, Ladouceur M, et al. Automated left ventricular diastolic function evaluation from phase-contrast cardiovascular magnetic resonance and comparison with Doppler echocardiography. J Cardiovasc Magn Reson. 2010 Dec;12(1):63.

19. Ashrafpoor G, Bollache E, Redheuil A, De Cesare A, Giron A, Defrance C, et al. Age-specific changes in left ventricular diastolic function: A velocity-encoded magnetic resonance imaging study. Eur Radiol. 2015 Apr;25(4):1077–86.

20. Westenberg JJM. CMR for Assessment of Diastolic Function. Curr Cardiovasc Imaging Rep. 2011 Apr;4(2):149–58.

21. Chamsi-Pasha MA, Zhan Y, Debs D, Shah DJ. CMR in the Evaluation of Diastolic Dysfunction and Phenotyping of HFpEF. JACC: Cardiovascular Imaging. 2020 Jan;13(1):283–96.

22. Caudron J, Fares J, Bauer F, Dacher JN. Evaluation of Left Ventricular Diastolic Function with Cardiac MR Imaging. RadioGraphics. 2011 Jan;31(1):239–59.

23. Backhaus SJ, Staab W, Steinmetz M, Ritter CO, Lotz J, Hasenfuß G, et al. Fully automated quantification of biventricular volumes and function in cardiovascular magnetic resonance: applicability to clinical routine settings. J Cardiovasc Magn Reson. 2019 Dec;21(1):24.

24. Kramer CM, Barkhausen J, Bucciarelli-Ducci C, Flamm SD, Kim RJ, Nagel E. Standardized cardiovascular magnetic resonance imaging (CMR) protocols: 2020 update. J Cardiovasc Magn Reson. 2020 Dec;22(1):17.

25. Cui C, Yin G, Lu M, Chen X, Cheng S, Li L, et al. Retrospective Electrocardiography-Gated Real-Time Cardiac Cine MRI at 3T: Comparison with Conventional Segmented Cine MRI. Korean J Radiol. 2019;20(1):114.

26. Schalla S, Nagel E, Lehmkuhl H, Klein C, Bornstedt A, Schnackenburg B, et al. Comparison of magnetic resonance real-time imaging of left ventricular function with conventional magnetic resonance imaging and echocardiography. The American Journal of Cardiology. 2001 Jan;87(1):95–9.

27. Vermersch M, Longère B, Coisne A, Schmidt M, Forman C, Monnet A, et al. Compressed sensing real-time cine imaging for assessment of ventricular function, volumes and mass in clinical practice. Eur Radiol. 2020 Jan;30(1):609–19.

28. Kühl HP, Spuentrup E, Wall A, Franke A, Schröder J, Heussen N, et al. Assessment of Myocardial Function with Interactive Non–Breath-hold Real-time MR Imaging: Comparison with Echocardiography and Breath-hold Cine MR Imaging. Radiology. 2004 Apr;231(1):198–207.

29. Hori Y, Yamada N, Higashi M, Hirai N, Nakatani S. Rapid Evaluation Of Right And Left Ventricular Function And Mass Using Real-time True-fisp Cine Mr Imaging Without Breath-hold: Comparison With Segmented True-fisp Cine Mr Imaging With Breath-hold. Journal of Cardiovascular Magnetic Resonance. 2003;5(3):439–50.

30. Ma Y, Hou Y, Ma Q, Wang X, Sui S, Wang B. Compressed SENSE single-breath-hold and free-breathing cine imaging for accelerated clinical evaluation of the left ventricle. Clinical Radiology. 2019 Apr;74(4):325.e9-325.e17.

31. Kaji S, Yang PC, Kerr AB, Tang WHW, Meyer CH, Macovski A, et al. Rapid evaluation of left ventricular volume and mass without breath-holding using real-time interactive cardiac magnetic resonance imaging system. Journal of the American College of Cardiology. 2001 Aug;38(2):527–33.

32. Costalat G, Pichon A, Joulia F, Lemaître F. Modeling the diving bradycardia: Toward an “oxygen-conserving breaking point”? Eur J Appl Physiol. 2015 Jul;115(7):1475–84.

33. Taboni A, Vinetti G, Bruseghini P, Camelio S, D’Elia M, Moia C, et al. Cardiovascular responses to dry apnoeas at exercise in air and in pure oxygen. Respiratory Physiology & Neurobiology. 2018 Sep;255:17–21.

34. Magnani S, Mulliri G, Sainas G, Ghiani G, Pinna V, Sanna I, et al. Occurrence of cardiac output decrease (via stroke volume) is more pronounced in women than in men during prolonged dry static apnea. Journal of Applied Physiology. 2018 Feb 1;124(2):349–55.

35. Russo MA, Santarelli DM, O’Rourke D. The physiological effects of slow breathing in the healthy human. Breathe. 2017 Dec;13(4):298–309.

36. Verhoeff K, Mitchell JR. Cardiopulmonary physiology: why the heart and lungs are inextricably linked. Advances in Physiology Education. 2017 Sep 1;41(3):348–53.

37. Palada I, Eterović D, Obad A, Bakovic D, Valic Z, Ivancev V, et al. Spleen and cardiovascular function during short apneas in divers. Journal of Applied Physiology. 2007 Dec;103(6):1958–63.

38. Albanese A, Limei Cheng, Ursino M, Chbat NW. Cardiorespiratory adaptation to breath-holding in air: Analysis via a cardiopulmonary simulation model. In: 2015 37th Annual International Conference of the IEEE Engineering in Medicine and Biology Society (EMBC) [Internet]. Milan: IEEE; 2015 [cited 2020 Mar 27]. p. 7788–91. Available from: http://ieeexplore.ieee.org/document/7320198/

39. Kido T, Kido T, Nakamura M, Watanabe K, Schmidt M, Forman C, et al. Assessment of Left Ventricular Function and Mass on Free-Breathing Compressed Sensing Real-Time Cine Imaging. Circ J. 2017;81(10):1463–8.

40. Roifman I, Gutierrez J, Wang E, Biswas L, Sparkes J, Connelly KA, et al. Evaluating a novel free-breathing accelerated cardiac MRI cine sequence in patients with cardiomyopathy. Magnetic Resonance Imaging. 2019 Sep;61:260–6.

41. Sudarski S, Henzler T, Haubenreisser H, Dösch C, Zenge MO, Schmidt M, et al. Free-breathing Sparse Sampling Cine MR Imaging with Iterative Reconstruction for the Assessment of Left Ventricular Function and Mass at 3.0 T. Radiology. 2017 Jan;282(1):74–83.

42. Wu Y, Wan Q, Zhao J, Liu X, Zheng H, Chung YC, et al. Improved workflow for quantifying left ventricular function via cardiorespiratory-resolved analysis of free-breathing MR real-time cines: Improved Workflow to Quantify LV Function. J Magn Reson Imaging. 2017 Sep;46(3):905–14.

43. Ramos JG, Fyrdahl A, Wieslander B, Thalén S, Reiter G, Reiter U, et al. Comprehensive Cardiovascular Magnetic Resonance Diastolic Dysfunction Grading Shows Very Good Agreement Compared With Echocardiography. JACC: Cardiovascular Imaging. 2020 Aug;S1936878X20306008.

44. Buss SJ, Krautz B, Schnackenburg B, Abdel-Aty H, Santos MFB, Andre F, et al. Classification of diastolic function with phase-contrast cardiac magnetic resonance imaging: validation with echocardiography and age-related reference values. Clin Res Cardiol. 2014 Jun;103(6):441–50.

45. Hartiala JJ, Mostbeck GH, Foster E, Fujita N, Dulce MC, Chazouilleres AF, et al. Velocity-encoded cine MRI in the evaluation of left ventricular diastolic function: Measurement of mitral valve and pulmonary vein flow velocities and flow volume across the mitral valve. American Heart Journal. 1993 Apr;125(4):1054–66.

46. Rubinshtein R, Glockner JF, Feng D, Araoz PA, Kirsch J, Syed IS, et al. Comparison of Magnetic Resonance Imaging Versus Doppler Echocardiography for the Evaluation of Left Ventricular Diastolic Function in Patients With Cardiac Amyloidosis. The American Journal of Cardiology. 2009 Mar;103(5):718–23.

47. Fyrdahl A, Ramos JG, Eriksson MJ, Caidahl K, Ugander M, Sigfridsson A. Sector-wise golden-angle phase contrast with high temporal resolution for evaluation of left ventricular diastolic dysfunction. Magn Reson Med. 2020 Apr;83(4):1310–21.

48. Paelinck BP, de Roos A, Bax JJ, Bosmans JM, van Der Geest RJ, Dhondt D, et al. Feasibility of tissue magnetic resonance imaging. Journal of the American College of Cardiology. 2005 Apr;45(7):1109–16.

49. Rathi VK, Doyle M, Yamrozik J, Williams RB, Caruppannan K, Truman C, et al. Routine evaluation of left ventricular diastolic function by cardiovascular magnetic resonance: A practical approach. J Cardiovasc Magn Reson. 2008 Dec;10(1):36.

50. Rajiah PS, Moore A, Broncano J, Anand V, Kolluri N, Shah DJ, et al. Diastology with Cardiac MRI: A Practical Guide. RadioGraphics. 2023 Aug 1;43(9):e220144.

51. Chamsi-Pasha MA, Zhan Y, Debs D, Shah DJ. CMR in the Evaluation of Diastolic Dysfunction and Phenotyping of HFpEF. JACC: Cardiovascular Imaging. 2020 Jan;13(1):283–96.

52. Ashkir Z, Myerson S, Neubauer S, Carlhäll CJ, Ebbers T, Raman B. Four-dimensional flow cardiac magnetic resonance assessment of left ventricular diastolic function. Front Cardiovasc Med. 2022 Jul 22;9:866131.

53. Dyverfeldt P, Bissell M, Barker AJ, Bolger AF, Carlhäll CJ, Ebbers T, et al. 4D flow cardiovascular magnetic resonance consensus statement. Journal of Cardiovascular Magnetic Resonance. 2015 Jan;17(1):72.

54. Bissell MM, Raimondi F, Ait Ali L, Allen BD, Barker AJ, Bolger A, et al. 4D Flow cardiovascular magnetic resonance consensus statement: 2023 update. Journal of Cardiovascular Magnetic Resonance. 2023 Feb;25(1):40.

55. Qin JJ, Indja B, Gholipour A, Gök M, Grieve SM. Evaluation of Left Ventricular Function Using Four-Dimensional Flow Cardiovascular Magnetic Resonance: A Systematic Review. JCDD. 2022 Sep 12;9(9):304.

56. Zhuang B, Sirajuddin A, Zhao S, Lu M. The role of 4D flow MRI for clinical applications in cardiovascular disease: current status and future perspectives. Quant Imaging Med Surg. 2021 Sep;11(9):4193–210.

57. Dyverfeldt P, Bissell M, Barker AJ, Bolger AF, Carlhäll CJ, Ebbers T, et al. 4D flow cardiovascular magnetic resonance consensus statement. J Cardiovasc Magn Reson. 2015 Dec;17(1):72.

58. Mukai K, Burris NS, Mahadevan VS, Foster ED, Ordovas KG, Hope MD. 4D flow image quality with blood pool contrast: a comparison of gadofosveset trisodium and ferumoxytol. Int J Cardiovasc Imaging. 2018 Feb;34(2):273–9.

59. Hanneman K, Kino A, Cheng JY, Alley MT, Vasanawala SS. Assessment of the precision and reproducibility of ventricular volume, function, and mass measurements with ferumoxytol-enhanced 4D flow MRI: 4D Flow MRI Assessment of Ventricular Mass. J Magn Reson Imaging. 2016 Aug;44(2):383–92.

60. Vial J, Bouzerar R, Pichois R, Lhostis F, Raad O, Mathiron A, et al. MRI Assessment of Right Ventricular Volumes and Function in Patients With Repaired Tetralogy of Fallot Using kat-ARC Accelerated Sequences. American Journal of Roentgenology. 2020 Oct;215(4):807–17.

61. Hsiao A, Lustig M, Alley MT, Murphy M, Chan FP, Herfkens RJ, et al. Rapid Pediatric Cardiac Assessment of Flow and Ventricular Volume With Compressed Sensing Parallel Imaging Volumetric Cine Phase-Contrast MRI. American Journal of Roentgenology. 2012 Mar;198(3):W250–9.

62. Yao X, Hu L, Peng Y, Feng F, Ouyang R, Xie W, et al. Right and left ventricular function and flow quantification in pediatric patients with repaired tetralogy of Fallot using four-dimensional flow magnetic resonance imaging. BMC Med Imaging. 2021 Dec;21(1):161.

63. Nayak KS, Nielsen JF, Bernstein MA, Markl M, D. Gatehouse P, M. Botnar R, et al. Cardiovascular magnetic resonance phase contrast imaging. J Cardiovasc Magn Reson. 2015 Dec;17(1):71.

64. Moon JCC, Lorenz CH, Francis JM, Smith GC, Pennell DJ. Breath-hold FLASH and FISP Cardiovascular MR Imaging: Left Ventricular Volume Differences and Reproducibility. Radiology. 2002 Jun;223(3):789–97.

65. Peng Y, Su X, Hu L, Wang Q, Ouyang R, Sun A, et al. Feasibility of Three-Dimensional Balanced Steady-State Free Precession Cine Magnetic Resonance Imaging Combined with an Image Denoising Technique to Evaluate Cardiac Function in Children with Repaired Tetralogy of Fallot. Korean J Radiol. 2021;22(9):1525.

66. Ramalho J, Semelka RC, Ramalho M, Nunes RH, AlObaidy M, Castillo M. Gadolinium-Based Contrast Agent Accumulation and Toxicity: An Update. American Journal of Neuroradiology. 2016 Jul 1;37(7):1192–8.

67. Vasanawala SS, Nguyen KL, Hope MD, Bridges MD, Hope TA, Reeder SB, et al. Safety and technique of ferumoxytol administration for MRI: Safety and Technique of Ferumoxytol Administration for MRI. Magn Reson Med. 2016 May;75(5):2107–11.

68. Ramos JG, Fyrdahl A, Wieslander B, Reiter G, Reiter U, Jin N, et al. Cardiovascular magnetic resonance 4D flow analysis has a higher diagnostic yield than Doppler echocardiography for detecting increased pulmonary artery pressure. BMC Med Imaging. 2020 06;20(1):28.

69. Pelc NJ, Bernstein MA, Shimakawa A, Glover GH. Encoding strategies for three-direction phase-contrast MR imaging of flow. J Magn Reson Imaging. 1991 Aug;1(4):405–13.

70. Schulz-Menger J, Bluemke DA, Bremerich J, Flamm SD, Fogel MA, Friedrich MG, et al. Standardized image interpretation and post-processing in cardiovascular magnetic resonance - 2020 update. Journal of Cardiovascular Magnetic Resonance. 2020 Jan;22(1):19.

71. Sievers B, Kirchberg S, Addo M, Bakan A, Brandts B, Trappe H. Assessment of Left Atrial Volumes in Sinus Rhythm and Atrial Fibrillation Using the Biplane Area?Length Method and Cardiovascular Magnetic Resonance Imaging with TrueFISP. J Cardiovasc Magn Reson. 2004;6(4):855–63.

72. Suinesiaputra A, Bluemke DA, Cowan BR, Friedrich MG, Kramer CM, Kwong R, et al. Quantification of LV function and mass by cardiovascular magnetic resonance: multi-center variability and consensus contours. Journal of Cardiovascular Magnetic Resonance. 2015 Jan;17(1):63.

73. Contijoch F, Witschey WRT, Rogers K, Gorman J, Gorman RC, Ferrari V, et al. Impact of end-diastolic and end-systolic phase selection in the volumetric evaluation of cardiac MRI. Magnetic Resonance Imaging. 2016 Mar;43(3):585–93.

74. Reiter G, Reiter U, Kovacs G, Olschewski H, Fuchsjäger M. Blood flow vortices along the main pulmonary artery measured with MR imaging for diagnosis of pulmonary hypertension. Radiology. 2015 Apr;275(1):71–9.

75. Reiter G, Kovacs G, Reiter C, Schmidt A, Fuchsjäger M, Olschewski H, et al. Left atrial acceleration factor as a magnetic resonance 4D flow measure of mean pulmonary artery wedge pressure in pulmonary hypertension. Front Cardiovasc Med. 2022 Aug 3;9:972142.

76. Mukaka MM. Statistics corner: A guide to appropriate use of correlation coefficient in medical research. Malawi Med J. 2012 Sep;24(3):69–71.

77. Koo TK, Li MY. A Guideline of Selecting and Reporting Intraclass Correlation Coefficients for Reliability Research. Journal of Chiropractic Medicine. 2016 Jun;15(2):155–63.

78. James SH, Wald R, Wintersperger BJ, Jimenez-Juan L, Deva D, Crean AM, et al. Accuracy of Right and Left Ventricular Functional Assessment by Short-Axis vs Axial Cine Steady-State Free-Precession Magnetic Resonance Imaging: Intrapatient Correlation with Main Pulmonary Artery and Ascending Aorta Phase-Contrast Flow Measurements. Can Assoc Radiol J. 2013 Aug;64(3):213–9.

79. Reiter G, Kovacs G, Reiter C, Schmidt A, Fuchsjäger M, Olschewski H, et al. Left atrial acceleration factor as a magnetic resonance 4D flow measure of mean pulmonary artery wedge pressure in pulmonary hypertension. Front Cardiovasc Med. 2022 Aug 3;9:972142.

80. Dorosz JL, Lezotte DC, Weitzenkamp DA, Allen LA, Salcedo EE. Performance of 3-Dimensional Echocardiography in Measuring Left Ventricular Volumes and Ejection Fraction. Journal of the American College of Cardiology. 2012 May;59(20):1799–808.

81. Zhao L, Lu A, Tian J, Huang J, Ma X. Effects of Different LVEF Assessed by Echocardiography and CMR on the Diagnosis and Therapeutic Decisions of Cardiovascular Diseases. Front Physiol. 2020 Jun 16;11:679.

82. Shimada YJ, Shiota T. A Meta-Analysis and Investigation for the Source of Bias of Left Ventricular Volumes and Function by Three-Dimensional Echocardiography in Comparison With Magnetic Resonance Imaging. The American Journal of Cardiology. 2011 Jan;107(1):126–38.

83. Whitlock M, Garg A, Gelow J, Jacobson T, Broberg C. Comparison of Left and Right Atrial Volume by Echocardiography Versus Cardiac Magnetic Resonance

Imaging Using the Area-Length Method. The American Journal of Cardiology. 2010 Nov;106(9):1345–50.

84. Rodevand O, Bjornerheim R, Ljosland M, Maehle J, Smith HJ, Ihlen H. Left atrial volumes assessed by three- and two-dimensional echocardiography compared to MRI estimates. The International Journal of Cardiac Imaging. 1999;15(5):397–410.

85. Alattar Y, Soulat G, Gencer U, Messas E, Bollache E, Kachenoura N, et al. Left ventricular diastolic early and late filling quantified from 4D flow magnetic resonance imaging. Diagnostic and Interventional Imaging. 2022 Jul;103(7–8):345–52.

86. Njoku P, Grafton-Clarke C, Assadi H, Gosling R, Archer G, Swift AJ, et al. Validation of time-resolved, automated peak trans-mitral velocity tracking: Two center four-dimensional flow cardiovascular magnetic resonance study. International Journal of Cardiology. 2022 Oct;364:148–56.

87. Fyrdahl A, Ramos JG, Eriksson MJ, Caidahl K, Ugander M, Sigfridsson A. Sector-wise golden-angle phase contrast with high temporal resolution for evaluation of left ventricular diastolic dysfunction. Magnetic Resonance in Med. 2020 Apr;83(4):1310–21.

88. Paelinck BP, De Roos A, Bax JJ, Bosmans JM, Van Der Geest RJ, Dhondt D, et al. Feasibility of tissue magnetic resonance imaging. Journal of the American College of Cardiology. 2005 Apr;45(7):1109–16.

89. Buss SJ, Krautz B, Schnackenburg B, Abdel-Aty H, Santos MFB, Andre F, et al. Classification of diastolic function with phase-contrast cardiac magnetic resonance imaging: validation with echocardiography and age-related reference values. Clin Res Cardiol. 2014 Jun;103(6):441–50.

90. Fujikura K, Sathya B, Acharya T, Benovoy M, Jacobs M, Sachdev V, et al. CMR provides comparable measurements of diastolic function as echocardiography. Sci Rep. 2024 May 22;14(1):11658.

91. Ramos JG, Fyrdahl A, Wieslander B, Thalén S, Reiter G, Reiter U, et al. Comprehensive Cardiovascular Magnetic Resonance Diastolic Dysfunction Grading Shows Very Good Agreement Compared With Echocardiography. JACC: Cardiovascular Imaging. 2020 Dec;13(12):2530–42.

92. Bahrami HSZ, Pedersen FHG, Myhr KA, Møgelvang R, Hassager C. Feasibility, repeatability, and reproducibility of contemporary diastolic parameters and classification. Int J Cardiovasc Imaging. 2021 Mar;37(3):931–44.

93. Holst K, Ugander M, Sigfridsson A. Respiratory variation in left ventricular cardiac function with 3D double golden-angle whole-heart cine imaging: Respiratory

Variation in LV Volumes With Golden-Angle Imaging. Magn Reson Med. 2018 May;79(5):2693–701.

94. Claessen G, Claus P, Delcroix M, Bogaert J, Gerche AL, Heidbuchel H. Interaction between respiration and right versus left ventricular volumes at rest and during exercise: a real-time cardiac magnetic resonance study. American Journal of Physiology-Heart and Circulatory Physiology. 2014 Mar 15;306(6):H816–24.

95. Graça B, Ferreira MJ, Donato P, Castelo-Branco M, Caseiro-Alves F. Cardiovascular magnetic resonance imaging assessment of diastolic dysfunction in a population without heart disease: a gender-based study. Eur Radiol. 2014 Jan;24(1):52–9.

96. Triulzi MO, Castini D, Ornaghi M, Vitolo E. Effects of preload reduction on mitral flow velocity pattern in normal subjects. The American Journal of Cardiology. 1990 Oct;66(12):995–1001.

97. Kebed K, Kruse E, Addetia K, Ciszek B, Thykattil M, Guile B, et al. Atrial-focused views improve the accuracy of two-dimensional echocardiographic measurements of the left and right atrial volumes: a contribution to the increase in normal values in the guidelines update. Int J Cardiovasc Imaging. 2017 Feb;33(2):209–18.

98. Reiter U, Reiter C, Kräuter C, Nizhnikava V, Fuchsjäger MH, Reiter G. Quantitative Clinical Cardiac Magnetic Resonance Imaging. Fortschr Röntgenstr. 2019 Nov 20;a-0999-5716.

99. Bertelsen L, Vejlstrup N, Andreasen L, Olesen MS, Svendsen JH. Cardiac magnetic resonance systematically overestimates mitral regurgitations by the indirect method. Open Heart. 2020 Jul;7(2):e001323.

100. Alattar Y, Soulat G, Gencer U, Messas E, Bollache E, Kachenoura N, et al. Left ventricular diastolic early and late filling quantified from 4D flow magnetic resonance imaging. Diagnostic and Interventional Imaging. 2022 Jul;103(7–8):345–52.

101. Marsan NA, Westenberg JJM, Tops LF, Ypenburg C, Holman ER, Reiber JHC, et al. Comparison Between Tissue Doppler Imaging and Velocity-Encoded Magnetic Resonance Imaging for Measurement of Myocardial Velocities, Assessment of Left Ventricular Dyssynchrony, and Estimation of Left Ventricular Filling Pressures in Patients With Ischemic Cardiomyopathy. The American Journal of Cardiology. 2008 Nov;102(10):1366–72.

102. Brandts A, Bertini M, van Dijk EJ, Delgado V, Marsan NA, van der Geest RJ, et al. Left ventricular diastolic function assessment from three-dimensional three-directional velocity-encoded MRI with retrospective valve tracking. J Magn Reson Imaging. 2011 Feb;33(2):312–9.

103. Chung CS, Karamanoglu M, Kovács SJ. Duration of diastole and its phases as a function of heart rate during supine bicycle exercise. American Journal of Physiology-Heart and Circulatory Physiology. 2004 Nov;287(5):H2003–8.

104. Njoku P, Grafton-Clarke C, Assadi H, Gosling R, Archer G, Swift AJ, et al. Validation of time-resolved, automated peak trans-mitral velocity tracking: Two center four-dimensional flow cardiovascular magnetic resonance study. International Journal of Cardiology. 2022 Oct;364:148–56.

105. Delfino JG, Bhasin M, Cole R, Eisner RL, Merlino J, Leon AR, et al. Comparison of myocardial velocities obtained with magnetic resonance phase velocity mapping and tissue doppler imaging in normal subjects and patients with left ventricular dyssynchrony. J Magn Reson Imaging. 2006 Aug;24(2):304–11.

106. Ajala A, Zhang J, Pednekar A, Buko E, Wang L, Cheong BY, et al. Mitral Valve Flow and Myocardial Motion Assessed with Dual-Echo Dual-Velocity Cardiac MRI. Radiology: Cardiothoracic Imaging. 2020 Jun 1;2(3):e190126.

107. Wu V, Chyou JY, Chung S, Bhagavatula S, Axel L. Evaluation of diastolic function by three-dimensional volume tracking of the mitral annulus with cardiovascular magnetic resonance: comparison with tissue Doppler imaging. J Cardiovasc Magn Reson. 2014 Dec;16(1):71.

108. Thavendiranathan P, Guetter C, da Silveira JS, Lu X, Scandling D, Xue H, et al. Mitral annular velocity measurement with cardiac magnetic resonance imaging using a novel annular tracking algorithm: Validation against echocardiography. Magnetic Resonance Imaging. 2019 Jan;55:72–80.

109. Nogami M, Ohno Y, Koyama H, Kono A, Takenaka D, Kataoka T, et al. Utility of phase contrast MR imaging for assessment of pulmonary flow and pressure estimation in patients with pulmonary hypertension: Comparison with right heart catheterization and echocardiography. Magnetic Resonance Imaging. 2009 Nov;30(5):973–80.

110. Reiter U, Reiter G, Fuchsjäger M. MR phase-contrast imaging in pulmonary hypertension. BJR. 2016 Jul;89(1063):20150995.

111. Chemla D, Castelain V, Herve P, Lecarpentier Y, Brimioulle S. Haemodynamic evaluation of pulmonary hypertension. European Respiratory Journal. 2002 Nov 1;20(5):1314–31.

112. Humbert M, Kovacs G, Hoeper MM, Badagliacca R, Berger RMF, Brida M, et al. 2022 ESC/ERS Guidelines for the diagnosis and treatment of pulmonary hypertension. European Heart Journal. 2022 Oct 11;43(38):3618–731.

113. Reiter G, Reiter U, Kovacs G, Olschewski H, Fuchsjäger M. Blood Flow Vortices along the Main Pulmonary Artery Measured with MR Imaging for Diagnosis of Pulmonary Hypertension. Radiology. 2015 Apr;275(1):71–9.

114. Chemla D, Castelain V, Provencher S, Humbert M, Simonneau G, Hervé P. Evaluation of Various Empirical Formulas for Estimating Mean Pulmonary Artery Pressure by Using Systolic Pulmonary Artery Pressure in Adults. Chest. 2009 Mar;135(3):760–8.

115. Ramos JG, Wieslander B, Fyrdahl A, Reiter G, Reiter U, Jin N, et al. Pulmonary Hypertension by Catheterization Is More Accurately Detected by Cardiovascular Magnetic Resonance 4D-Flow Than Echocardiography. JACC: Cardiovascular Imaging. 2023 Apr;16(4):558–9.

116. Venkateshvaran A, Tureli HO, Faxén UL, Lund LH, Tossavainen E, Lindqvist P. Left atrial reservoir strain improves diagnostic accuracy of the 2016 ASE/EACVI diastolic algorithm in patients with preserved left ventricular ejection fraction: insights from the KARUM haemodynamic database. European Heart Journal - Cardiovascular Imaging. 2022 Aug 22;23(9):1157–68.

117. Andersen OS, Smiseth OA, Dokainish H, Abudiab MM, Schutt RC, Kumar A, et al. Estimating Left Ventricular Filling Pressure by Echocardiography. Journal of the American College of Cardiology. 2017 Apr;69(15):1937–48.

118. Barberato SH, Bucharles SGE, Sousa AM, Costantini CO, Costantini CRF, Pecoits-Filho R. Prevalência e impacto prognóstico da disfunção diastólica na doença renal crônica em hemodiálise. Arq Bras Cardiol. 2010 Apr;94(4):457–62.

119. De Lima JJG, Macedo TA, Gowdak LHW, David-Neto E, Bortolotto LA. Diastolic and systolic left ventricular dysfunction and mortality in chronic kidney disease patients on haemodialysis. Nephrology. 2022 Jan;27(1):66–73.

120. Suh SH, Oh TR, Choi HS, Kim CS, Bae EH, Oh KH, et al. Association of Left Ventricular Diastolic Dysfunction With Cardiovascular Outcomes in Patients With Pre-dialysis Chronic Kidney Disease: Findings From KNOW-CKD Study. Front Cardiovasc Med. 2022 Mar 25;9:844312.

121. Playford D, Strange G, Celermajer DS, Evans G, Scalia GM, Stewart S, et al. Diastolic dysfunction and mortality in 436 360 men and women: the National Echo Database Australia (NEDA). European Heart Journal - Cardiovascular Imaging. 2021 Apr 28;22(5):505–15.

122. Pezawas T, Burger AL, Binder T, Diedrich A. Importance of Diastolic Function for the Prediction of Arrhythmic Death: A Prospective, Observer-Blinded, Long-Term Study. Circ: Arrhythmia and Electrophysiology. 2020 Feb;13(2):e007757.

123. Kim KH, She L, Lee KL, Dabrowski R, Grayburn PA, Rajda M, et al. Incremental prognostic value of echocardiography of left ventricular remodeling and diastolic function in STICH trial. Cardiovasc Ultrasound. 2020 Dec;18(1):17.

124. Metkus TS, Suarez-Pierre A, Crawford TC, Lawton JS, Goeddel L, Dodd-o J, et al. Diastolic dysfunction is common and predicts outcome after cardiac surgery. J Cardiothorac Surg. 2018 Dec;13(1):67.

125. Asami M, Lanz J, Stortecky S, Räber L, Franzone A, Heg D, et al. The Impact of Left Ventricular Diastolic Dysfunction on Clinical Outcomes After Transcatheter Aortic Valve Replacement. JACC: Cardiovascular Interventions. 2018 Mar;11(6):593–601.

126. Kampaktsis PN, Kokkinidis DG, Wong SC, Vavuranakis M, Skubas NJ, Devereux RB. The role and clinical implications of diastolic dysfunction in aortic stenosis. Heart. 2017 Oct;103(19):1481–7.

127. Sharifov OF, Schiros CG, Aban I, Denney TS, Gupta H. Diagnostic Accuracy of Tissue Doppler Index E/è for Evaluating Left Ventricular Filling Pressure and Diastolic Dysfunction/Heart Failure With Preserved Ejection Fraction: A Systematic Review and Meta-Analysis. JAHA [Internet]. 2016 Jan 13 [cited 2020 Jan 22];5(1). Available from: https://www.ahajournals.org/doi/10.1161/JAHA.115.002530

128. Lancellotti P, Galderisi M, Edvardsen T, Donal E, Goliasch G, Cardim N, et al. Echo-Doppler estimation of left ventricular filling pressure: results of the multicentre EACVI Euro-Filling study. European Heart Journal - Cardiovascular Imaging. 2017 Sep 1;18(9):961–8.

129. Ran H, Schneider M, Pistritto AM, Gerges C, Heidari H, Binder T, et al. Echocardiographic evaluation of left ventricular filling pressures in patients with pulmonary hypertension. Int J Cardiovasc Imaging. 2019 May;35(5):861–8.

130. D'Alto M, Romeo E, Argiento P, Pavelescu A, Mélot C, D'Andrea A, et al. Echocardiographic prediction of pre- versus postcapillary pulmonary hypertension. J Am Soc Echocardiogr. 2015 Jan;28(1):108–15.

131. Geske JB, Sorajja P, Nishimura RA, Ommen SR. Evaluation of Left Ventricular Filling Pressures by Doppler Echocardiography in Patients With Hypertrophic Cardiomyopathy: Correlation With Direct Left Atrial Pressure Measurement at Cardiac Catheterization. Circulation. 2007 Dec 4;116(23):2702–8.

132. Mullens W, Borowski AG, Curtin RJ, Thomas JD, Tang WH. Tissue Doppler Imaging in the Estimation of Intracardiac Filling Pressure in Decompensated Patients With Advanced Systolic Heart Failure. Circulation. 2009 Jan 6;119(1):62–70.

133. Tomlinson S, Scalia GM, Appadurai V, Edwards N, Savage M, Lam AK, et al. Left atrial reservoir strain provides incremental value to left atrial volume index for evaluation of left ventricular filling pressure. Echocardiography. 2021 Sep;38(9):1503–13.

134. Romano G, Magro S, Agnese V, Mina C, Di Gesaro G, Falletta C, et al. Echocardiography to estimate high filling pressure in patients with heart failure and reduced ejection fraction. ESC Heart Failure. 2020 Oct;7(5):2268–77.

135. Borde D, Joshi S, Jasapara A, Joshi P, Asegaonkar B, Apsingekar P. Left Atrial Strain as a Single Parameter to Predict Left Ventricular Diastolic Dysfunction and Elevated Left Ventricular Filling Pressure in Patients Undergoing Off-Pump Coronary Artery Bypass Grafting. Journal of Cardiothoracic and Vascular Anesthesia. 2021 Jun;35(6):1618–25.

136. Mandoli GE, Sisti N, Mondillo S, Cameli M. Left atrial strain in left ventricular diastolic dysfunction: have we finally found the missing piece of the puzzle? Heart Fail Rev. 2020 May;25(3):409–17.

137. Cameli M, Lisi M, Mondillo S, Padeletti M, Ballo P, Tsioulpas C, et al. Left atrial longitudinal strain by speckle tracking echocardiography correlates well with left ventricular filling pressures in patients with heart failure. Cardiovasc Ultrasound. 2010 Apr 21;8:14.

138. Sato K, Grant ADM, Negishi K, Cremer PC, Negishi T, Kumar A, et al. Reliability of updated left ventricular diastolic function recommendations in predicting elevated left ventricular filling pressure and prognosis. American Heart Journal. 2017 Jul;189:28–39.

139. Johansson B, Lundin F, Tegeback R, Bojö L. E/a′ ratio is closely related to pulmonary vein flow profile in patients with normal ejection fraction. Scandinavian Cardiovascular Journal. 2019 Nov 2;53(6):312–6.

140. Abdula G, Ramos JG, Marlevi D, Fyrdahl A, Engblom H, Sörensson P, et al. Noninvasive estimation of mean pulmonary artery pressure by CMR in under 2 minutes scan time [Internet]. Cardiovascular Medicine; 2023 Apr [cited 2023 Aug 22]. Available from: http://medrxiv.org/lookup/doi/10.1101/2023.04.04.23288073

141. Varga-Szemes A, Halfmann M, Schoepf UJ, Jin N, Kilburg A, Dargis DM, et al. Highly Accelerated Compressed-Sensing 4D Flow for INTRACARDIAC Flow Assessment. Magnetic Resonance Imaging. 2022 Oct 20;jmri.28484.

142. Reiter C, Reiter G, Kräuter C, Scherr D, Schmidt A, Fuchsjäger M, et al. Evaluation of left ventricular and left atrial volumetric function from native MR multislice 4D flow magnitude data. Eur Radiol [Internet]. 2023 Aug 15 [cited 2023 Aug 22]; Available from: https://link.springer.com/10.1007/s00330-023-10017-3

143. Ley S, Fink C, Puderbach M, Zaporozhan J, Plathow C, Eichinger M, et al. MRI Measurement of the Hemodynamics of the Pulmonary and Systemic Arterial Circulation: Influence of Breathing Maneuvers. American Journal of Roentgenology. 2006 Aug;187(2):439–44.

144. Sakuma H, Kawada N, Kubo H, Nishide Y, Takano K, Kato N, et al. Effect of breath holding on blood flow measurement using fast velocity encoded cine MRI. Magn Reson Med. 2001 Feb;45(2):346–8.

145. Cross TJ, Kim CH, Johnson BD, Lalande S. The interactions between respiratory and cardiovascular systems in systolic heart failure. J Appl Physiol (1985). 2020 Jan 1;128(1):214–24.

146. Tsuchiya N, Nagao M, Shiina Y, Miyazaki S, Inai K, Murayama S, et al. Circulation derived from 4D flow MRI correlates with right ventricular dysfunction in patients with tetralogy of Fallot. Sci Rep. 2021 Jun 2;11(1):11623.

147. Yuan L, Cao T, Zang Y, Pei J, Duan Y, Gao F. Reversal E/A Value at End-Inspiration Might Be More Sensitive and Accurate for Diagnosing Abnormal Left Ventricular Diastolic Function. Echocardiography. 2007 May;24(5):472–7.

148. Pelc NJ, Bernstein MA, Shimakawa A, Glover GH. Encoding strategies for three-direction phase-contrast MR imaging of flow. J Magn Reson Imaging. 1991 Jul;1(4):405–13.

149. Bissell M, Raimondi F, Ait Ali L, Allen BD, Barker AJ, Bolger A, et al. 4D Flow cardiovascular magnetic resonance consensus statement: 2023 update. J Cardiovasc Magn Reson. 2023;25:40.

150. Hedström E, Bloch KM, Bergvall E, Ståhlberg F, Arheden H. Effects of gadolinium contrast agent on aortic blood flow and myocardial strain measurements by phase-contrast cardiovascular magnetic resonance. J Cardiovasc Magn Reson. 2010 Dec;12(1):70.